ADDIS ABABA UNIVERSITY

SCHOOL OF GRADUATE STUDIES

BULK HETEROJUNCTION, NATURAL, AND SYNTHETIC DYE SENSITIZED PHOTOELECTROCHEMICAL SOLAR ENERGY CONVERSION

By

Sisay Tadesse

A Thesis Submitted to

The Department of Chemistry

Presented in Fulfillment of the requirements for the degree of Doctor of Philosophy (Physical Chemistry)

Addis Ababa, Ethiopia

BULK HETEROJUNCTION, NATURAL AND SYNTHETIC DYE SENSITIZED PHOTOELECTROCHEMICAL SOLAR ENERGY CONVERSION

Sisay Tadesse

A Thesis Submitted to

The Department of Chemistry

Presented in Fulfillment of the requirements for the degree of

Doctor of Philosophy (Physical Chemistry)

Addis Ababa University

Addis Ababa, Ethiopia

May, 2012

Addis Ababa University

School of Graduate Studies

This is to certify that the thesis prepared by Sisay Tadesse Anshebo entitled: *Heterojunction, Natural and Synthetic Dye Sensitized Photoelectrochemical Solar En Conversion* and submitted in partial fulfillment of the requirements for the Degre Doctor of Philosophy (Physical Chemistry) complies with the regulations of University and meets the accepted standards with respect to originality and quality.

Signed by the Examining Committee

Name	Signature	Date
Prof. Carlo A. Bignozzi External Examiner		19 June 2012
Prof. Theodros Solomon Examiner		19 June 2012
Dr. Ahmed Mustefa Examiner		19 June 2012
Dr. Shimelis Admassie Examiner		19 June 2012
Prof. Teketel Yohannes Advisor		19 June 2012

Chair of Department or Graduate Program Coordinator

Abstract

Bulk Heterojunction, Natural and Synthetic Dye Sensitized Photoelectrochemical Solar Energy Conversion

Sisay Tadesse

Addis Ababa University, 2012

A solid-state photoelectrochemical solar energy conversion device based on blend of poly(3-hexylthiophene) (P3HT) and 1- (3-methoxycarbonyl)propyl-1-phenyl [6,6]C_{61} (PCBM), and an amorphous poly(ethylene oxide) complexed with I_3^-/I^- redox couple has been constructed and characterized. The photoelectrochemical performance parameters of the device were compared with pure P3HT and P3HT:C_{60} blend solid-state photoelectrochemical cell. The current density–voltage characteristics in the dark and under white light illumination and photocurrent spectra for front and backside illuminations have been studied. An open-circuit voltage of 140 mV and a short circuit current density of 28.4 $\mu A/cm^2$ at light intensity of 100 mW/cm^2; IPCE% of 1.52% for front side illumination (ITO|PEDOT) and IPCE% of 0.17% for backside illumination (ITO|P3HT:PCBM) at a wavelength of 510 nm were obtained. The dependence of the short-circuit current density and an open-circuit voltage on the light intensity and time have also been studied.

A solid-state photoelectrochemical solar energy conversion device based on nc-TiO sensitized with Di-Tetrabutylammoniumcis-bis(isothiocyanato)bis(2,2'-bipyridyl 4,4'-dicarboxylato)-ruthenium(II) (N-719) dye has been constructed and characterized. The current–voltage characteristics in the dark and under white light illumination and action spectra under monochromatic illuminations have been studied. The following device parameters were obtained: an open-circuit voltage of 762.5 m

and a short circuit current density of 33.2 $\mu A/cm^2$ at light intensity 100 mW/cm^2; the IPCE% obtained was 1.7% at 330 nm. The dependence of the short-circuit current and an open-circuit voltage on the incident light intensity and illumination time have also been studied.

DSSCs were assembled using natural dye extracted from fruits of Dokma (*Syzygium guineense)* as sensitizer. The photoelectrochemical performance of the quasi-solid state DSSCs based on the ethanol extract dye showed V_{OC} of 0.506 V and J_{SC} of 2.03 $mAcm^{-2}$; and a power conversion efficiency of 0.51%. UV–vis spectroscopy studies of light absorption of the natural dye were done. Furthermore, the ethanol extract obtained from *Syzygium guineense* was further purified stepwise through solvent-solvent extraction. The photoelectrochemical performance for the extracts with different solvents indicated that the individual components have synergistic effect in the performance of the DSSC.

Quasi-solid state dye-sensitized solar cells (DSSCs) were assembled by using the lea extracts of *Amaranthus caudatus* and *Iresine herbstii,* and flower extract of *Ipomoea indica* and *Hibiscus sabdariffa* as natural sensitizers of TiO_2 films. 0.1 M HCl lea extracts of *Amaranthus caudatus* and *Iresine herbstii* mainly contains the yellow orange indicaxanthin and the red purple betacyanin whereas their respective ethanc extract is mainly chlorophyll. In ethanol and 0.1 M HCl extract of *Ipomoea indica* an *Hibiscus sabdariffa* anthocyanins are the main components. The best overall sola energy conversion efficiency of 1% was obtained, under 100 mW/cm^2 irradiation with ethanol extract of *Amaranthus caudatus*, that showed a current density (J_{SC} = 3.44 mA/cm^2), open circuit voltage (V_{OC} = 0.57 V), and a high IPCE value (77% at = 410 nm). Also the ethanol extract of *Ipomoea indica* flower showed interestin

performances, with a J_{SC} of 3.11 mA/cm^2, V_{OC} of 0.55 V, the corresponding solar to electrical power conversion of efficiency of 0.94% and IPCE value (75% at λ = 420 nm). The ethanol extract of *Hibiscus sabdariffa* flower showed J_{SC} of 3.21 mA/cm^2, V_{OC} of 0.49 V, the corresponding solar to electrical power conversion of efficiency of 1% and IPCE value (50.2% at λ = 600 nm).

Key Words: Photoelectrochemical cell, Solid State Electrolyte, Quasi-Solid State Electrolyte, Dye Sensitized Solar Cells, Natural Dyes

Acknowledgements

First and foremost, praise to God for His blessings and mercy for giving me an excellent health and strength in completing this work. I would like to express my earnest appreciation to my supervisor Prof. Teketel Yohannes for his tremendous support, excellent guidance, and encouragement during the entire period of my PhD study. I really appreciate his willingness to solve problems that I encountered during the whole period of my PhD study. His patience to read all seminar papers, progress report, my PhD thesis, and manuscripts was exemplary. The comments and corrections to my documents were very valuable. I gratefully acknowledge for the opportunity to be supervised by him.

I thank the Austrian Academic Exchange Service (ÖEAD) for giving me scholarshi for a one year research work as part of my PhD work. The experience of working a Linz Institute for Organic Solar Cells (LIOS), Johannes Kepler University, Linz i Austria is invaluable to me. I would like to thank Prof. N.S. Sariciftci for giving m the opportunity to do part of my research work under his supervision at LIOS. I woul also thank Dr. H. Neugebauer for his guidance, Dr. Daniel Egbe for providing m some chemicals I needed for my work and members of the institution for thei cooperation during my stay at LIOS. I am deeply grateful for the opportunity to worl with and learn from them.

I am indebted to the Hawassa University for giving me the sponsorship an continuous support during my study. I greatly appreciate the department c Chemistry, Addis Ababa University, and staff members for their sincere cooperatio during my study. I specially thank Prof. Wondimagegn Mammo and Dr. Yona Chebude for allowing me to use their lab for part of my work. I am thankful to Pro

Theodros Solomon for reviewing and giving me his genune comments on my manuscripts. I also thank with gratitude Ato Atakilt Abebe for his encouragement and generously providing the ionic liquids that I need for my research work. My special thanks also go to Ato Sahlemichael Deme for his kind support in getting the chemicals and other materials I need.

With only limited access to research journals, getting literatures would have been very difficult had there not been the cooperation of my friends, Dr. Alemayehu Mekonnen and Ato Alemayehu Esayas from Norway, Dr. Dereje Taffa from Germany, Ato Ajawmolla Abere from Canada and Dr. Bitu Birru from UK. I thank you very much. Furthermore, I express my deepest appreciation to my Friends Getachew Adam, Siraye Esubalew, Minaleshewa Atlabachew, and all individuals that have contributed ideas, comments, criticized and for having made my time in completing this work so pleasant and enjoyable, thank you so much.

My warmest thanks are due to my father Ato Tadesse Anshebo and my mother, W/ro Ayelech Abiyo, and all my family members for never-ending support and encouragement all this time. I specially thank with gratitude my brother Mesfin Tadesse and his family from USA for their encouragement and material support.

Finally, I would like to express my sincere gratitude to the support and encouragement I got from my beloved wife W/ro Abaynesh Bekele. Indeed it is you greatest support, encouragement and scarifies that brought this work to a successfu end. You showed great endurance in taking care of me and our two sons, Nathan and Abenezer, while I go through the hard way. I thank you very much from the bottom o my heart. May God give you His rewards for your sacrifices!

Sisay Tadesse

Table of Contents

List of Figures

List of Tables

1. INTRODUCTION AND MOTIVATION

One of the many challenges we face today is the steady increase in energy consumption. With a constantly growing human population and improved living standards, more energy will be needed, with the result that the worldwide power consumption is expected to double within the next 30 years [1]. Mankind's overall energy consumption came to be 13 terawatts (TW). It has been predicted that by the year 2050, between 26.4 and 32.9 TW will be required to meet our demand for energy. If fossil fuels continue to be the main source of energy, this could lead to atmospheric CO_2 levels exceeding 750 ppm, with devastating effects on ecosystems, animal species and populations throughout the globe. If this catastrophe is to be prevented, production of CO_2-neutral energy is of utmost importance. There are many renewable energy sources, of which the most abundant, but also the most difficult to harness, is solar energy. Indeed, the solar energy reaching the Earth's surface in one hour surpasses the yearly expenditure of energy by humankind. The challenge that now faces a section of the scientific community is to find an economically viable way to utilize this energy [2]. There are essentially three ways to harness the sun's energy. The simplest is by capturing the thermal energy, which can either be used directly for domestic use, or concentrated as a heat engine to drive a turbine to generate electricity. The second has been implemented by nature since the beginnings of life on Earth. Photosynthesis is an example of a photochemical energy converter, whereby the photon's energy is stored in the form of chemical energy. A promising example of a renewable energy source is using sunlight to drive water splitting into hydrogen which can later be used as a fuel [3 – 4]. Photovoltaic devices constitute the third method to harness the sun's energy.

The availability of energy is not only necessary for people in their daily life; it is also among the major driving forces of the global economy [5]. Everything, from politics to economy and even further to individuals, is directly dependent on it. As it is mentioned earlier, currently, the total energy usage is about 13 TW, where fossil fuel (coal, oil, and natural gas) is the main source. There are however concerns on maintaining the usage of fossil fuels as the main source of energy. Basically, energy from fossil fuels faces two problems, the first being the limitation of resources and the second their environmental impact. For these two reasons, there has been an urge to develop sustainable energy solutions. The supply of clean sustainable energy is considered as one of the most important scientific and technical challenges facing humanity in the 21st century [5].

Among the different alternative power sources existing today (e.g. nuclear, hydroelectric, geothermal, wind, biomass, and solar), solar energy has the most potential [5]. In fact, several of the alternative energy sources used today are indirectly derived from solar energy [6]. The sun provides the earth with approximately 100,000 TW which is almost 10,000 times more than the current energy consumption [7]. The practical global solar potential is about 600 TW [8]. This abundance of energy makes solar cells very attractive for electricity production. The solar cell that currently has the largest share in the market is based on crystalline silicon and was first reported by Chapin et al. in 1954 [9]. Even if the efficiency since then has increased and the production cost decreased, it is still too expensive to be able to compete with the conventional energy sources. This has lead to a great research interest in finding new ways of utilizing the solar energy with cheaper and more efficient methods.

In this framework, we studied photoelectrochemical solar energy conversion based on polymer PCBM, natural (dyes extracted from plants) and commercial dye based solid state and quasi-solid state dye sensitized solar cells (DSSCs) with the interest to investigate the photoelectrochemical properties of polymer:PCBM, commercial, and natural dyes adsorbed on nanocrystalline TiO_2 film, with solid state electrolyte based amorphous polymer poly[oxymethylene-oligo(oxyethylene)] (POMOE) complexed with the redox couple I_3^-/I^- and the polymer polyvinylpyrrolidone (PVP) mixed with 1-ethyl-3-methylimmidazolium iodide (EMIm-I), sodium iodide, and iodine as quasi-solid state electrolyte.

General Objectives of this work was:

To design and characterize polymer based solid state photoelectrochemical cells, solid state and quasi-solid state Dye Sensitized Solar Cells based on nanocrystalline-TiO_2 sensitized with natural pigments and ruthenium dyes for use in photoelectrochemical solar energy conversion. The specific objectives include:

(i) To produce bulk heterojunction all-solid-state photoelectrochemical solar cells using conjugated polymer poly (3-hexylthiophene), P3HT, by blending with 1-(3-methoxycarbonyl) propyl-1-phenyl [6, 6]C_{61} PCBM as photoactive materials and study the photovoltaic properties of polymer:PCBM photoelectrochemical cells with basic structure: ITO|polymer:PCBM | polymer electrolyte with redox couple| Pt or PEDOT| ITO.

(ii) To produce all-solid-state Dye sensitized solar cell based on nc-TiO sensitized with synthetic dyes like N-719 Dye and study the photovoltaic properties of hybrid solar cells with the basic structure; ITO|TiO_2| Dye polymer electrolyte with redox couple| Pt or PEDOT|ITO.

(iii) To produce quasi-solid state dye sensitized solar cell based on nc-TiO_2 sensitized with ruthenium dye and various natural dyes from plant sources, polymer gel electrolyte composed of 1-ethyl-3-methylimmidazolium iodide (EMImI), NaI, I_2 and polyvinylpyrrolidone (PVP) dissolved in acetonitrile and study the photovoltaic properties of dye sensitized solar cells with the basic structure; ITO|TiO_2 |Dye|Quasi-solid state polymer electrolyte with redox couple|Pt or PEDOT|coated ITO.

This thesis is organized as follows:

Chapter 1 is an introductory chapter presenting the general motivation of this thesis.

In Chapter 2 the fundamental theoretical background for the understanding of the work is described. Accordingly, photoelectrochemical cells without dyes (photoelectrochemical cells based on photoactive polymers) and dye sensitized solar cells, their operation principle and things to be done in order to improve the performance of dye sensitized solar cells etc, are given.

Chapter 3 presents experimental procedures, materials, and methods used for the preparations of the various photoelectrochemical cells. Detailed preparation steps for an all solid state photoelectrochemical cell based on blend of P3HT and PCBM or dye coated nanocrystalline TiO_2 as photoactive material and amorphous polyethylene oxide complexed with the I_3^-/I^- redox couple used as an electrolyte are described. Preparation of quasi-solid state dye sensitized solar cells using natural dyes as sensitizer and polymer polyvinylpyrrolidone (PVP) mixed with an ionic liquid 1-ethyl-3-methylimmidazolium iodide (EMIm-I), sodium iodide and iodine as quasi-solid state electrolyte are described.

In Chapter 4 Experimental results are discussed. The first section (Section 4.1) presents experimental results on the behaviour of a solid-state PEC containing a mixture of poly(3-hexylthiophene) (P3HT) and PCBM coated on indium-doped tin oxide (ITO) used as a photoactive electrode; amorphous polyethylene oxide complexed with the I_3^-/I^- redox couple used as an electrolyte; and a thin transparent layer of poly(3,4-ethylenedioxythiophene), PEDOT, electrochemically coated on ITO as a counter electrode.

The second section (Section 4.2) describes the study of solid state photoelectrochemicl cell based on dye sensitized TiO_2 and polymer electrolyte complexed with I_3^-/I^-. In this section the studies made on an all-solid-state PEC constructed with nc-TiO_2 coated onto ITO that is covered with N-719 dye and used as a photoactive electrode, the ion conducting polymer, POMOE, complexed with redox couple as a solid polymer electrolyte, and a PEDOT coated on ITO as counter electrode are discussed.

The third section (Section 4.3) describes the work on natural dye sensitized solar cells using pigments extracted from fruit of *Syzygium guineense*. The photoelectrochemical properties of the quasi–solid state DSSCs using these extracts as sensitizer and polymer polyvinylpyrrolidone (PVP) mixed with 1-ethyl-3-methylimmidazolium iodide (EMIm-I), sodium iodide, and iodine as quasi-solid state electrolyte complexed with redox couple were investigated.

The fourth section (Section 4.4) describes the results of the study on solar energy conversion based on quasi-solid state dye-sensitized solar cells using leaf and flower extracts as sensitizers are described. Here the results of a series of experiments carried out on raw leaf extracts of *Amaranthus caudatus* and *Iresine herbstii,* and flower o

morning glory (*Ipomoea indica*) and Karkade (*Hbiscus sabdariffa*) are described. The photoelectrochemical properties of the quasi–solid state DSSCs using these extracts as sensitizer and polymer PVP mixed with EMIm-I, sodium iodide and iodine as quasi-solid state electrolyte were investigated.

2. PHOTOELECTROCHEMICAL CELLS

2.1. Introduction

A typical type of the photocurrent-generated device has a semiconductor in contact with an electrolyte, and this is often referred as photoelectrochemical cells (PECs). A photoelectrochemical cell consists of a photoactive semiconductor working electrode (either n- or p-type) and counter electrode made of metal (e.g. Pt). Both electrodes are immersed in the electrolyte containing suitable redox couples. In a metal-electrolyte junction, the potential drop occurs entirely on the solution side, whereas in a semiconductor-electrolyte junction, the potential drop occurs on the semiconductor side as well as the solution side. The charge on the semiconductor side is distributed deep in the interior of the semiconductor, creating a space charge region. If the junction of the semiconductor-electrolyte is illuminated with a light having energy greater than the bandgap of the semiconductor, photogenerated electrons/holes are separated in the space charge region. The photogenerated minority carriers arrive at the interface of the semiconductor-electrolyte.

Photogenerated majority carriers accumulate at the backside of the semiconductor. With the help of a connecting wire, photogenerated majority carriers are transported *via* a load to the counter electrode where these carriers electrochemically react with the redox electrolyte. A pioneering photoelectrochemical experiment was realized by obtaining photocurrent between two platinum electrodes immersed in the electrolyte containing metal halide salts [10]. It was later found that the photosensitivity can be extended to longer wavelengths by adding a dye to silver halide emulsions [11].

The interest in photoelectrochemistry of semiconductors led to the discovery of wet type photoelectrochemical solar cells [12–14]. These studies showed electron transfe

to be the prevalent mechanism for photoelectrochemical sensitization processes. Grätzel has then extended the concept to the dye sensitized solar cells (DSSC), which will be discussed further in the later part. The PECs that convert light into electricity are termed "electrochemical photovoltaic" or "regenerative cells" and those that generate chemical fuels are "photoelectrosynthetic" or "non-regenerative cells". Figure 2.1 shows various types of the photoelectrochemical cells.

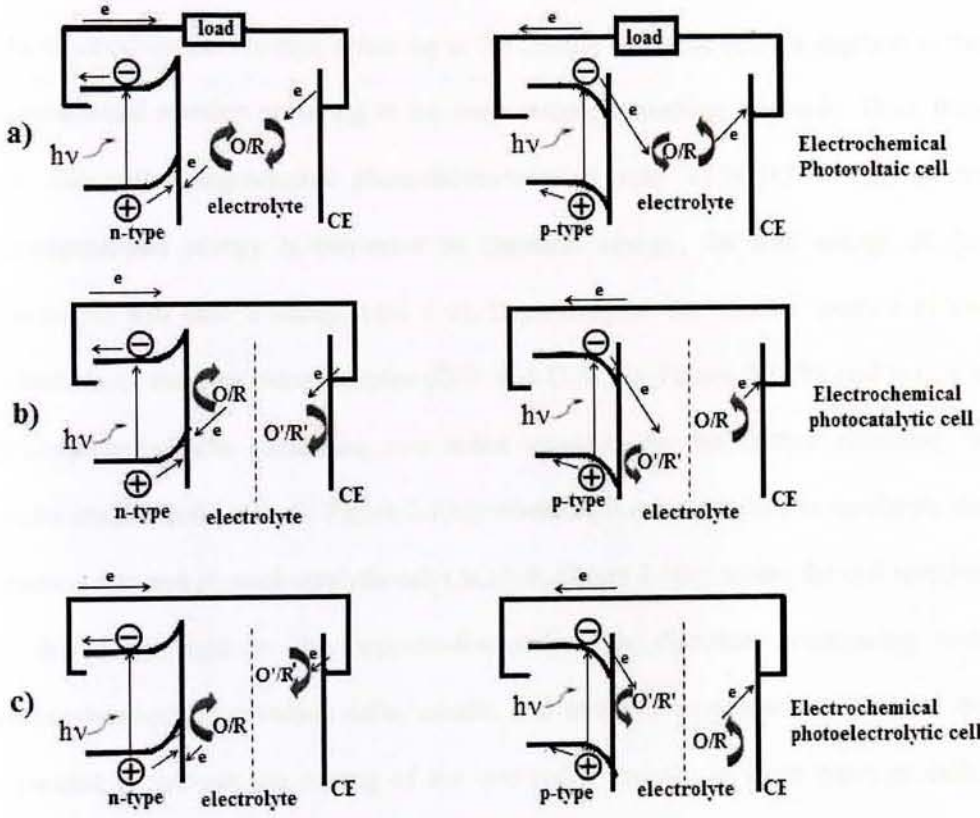

Figure 2. 1: Different types of photoelectrochemical cells with the working electrode (WE) made of semiconductor (n- or p-type) and the counter electrode (CE), (a) regenerative photoelectrochemical cell (b) photocatalytic cell (non-regenerative photoelectrochemical cell) (c) photoelectrolytic cell (non-regenerative photoelectrochemical cell).

When shining the light, oxidation reaction will happen on the surface of n-type semiconductors, whilst reduction reaction will happen on the surface of p-type semiconductors. In the regenerative photoelectrochemical cell, which is based on a narrow bandgap semiconductor and a redox couple as shown in Figure 2.1a, solar energy is converted into electrical energy without change of the free energy of the redox electrolyte ($\Delta G = 0$).

The electrochemical reaction occurring at the counter electrode (CE) is opposite to the photoassisted reaction occurring at the semiconductor working electrode. Thus, they are also called regenerative photoelectrochemical solar cells [15 – 18]. If the photogenerated energy is converted to chemical energy, the free energy of the electrolyte will have a change ($\Delta G \neq 0$). Depending on the relative location of the potentials of the two redox couples (O/R and O'/R' in Figure 2.1 (b) and (c)), the photosynthetic cells containing two redox couples, can be further classified as photocatalytic cell ($\Delta G < 0$, Figure 2.1(b)) where light merely serves to accelerate the reaction rate and photoelectrolytic cell ($\Delta G > 0$, Figure 2.1(c)) where the cell reaction is driven by light in the opposite-thermodynamic direction. Comparing with electrochemical photovoltaic cells, anodic and cathodic compartments need to be separated to prevent the mixing of the two redox couples in these types of cells. Titanium dioxide (TiO_2) has been favored semiconductor for such studies [19]. As early as 1971, photoelectrolysis of water was reported in an electrochemical cell with a TiO_2 photoanode and a Pt cathode without an external source [20]. A novel microreactor for TiO_2-assisted photocatalysis in a microfluidic electrochemical cell was designed with TiO_2 nanoparticles embedded in a gold electrode matrix [21]. The metal ions in aqueous solution can be determined by voltammetry after *in sit*

photocatalytic digestion of interfereing organic matter. This is very important for environmental analysis.

Here we will mainly focus on the development of regenerative electrochemical photovoltaic cells and dye sensitized solar cells. Absorption of light by the semiconductor or the sensitizer layer gives rise to a photocurrent and/or a photovoltage, which can be measured in the external circuit.

2.2. Electrochemical Photovoltaic Cells

One of the most important aspects in using solar energy is its conversion from solar radiation into electric energy. Electrochemical photovoltaic cells have the following advantages comparing with the solid photovoltaics.

1. It is not sensitive to the defects in semiconductors.
2. The solid/liquid junction is easy to form and the production price will be much reduced.
3. It is possible to realize the direct energy transfer from photons to chemical energy.

Unlike conventional solid state photovoltaic cells, the potential of the working electrode can be varied with respect to the reference electrode by means of an external voltage source connected between working and counter electrode.

The most striking difference between a photoelectrochemical photovoltaic cell and the conventional Si based photovoltaics is that the former contains two interfaces at which charge transport has to switch from electronic to ionic and *vice versa*, as in batteries. In electrochemical photovoltaic cells without dyes, both the semiconductor electrode and the counter electrode are immerged in the redox electrolyte. The

incident light excites the semiconductor electrode and the photogenerated electrons and holes are seperated in the space charge region. Specific reactions occur only at the semiconductor and the metal as shown in Figure 2.1(a). In these kinds of cell, charge balance due to oxidation and reduction processes is maintained. However, the wet-type photoelectrochemical cells suffer from instability of semiconductor in aqueous media. Unsensitized photoelectrochemical photovoltaic cells cannot replace the silicon based photovoltaics unless some photoelectrochemically stable semiconductor materials possessing band gap approximately 1.4 eV can be found [15 – 18].

2.3. Photoelectrochemical Cells based on Photoactive Polymers

2.3.1. Semiconductor-electrolyte interfaces

Photoelectrochemical cells allow the conversion of light to electricity. Their main characteristic is a semiconductor-electrolyte solution interface, which was intensely studied by Gerischer [22, 23]. For an n-type semiconductor, a scheme of the energetics of the interface before and after contact is shown in Figure 2.2.

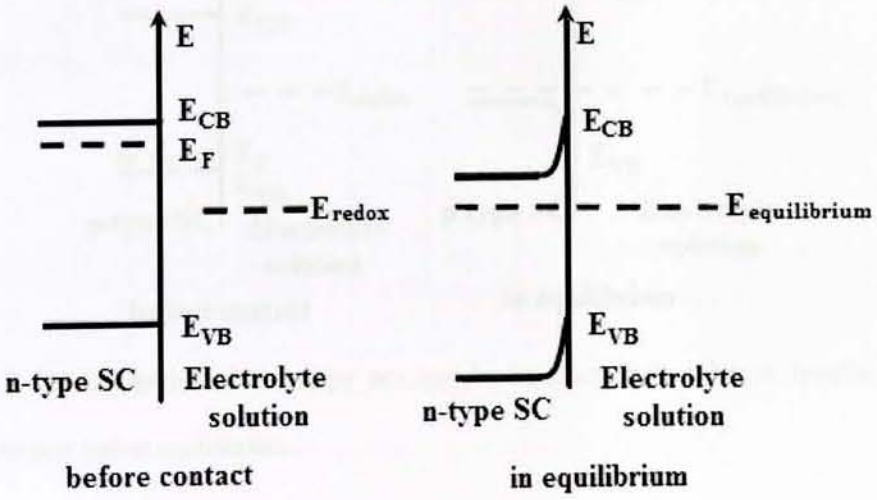

Figure 2. 2: Energetics of an n-type semiconductor-electrolyte solution interface before contact and at equilibrium.

After contact, the former different redox potential E_{redox} of the electrolyte solution and the Fermi level E_F of the semiconductor equilibrate. As a result, the interface gets charged, which leads to a bending of the valence band (VB) and the conduction band (CB) of the semiconductor. Due to illumination of the semiconductor, electrons may be excited, jumping from the valence band to the conduction band. In the space charge layer the generated charges are now separated, because the holes are attracted towards the interface and the electrons to the opposite direction. As a result, a current is observed in an outer circuit.

For a p-type semiconductor the situation is reversed. Valence and conduction bands are now bent downwards, and consequently the electrons excited by illumination are attracted by the interface, pushing the holes away. The current flowing through an outer circuit is now opposite in sign. A scheme of the situation in a p-type semiconductor is shown in Figure 2.3.

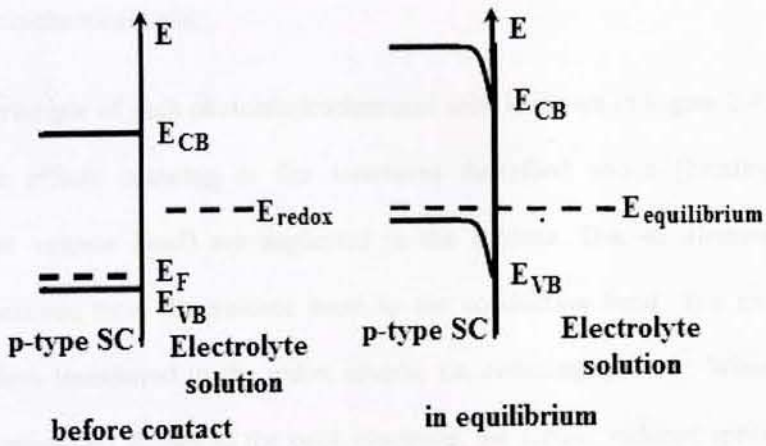

Figure 2. 3: Energetics of a p-type semiconductor-electrolyte solution interface before contact and at equilibrium.

When the high electrical conductivity of oxidised polyacetylene was discovered by Shirakawa, Heeger and MacDiarmid [24 – 26], suddenly a new class of materials wa

available. Dependig on their doping state, conjugated polymers offer beside insulating and metal-like conducting behaviour also semiconductor properties.

Moreover, they can be processed like other polymers [27]. The application of conjugated polymers has been investigated in many fields, e.g. in batteries [28], transistors [29], photodiodes [30], lasers [31], solar cells [32–36] and light emitting diodes [37].

2.3.2. Conjugated polymers in photoelectrochemical cells

Conjugated polymers are also of interest in the studies of photoelectrochemical cells because of their semiconductor behaviour and, as a result, their photoactivity. Besides many other polymers like polyacetylenes, polyanilines (PANI), and polyphenylene-vinylenes (PPV), polythiophenes were of great interest [38–42]. Even solid electrolytes were applied in photoelectrochemical cells [43], paving a way to all-solid state photoelectrochemical cells.

The working principle of such photoelectrochemical cells is shown in Figure 2.4. For simplicity, the effects occuring at the interfaces described above (bending of conduction and valence band) are neglected in the scheme. Due to illumination electrons are excited from the valence band to the conduction band. The excited electrons are then transferred to the redox couple, i.e. reducing I_3^- to I^-. When the electrons are transferred further to the back electrode, the former reduced species is oxidised back, leaving no net chemical reaction [44]. The hole left in the valence band is refilled from the front side by transfer of an electron from the ITO electrode to the polymer.

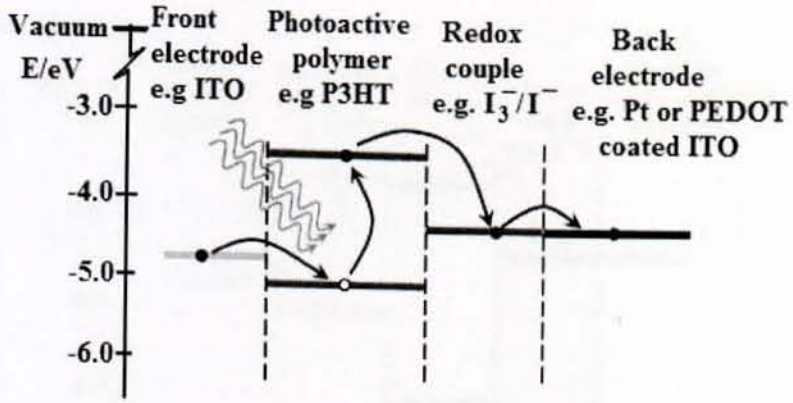

Figure 2. 4: Working principle of a photoelectrochemical cell.

2.3.3. Fullerenes in photoelectrochemical cells

In typical organic polymeric solid-state solar cells the photoactive conjugated polymer is blended with electron acceptors like methanofullerenes. These materials improve the charge separation, allowing efficiencies of 2.5% [35] and recently up to 7.4% [45]. Therefore, regarding the ultra fast electron transfer from the polymer to the electron acceptor, they might also be useful in photoelectrochemical cells: Electron acceptor intermediate layers could improve the charge separation before the electrons would be transferred further to the redox couple. Moreover, photoelectrochemical cells using C_{60} as photoactive material were investigated [46]. From this point of view, conjugated polymers which have better light absorption properties could improve the cell's characteristics. In Figure 2.5 the energetic levels of such a device is shown.

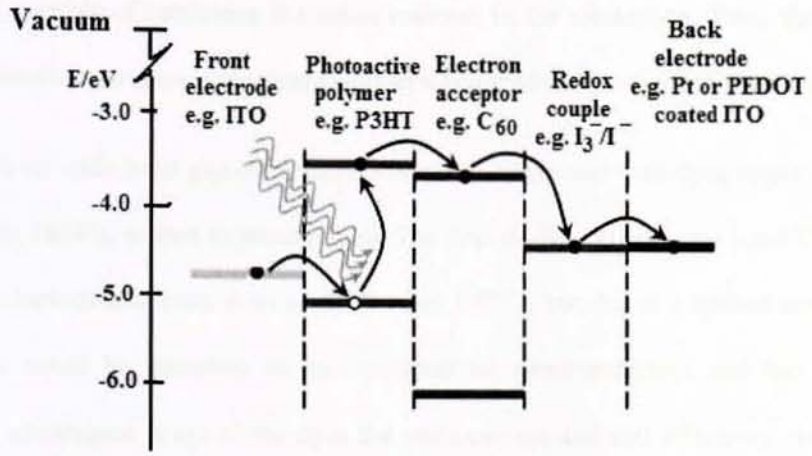

Figure 2. 5: Modification of a photoelectrochemical cell by addition of acceptor materials.

The conduction band of the electron acceptor has to be lower than the photoactive polymer. So the excited electrons can be transfered from the lowest unoccupied molecular orbital (LUMO) of the polymer to the LUMO of the acceptor and further to the electrolyte.

2.4. Dye Sensitized Photoelectrochemical Cells

2.4.1. Dye Sensitized Solar Cell (DSSC) structure and operating principle

The DSSC differs from other solar cell types both by its basic construction and the physical processes behind its operation. Unlike the first and second generation PV devices based on solid semiconductor materials, the typical DSSC configuration combines solid and liquid phases. Electricity is generated on the photoelectrode which is a nanoporous TiO_2 film sensitized with a monolayer of visible light absorbing dye and penetrated with a redox electrolyte. The TiO_2-electrolyte network is sandwiched between two conductive substrates that also work as current collectors. The opposite substrate to the TiO_2 layer, the counter electrode, is coated with

material capable of catalyzing the redox reaction in the electrolyte. Thus, the DSSC resembles more an electrochemical cell than a conventional *p-n* junction solar cell.

Research on wide band gap oxide semiconductors sensitized with dyes began already in the late 1800's, related to photography. The first studies on dye-sensitized TiO_2 and ZnO photoelectrodes were done in 1960's and 1970's, but due to a limited amount of dye that could be adsorbed on macrocrystalline semiconductors and too narrow spectral absorbance range of the dyes the photocurrent and cell efficiency stayed on very modest level [47]. Improvement to this was achieved in the early 1990's, thanks to nanotechnology and development of better dyes. Nanocrystalline TiO_2 enabled drastic multiplying of the effective surface area of the photoelectrode for the dye to adsorb, and the new ruthenium bipyridyl organometallic complexes (Figure 2.6) had absorbance range from visible to near-infrared wavelengths [47].

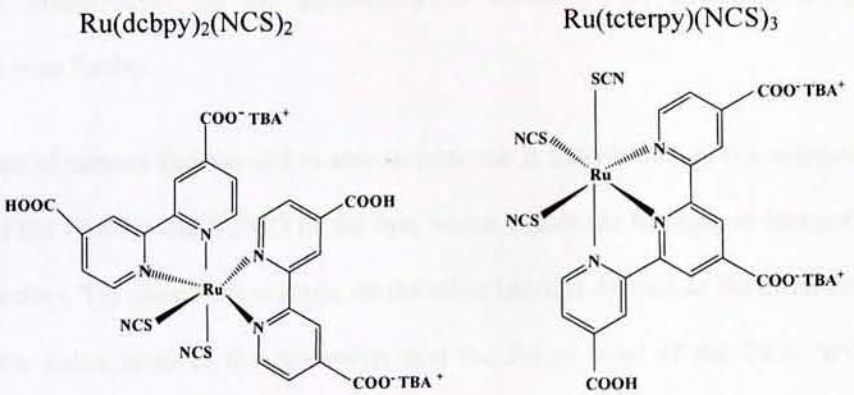

N719 Black dye

Figure 2. 6: Molecular structures of some common dyes, N 719 and black dye [47].

The basic DSSC structure and operating principle are presented in Figure 2.7. Photon absorption induces a metal-to-ligand type electronic transition between the HOMO (highest occupied molecular orbital) and LUMO of the dye. Since the LUMO is located in the vicinity of the ligands (pyridyl π-orbitals) the electron injection to the

TiO_2 is spatially favorable. Efficient electron injection is further enhanced by the strong electronic interaction that forms when the dye bonds to the TiO_2 with the ligand carboxyl groups and the energetic location of the TiO_2 conduction band in relation to the LUMO of the dye. Efficient charge separation is, on the other hand, achieved because the electrons and holes travel in different mediums. This prevents bulk recombination which is a problem in conventional *p-n* junction cells. The competing reactions, i.e. recombination of the photogenerated electrons with the oxidized form of the dye or the redox species in the electrolyte (Figure 2.8; the latter reaction referred to as "dark current" in the picture) proceed also several decades slower than the electron injection process. In addition to that, the electrolyte cations and protons released in the dye adsorption process intercalate to the TiO_2 surface and lattice where they, together with the negative species in the electrolyte, form a Helmholtz dipole layer on the photoelectrode surface. This enhances charge separation even further.

The amount of current that the cell is able to generate is determined by the energetic distance of the HOMO and LUMO of the dye, which equals the bandgap in inorganic semiconductors. The maximum voltage, on the other hand, is defined as the difference between the redox level of the electrolyte and the Fermi level of the TiO_2. With iodide/triiodide redox couple, this difference is about 0.9 V, though slight variation is caused by the electrolyte composition due to species adsorbed on the TiO_2 surface which may alter the Fermi level position somewhat. Also, there is always some recombination in the cell which lessens the amount of electrons in the TiO_2 film, thus lowering the Fermi level and decreasing the cell voltage.

After injection, electrons diffuse in the nanocrystalline TiO_2 network to the conductive coating of the substrate, from which they can be transferred to an external circuit. There exist various models for the electron diffusion in the TiO_2 film but thermally activated trapping/detrapping mechanism along localized energy levels below the TiO_2 conduction band edge seems the most realistic one, in the light of experimental evidence [48 – 51].

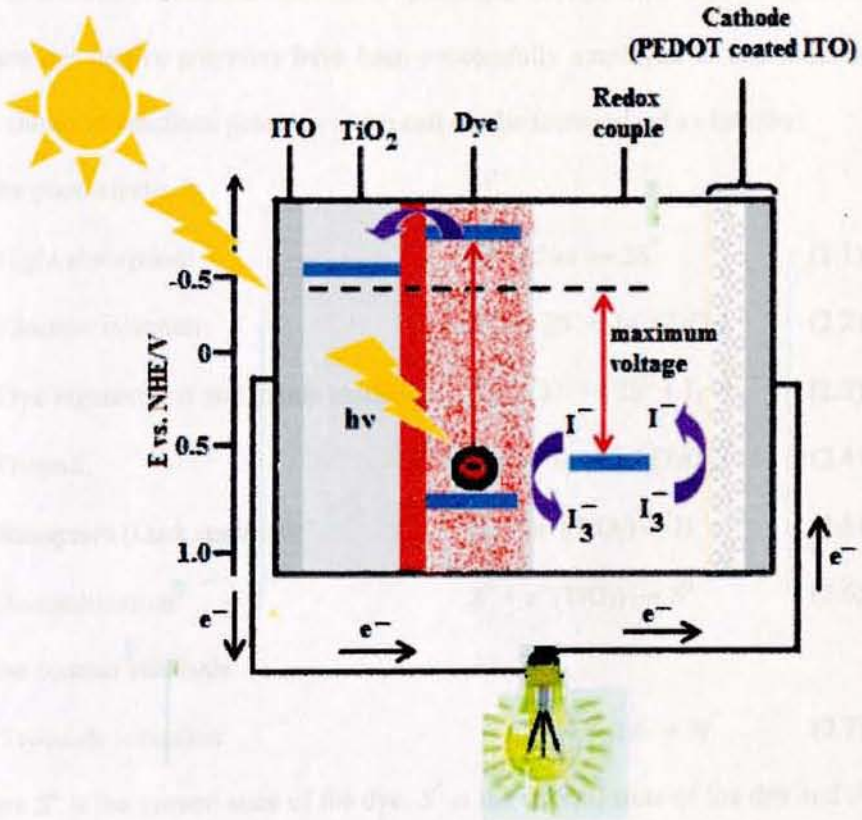

Figure 2. 7: The structure and operating principle of the DSSC.

The electron injection to the TiO_2 leaves the dye molecule on an oxidized state, S^+, in order for the current generation to continue, the dye must be reduced back to its ground state. This is done by the redox couple in the electrolyte. The most commonly used redox couple, and the one that gives the best cell efficiencies when combined with TiO_2, is iodide/triiodide. The oxidized dye gets electrons from the iodide ions

which, in turn, get oxidized to triiodide in the process. The triiodide ions then diffuse to the counter electrode, where they get reduced back to iodide by the electrons returning from the external load. Thus, the cell operation is based on consecutive reduction/oxidation cycles and, in an ideal cell, no chemical substances are permanently transmuted. The most often used counter electrode catalyst for the triiodide/iodide reduction reaction is platinum, though also carbon materials and certain conductive polymers have been successfully employed in this function [52].

The chemical reactions going on in the cell can be summarized as follows:

At the photoelectrode

- Light absorption: $2S^0 + 2hv \rightarrow 2S^*$ (2.1)
- Electron injection: $2S^* \rightarrow 2S^+ + 2e^-(TiO_2)$ (2.2)
- Dye regeneration and iodide oxidation: $2S^+ + 3I^- \rightarrow 2S^0 + I_3^-$ (2.3)
- Overall: $3I^- + 2hv \rightarrow I_3^- + 2e^-(TiO_2)$ (2.4)
- Recapture (Dark reaction): $I_3^- + 2e^-(TiO_2) \rightarrow 3I^-$ (2.5)
- Recombination: $S^+ + e^-(TiO_2) \rightarrow S^0$ (2.6)

At the counter electrode:

- Triiodide reduction: $I_3^- + 2e^- \rightarrow 3I^-$ (2.7)

where S^0 is the ground state of the dye; S^* is the excited state of the dye and S^+ is the oxidized state of the dye.

The high solar energy conversion efficiencies of solar cells employing dye-sensitized nanocrystalline films of TiO_2 [53] have spawned many recent studies of similar photoelectrochemical systems based on dye sensitization [54 – 59]. A detailed understanding of the mechanism and time scale of electron transfer from surface adsorbed dyes to semiconductors will help to explain the high conversion efficiencies

and to improve them further. Femtosecond laser techniques make it possible to explore the initial steps of the electron injection and recombination [60 – 63].

Comparison of the injection time and the recombination time measured in these experiments should allow for selection of efficient dye compounds for the nanocrystalline solar cell (or light detector).

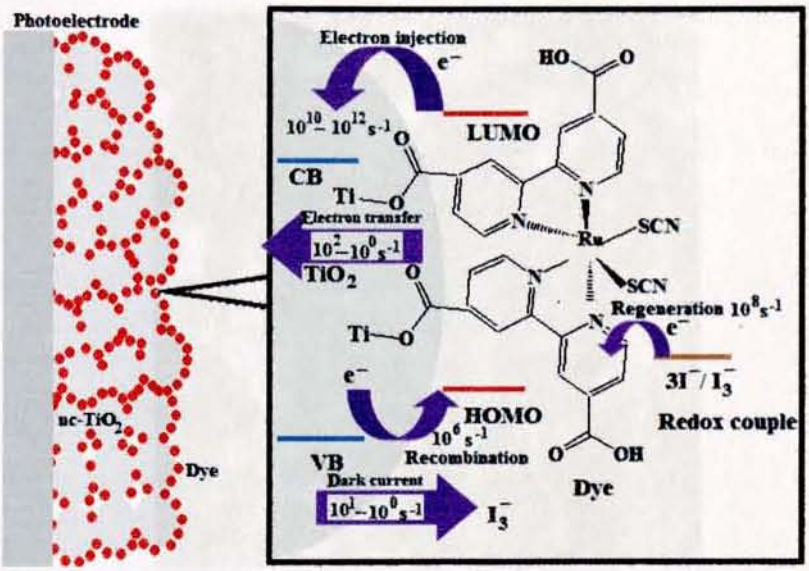

Figure 2. 8: The electron transfer reactions and their time scales in the dye-TiO_2-electrolyte system [47].

2.4.2. Nanocrystalline Film Morphology

A photovoltaic conversion system based on light harvesting by a molecular absorber attached to a wide bandgap semiconductor surface faces two problems [64]:

1. A monolayer of dye on a flat surface absorbs at most a few percent of light because it occupies an area that is much larger than its optical cross section. Therefore it can only harvest a negligibly small fraction of the incoming light.
2. Compact oxide semiconductor films need to be n-doped to conduct electrons.

Therefore it is detrimental to enlarge the interface between oxide semiconductor phase and the sensitizing dye. This is successfully achieved by introducing a nanoparticle based electrode construction which enhances the photoactive interface by orders of magnitude [65]. Figure 2.9 shows scanning electron micrograph of a TiO_2 anatase colloid film.

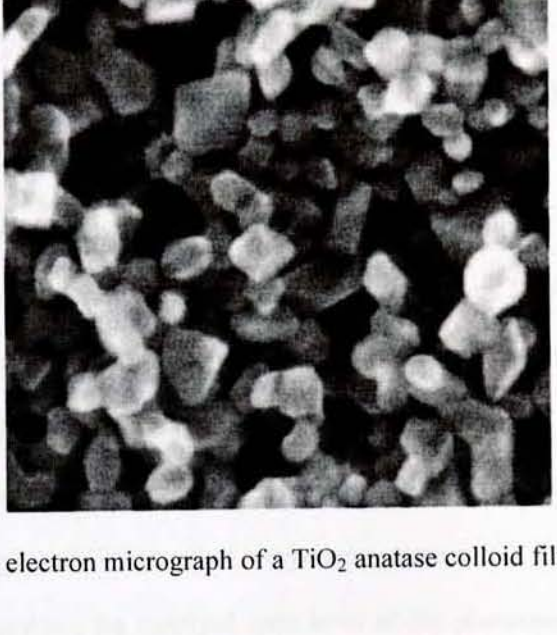

Figure 2. 9: Scanning electron micrograph of a TiO_2 anatase colloid film [65].

2.4.3. The Choice of the Sensitizer (Light Absorption)

While the high efficiency of the dye sensitized solar cells arises from a collective effect of numerous physical-chemical nanoscale properties, the key issue is the principle of dye sensitization of large band-gap semiconductor electrodes. In the dye sensitized solar cells this is accomplished by coating the internal surfaces of porous TiO_2 electrode with special dye molecules tuned to absorb the incoming photons [66].

The actual sensitization effect can be seen in Figure 2.10 [64] as a shift of the incident photon to current conversion efficiency (IPCE) curve of the bare TiO_2 to higher wavelengths when coated with the dye. The current efficiency of the cell is related to

the 'height' of the IPCE curve, which depends on the charge separation and charge collection efficiencies [66].

The ideal sensitizer for a single junction solar cell converting global AM 1.5 sunlight to electricity should fullfill the following requirements [64, 65, 67]:

1. The absorption spectrum of the photosensitizer should cover the whole visible region and even the part of the near-infrared (NIR).
2. The photosensitizer should have anchoring groups (-COOH, $-H_2PO_3$, $-SO_3H$, etc.) to strongly bind the dye onto the semiconductor surface.
3. The excited state level of the photosensitizer should be higher in energy than the conduction band edge of n-type semiconductor (n-type DSSCs), so that an efficient electron transfer process between the excited dye and conduction band (CB) of the semiconductor can take place. In contrast, for p-type DSSCs the HOMO level of the photosensitizer should be at more positive potential than the valence band (VB) level of p-type semiconductor.
4. For dye regeneration, the oxidized state level of the photosensitizer must be more positive than the redox potential of electrolyte.
5. Unfavorable dye aggregation on the semiconductor surface should be avoided through optimization of the molecular structure of the dye or by addition of coadsorbers that prevent aggregation.
6. The photosensitizer should be photostable, and electrochemical and thermal stability are also required.

Based on these requirements, many different compounds have been investigated for semiconductor sensitization, such as porphyrins [68 – 70], phthalocyanines [71 – 73]

transition metal complexes [74, 75], coumarin [62] and transition metal complexes have been the best so far.

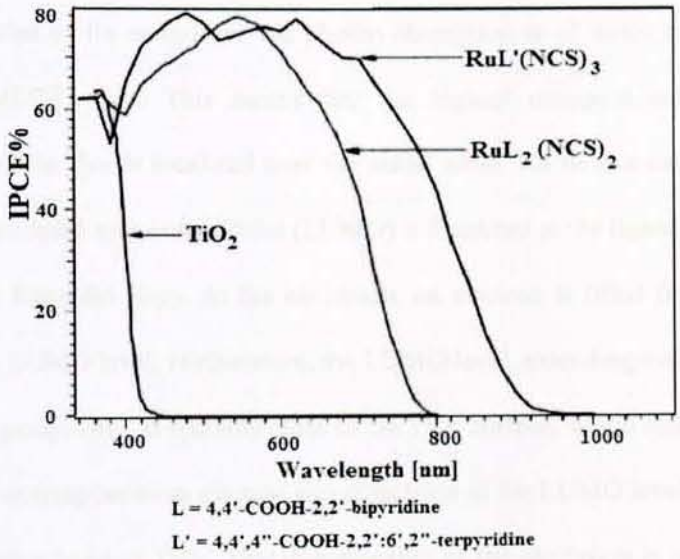

Figure 2. 10: Sensitization effect can be seen as the shift of IPCE curves to higher wavelengths when coated with dye as compared with that of naked TiO_2 [64].

Metal complex sensitizers usually have anchoring ligands (Figure 2.6). Anchoring ligands are responsible for the complex adsorption onto the semiconductor surface and are also chromophoric groups. Ancillary ligands are not directly attached onto the semiconductor surface and can be used for tuning the overall properties of the complexes [67].

The breakthrough in dye sensitization of semiconductor electrodes for solar cells was made by the use of metallo-organic ruthenium complexes along with nanostructured TiO_2 electrodes. The dyes having the general structure of $ML_2(X)_2$, where L stands for 2,2'-bipyridyl-4-4'-dicarboxylic acid, M for ruthenium or osmium and X for halide, cyanide, thiocynate, or water have been found promising [66, 76, 77]. Among

these N3 dye has shown superior performance and has been the top choice for dye sensitized solar cells.

The excitation of Ru complexes *via* photon absorption is of metal to ligand charge transfer (MLCT) type. This means that the highest occupied molecular orbital (HOMO) of the dye is localized near the metal atom, Ru in this case, whereas the lowest unoccupied molecular orbital (LUMO) is localized at the ligand species, in this case at the bipyridyl rings. At the excitation, an electron is lifted from the HOMO level to the LUMO level. Furthermore, the LUMO level, extending even to the COOH anchoring groups [66], is spatially close to the TiO_2 surface, which means that there is significant overlap between electron wavefunctions of the LUMO level of the dye and the conduction band of TiO_2. This directionality of the excitation is proposed as one of the reasons for the fast electron transfer process at the dye- TiO_2 interface [66].

2.4.4. Electrolytes for Dye Sensitized Solar Cells

It can be seen that DSSCs are a kind of complex system for light-to-electricity conversion. As a basic component, the electrolyte plays an important role in the process of light-to-electricity conversion in DSSCs. The electrolytes employed in DSSCs can be classified as liquid, solid state, or quasi solid state. Several aspects are essential for any electrolytes in a DSSC [78, 79].

1. The electrolyte must be able to transport the charge carrier between photoanode and counter electrode. After the dye injects electrons into the conduction band of TiO_2, the oxidized dye must be reduced to its ground state rapidly. Thus, the choice of the electrolyte should take into account the dye redox potential and regeneration of itself.

2. The electrolyte must be able to permit the fast diffusion of charge carriers (higher conductivity) and produce good interfacial contact with the porous nanocrystalline layer and the counter electrode. For liquid electrolytes, it is necessary to prevent the loss of the liquid electrolyte by leakage and/or evaporation of solvent.
3. The electrolyte must have long-term stability, including chemical, thermal, optical, electrochemical, and interfacial stability, which does not cause the desorption and degradation of the dye from the oxide surface.
4. The electrolyte should not exhibit a significant absorption in the range of visible light. For the electrolyte containing I_3^-/I^- redox couple, since I_3^- shows color and reduces the visible light absorption by the dye, and I_3^- ions can react with the injected electrons and increase the dark current. Thus, the concentration of I_3^-/I^- must be optimized.

Transport of the redox mediator between the electrodes is mainly driven by diffusion. Typical redox electrolytes have a high conductivity and ionic strength so that the influence of the electric field and transport by migration is negligible. In viscous electrolytes, such as ionic liquids, diffusion coefficients can be too low to maintain a sufficiently large flux of redox components, which can limit the photocurrent of the DSSC [80]. Transport of the redox mediator in the electrolyte gives rise to a diffusion impedance, which acts as a series resistance in the solar cell. The diffusion impedance depends on the diffusion coefficient and concentration of the redox mediator and on the distance between the electrodes [81]. Han et al. [82] optimized dye-sensitized solar cells with the help of impedance spectroscopy measurements and achieved a value for the diffusion resistance as low as 0.7 Ω cm^2 by minimizing the distance between the working and counter electrodes, while a separation of 20 μm led to

value of 2 Ω cm^2. In the case of the iodide/triiodide electrolyte, an alternative type of charge transport can occur when high mediator concentrations are used, the Grotthus mechanism [80]. In this case, charge transport corresponds to formation and cleavage of chemical bonds:

$$I_3^- + I^- \rightarrow I^- \cdots I_2 \cdots I^- \rightarrow I^- + I_3^- \qquad (2.8)$$

In viscous electrolytes, such as ionic liquid based electrolytes, this mechanism can contribute significantly to charge transport in the electrolyte [80].

The first DSSC was reported in 1991 by O'Reagan and M. Grätzel [33] using organic liquid electrolyte containing LiI/I_2, which obtained an overall light-to-electricity conversion efficiency of about 7.1% under irradiation of AM 1.5, 100 mW cm^{-2}. Later, many kinds of liquid electrolytes containing iodide/triiodide redox couple and high dielectric constant organic solvents such as acetonitrile (AcN), ethylene carbonate (EC), 3-methoxypropionitrile (MePN), propylene carbonate (PC), γ-butyrolactone (GBL), and N-methylpyrrolidone (NMP) were investigated, and some DSSCs with high photovoltaic performance were obtained [83 – 87]. Research during the past decade shows that each component of liquid electrolyte such as solvent, redox couple, and additive plays a different role in the photovoltaic performance of DSSCs.

A. Organic solvents

The organic solvent is a basic component in liquid electrolytes, it gives a environment for iodide/triiodide ions' dissolution and diffusion. The physical characteristics of organic solvent including donor number, dielectric constant, viscosity, etc. affect the photovoltaic performance of DSSCs. Especially, the donor number of solvent shows obvious influence on the open-circuit voltage (V_{OC}) and short-circuit current density (J_{SC}) of DSSCs. The donor–acceptor reaction between

non-aqueous solvents and iodide to generate triiodide in DSSCs was investigated, the results showed [62] that the extent of transformation from iodide to triiodide ions in a given solvent could be predicted according to the donor number of the solvent. Therefore, the V_{OC} increased and J_{SC} decreased with the increase of the donor number of solvent in liquid electrolytes in DSSCs [85].

The influence of the donor number of solvent on the V_{OC} is related to the following three factors:

1. The electron donor–acceptor reaction between organic solvent and triiodide [84]:

$$\text{solvents} + I_3^- \rightarrow \text{solvent}\cdots I_3^- \leftrightarrow \text{solvents}\cdots I_2 + I^- \qquad (2.9)$$

The above reaction equilibrium depends on the donor number of single or mixed solvent. The higher donor number of solvent leads to the incline of reaction equilibrium to the right [53, 56, 88, 89], which gives a lower concentration of triiodide and causes a decrease of dark reaction (Equation 2.5) and an increase of V_{OC} according to Equation 2.10.

$$V_{OC} = \left[\frac{kT}{e}\right] \ln\left\{\frac{I_{inj}}{n_{cb} k_{et} [I_3^-]}\right\} \qquad (2.10)$$

where k is the Boltzmann constant, T is absolute temperature, e is an electronic charge, I_{inj} is the flux of charge resulting from sensitized injection, n_{cb} is the concentration of electrons on the surface of TiO_2, k_{et} is the reaction rate constant of I_3^- dark reaction on TiO_2 (Equation 2.5), $[I_3^-]$ is the concentration of I_3^- in liquid electrolyte.

2. According to Grätzel's hypothesis [53], the reaction between the bare Lewis acidic TiO_2 surface and the Lewis basic solvent blocks the surface active site of TiO_2, electrode which is responsible for the dark reaction (Equation 2.5

The solvent with higher donor number has higher Lewis basicity, which shows a stronger function of blocking the active sites of TiO_2 electrode and decreasing the rate constant (k_{et}) of triiodide reduction. According to Equation 2.10, V_{OC} increases with decreasing of k_{et}.

3. The flatband potential (V_{fb}) of the TiO_2 electrode soaked in solvent was an important factor affecting V_{OC} [90], and the V_{fb} of TiO_2 electrode is sensitive to the contact solvent [44]. The contact solvent with higher donor number causes an increase in V_{fb} of the TiO_2 electrode [91]. Under Fermi level pinning, these two parameters are linked by the following equation:

$$V_{OC} = \left| V_{fb} - V_{red} \right| \tag{2.11}$$

where V_{red} is the standard reduction potential of a redox couple, it remains constant [92]. So the V_{OC} increases with the increase of the donor number of solvent. The decrease of J_{SC} is also related to the increasing of V_{fb} of TiO_2 electrode. The increase of V_{fb} also causes a negative shift in the conduction band edge of TiO_2, which decreases the energy bandgap between the conduction band of TiO_2 and LUMO of photoexcited dye, and causes a decrease of driving force for the excited dye to inject electron into the conduction band of TiO_2. So the J_{SC} decreases with the increase of the donor number of solvent.

B. Redox couples

Although iodide/triiodide has been demonstrated as the most efficient redox couple for regeneration of the oxidized dye, its severe corrosion for many sealing materials especially metals, causes a difficult assembling and sealing for a large-area DSSC and poor long-term stability of DSSC [93]. Therefore, other kinds of redox couples such as Br^-/Br_3^-, $SCN^-/(SCN)_3^-$, $SeCN^-/(SeCN)_3^-$, and bipyridine cobalt (III/II) complexes

were investigated for use in DSSCs. Owing to their energy unmatchable with sensitized dyes or their intrinsic low diffusion coefficients in electrolyte, these redox couples show lower DSSCs' light-to-electricity conversion efficiencies than the iodide/triiodide redox couple does [78, 94 – 98]. Cations in liquid electrolytes seem to function in the light-to-electricity conversion process of DSSCs. As a band bending and a depletion layer, which usually exist in bulk, semiconductor materials contacted with liquid electrolyte-containing redox couples [44] are considered unlikely in nanocrystalline TiO_2 electrodes owing to the extremely small size of the particle [55, 99]. In fact, cations, particularly small cations such as protons, Li^+, etc. play an important role in the photoelectrochemical performance of DSSCs. This is due to the fact that diffusion of electrons in the conduction band of TiO_2 is considered as an ambipolar diffusion mechanism, namely, ion diffusion is strongly correlated with electron transport to ensure that electroneutrality is obeyed throughout the TiO_2 network [100 – 104]. For example, the addition of LiI into liquid electrolyte can enhance the J_{SC} of DSSCs. The reason is that the small-radius of Li^+ can deeply penetrate into the mesoporous dye-coated nanocrystalline TiO_2 film and form an ambipolar Li^+-e^- with the electrons in the conduction band of TiO_2, which increases the transport speed of electrons in nanocrystalline TiO_2 network and enhances the J_{SC} of DSSCs [105 – 107]. However, the negative influence of ambipolar Li^+-e^- on DSSCs is its easy combination with triiodide, which leads to the decrease of V_{OC} of the DSSCs [105, 108]. In order to overcome this negative influence, an imidazole cation with larger ionic radii is used in liquid electrolyte to form a Helmholtz layer on the surface of TiO_2 film and block the direct contact of triiodide with ambipolar Li^+-e , which has an efficient result for suppressing the reaction between ambipolar Li^+-e and triiodide and enhancing the V_{OC} of the DSSC [106, 108].

C. Additives

Additive is another important component in liquid electrolytes for optimizing the photovoltaic performance of DSSCs. It is found that the photovoltaic performance of DSSCs can be enhanced hugely by adding a small amount of electric additive [53]. The influence of nitrogen-containing heterocyclic additives on the photovoltaic performance of DSSCs was investigated, and it was found [109 – 115] that some efficient additives such as 4-tert-butylpyridine, pyridine could enhance V_{OC} but decrease J_{SC} owing to the same aforementioned reasons about the donor number of solvent on the photovoltaic performance of DSSC. The difference is that the function of additive for optimizing the photovoltaic performance of DSSCs is more efficient than that of the donor number of solvent. On the other hand, it is only a small amount of additive added into the electrolyte, the excessive amount of additive, will cause a poor photovoltaic performance of DSSCs [87, 116].

D. Ionic liquids

Room-temperature ionic liquid (RTIL) has good chemical and thermal stability negligible vapor pressure, nonflammability, and high ionic conductivity [117, 118] When incorporated into DSSCs, RTIL can be both the source of iodide and the solvent itself [119]. N. Papageorgiou et al. [120] reported in 1996 that these unique properties of RTIL were effective for long-term operation of electrochemical device such as DSSCs. They employed methyl-hexyl-imidazolium iodide (MHImI) as a involatile electrolyte. The DSSC performance showed outstanding stability, with a estimated sensitizer redox turnover number in excess of 50 million. However, pure Il usually has higher viscosity than that of organic solvent, which limits th iodide/triioide transport speed and the restoration of oxidized dye, so the photovoltai

performance of these DSSCs is not so good as that of DSSCs using liquid electrolyte-containing organic solvents. In 2004, a solvent-free IL electrolyte-based $SeCN^-/(SeCN)_3^-$ redox couple was reported [121].

The viscosity of this IL, 1-ethyl-3-methylimidazolium selenocyanate (EMImSeCN), was determined to be 25 cP at 21^0C, and the specific conductivity of EMImSeCN was 14.1 mS/cm. Thus, an unprecedented 7.5 – 8.3% light-to-electricity conversion efficiency under AM 1.5 sunlight was achieved for DSSCs. The low viscosity, higher conductivity, and visible-light absorbency of this kind of IL electrolyte ensure the high photovoltaic performance of DSSCs. Liquid electrolyte-based organic solvent usually has high ionic conductivity and excellent interfacial contact property, which are the prerequisites for high photovoltaic performance of DSSCs. Although a photoelectric conversion efficiency of 11% for the DSSC-containing liquid electrolyte has been achieved [64, 65], the potential problems caused by liquid electrolytes, such as leakage and volatilization of organic solvents, are considered as some of the critical factors limiting the long-term performance and practical use of DSSCs. Although the electrolyte using low-viscosity IL achieves a high photovoltaic performance for DSSCs, the sealing and leaking problems by liquid the same as liquid electrolytes with organic solvents still exist for high long-term stability of DSSCs. Thus, solid state and quasi-solid-state electrolytes [83, 86, 122 – 124] with high long-term stability are attempted to replace liquid electrolytes.

2.4.5. Solid –State DSSCs

There are two kinds of solid-state DSSCs, one uses hole transport materials (HTMs) as medium, the other uses a solid-state electrolyte containing iodide/triiodide redox couple as medium.

A. Hole transport materials (HTMs) for Solid-State DSSC

Familiar large-bandgap HTMs such as SiC and GaN are not suitably used in DSSCs since the high-temperature deposition process for these materials will certainly degrade the sensitized dyes on the surface of nanocrystalline TiO_2 [79]. Researchers found [125 – 128] that a kind of inorganic HTM based on copper compounds such as CuI, CuBr, or CuSCN could be used in fabricating DSSCs. These copper-based materials can be cast from solution or vacuum deposition to form a complete hole-transporting layer, and CuI and CuSCN share good conductivity in excess of 10^{-2} S/cm, which facilitates their hole-conducting ability. For example, the DSSC based on CuI HTM obtained as high as 2.4% light-to-electricity conversion efficiency under irradiation of AM 1.5, 100 mW cm^{-2} [129]. However, its stability is quite poor, even worse than the traditional organic photovoltaic cell, which is also a common problem existing in DSSCs based on this kind of inorganic HTMs. Therefore, researchers put their vision into organic HTMs.

Compared with inorganic HTMs, organic HTMs possess the advantages of plentiful sources, easy preparation, and low cost. In 1998, an efficient solid-state DSSC based on organic HTM 2, 2', 7, 7'-tetrakis(N,N-di-p-methoxyphenyl-amine) 9, 9'-spirobifluorene (spiro-OMeTAD) was reported [130], although the overall light-to-electricity conversion efficiency of this DSSC only reached 0.74% under irradiation of 9.4 mW cm^{-2}, it is a pioneer for fabricating DSSCs with organic HTMs. Later, by improving the dye adsorption in the presence of silver ions in the dye solution [85, 86], the efficiency of the solid-state DSSC employing spiro-OMeTAD was enhanced to 3.2%. For DSSCs based on typical inorganic or organic HTMs, the overall light-to-electricity conversion efficiencies are all much lower than that of the DSSCs based on liquid electrolytes. This is due to the low intrinsic conductivities of HTMs, the high

frequencies of charge recombination from TiO_2 to HTMs, and the poor electronic contact between dye molecules and HTMs caused by incomplete penetration of solid HTMs into the pores of the mesoporous TiO_2 electrodes.

B. Solid-State Polymer Electrolyte with Redox Couple for Solid-state DSSC

Organic or inorganic HTM as a transport material for DSSCs cannot satisfy the practical application due to their low power conversion efficiencies. On the other hand, some remarkable results have already been achieved by introducing iodide/triioide redox couple into solid-state electrolytes as a transport medium for DSSCs. For example, a solid-state electrolyte containing iodide/triiodide redox couple by introducing TiO_2 nanoparticle into poly(ethylene oxide) (PEO) was prepared, the overall light-to-electricity conversion efficiency of 4.2% for the DSSC with this solid-state electrolyte was obtained under irradiation of AM 1.5, 100 mW cm^{-2} [131]. A kind of ambient-temperature plastic crystal electrolyte containing iodide/triiodide redox couple was used to fabricate DSSCs and achieved a high overall light- to-electricity conversion efficiency of 6.5% under irradiation of AM 1.5, 100 mWcm^{-2} [132]. A solid-state electrolyte based on $LiIC_6H_{10}N_2O_2$ [LiI(HPN)$_2$] single crystal and iodide/triiodide was prepared. This solid-state electrolyte can be optimized by adding SiO_2 nanoparticles and put into DSSCs to enhance light-to-electricity conversion efficiency [133].

Higher photovoltaic performance for DSSCs using iodide/triiodide redox couple than using HTMs is due to the fact that the iodide/triiodide can efficiently regenerate oxidized dyes, and the dark reactions in these solid-state electrolytes are lower than in HTMs. Another reason is that the interfacial contact properties of these solid-state

electrolytes are better than that of HTMs. This kind of solid-state electrolyte has a good prospect in practical DSSCs.

2.4.6. Quasi-Solid-State Electrolytes with Redox Couple for Quasi-Solid-state DSSC

The quasi-solid-state, or gel state, is a particular state of matter, neither liquid nor solid, or conversely both liquid and solid. Generally, a quasi-solid-state electrolyte is defined as a system which consists of a polymer network (polymer host) swollen with liquid electrolytes [58, 83, 134 – 137]. Owing to its unique hybrid network structure, quasi-solid-state electrolytes always possess, simultaneously, both the cohesive property of a solid and the diffusive transport property of a liquid. Namely, quasi-solid-state electrolytes show better long-term stability than liquid electrolytes do and have the merits of liquid electrolytes including high ionic conductivity and excellent interfacial contact property [78, 134, 135]. These unique characteristics of quasi-solid-state electrolytes have been actively developed as highly conductive electrolyte materials for DSSCs, lithium secondary batteries, and fuel cells [136]. Quasi-solid-state electrolytes are usually prepared by incorporating a large amount of a liquid electrolyte into organic monomer or polymer matrix, forming a stable gel with a network structure *via* a physical or chemical method. The quasi-solid-state electrolyte formed *via* physical cross-linking is called "entanglement network", which is thermo reversible (thermoplastic). By contrast, chemical or covalent crosslinking leads to the formation of thermo-irreversible (thermosetting) gel electrolyte [78].

A. Thermoplastic gel electrolytes (TPGEs)

The formation of the TPGE is based on physical cross-linking of gelators to form "entanglement network" to solidify liquid electrolyte. The main characteristic of thi

kind of gel electrolyte is the gel-sol state reversible conversion with the change of temperature, which is a benefit of deep penetration of the electrolyte into mesoporous dye-coated nanocrystalline TiO_2 film [78, 79, 137]. The interfacial contact between the electrolyte layer and nanocrystalline TiO_2 film or counter electrode is one of the most important factors influencing the photovoltaic performance of DSSCs besides the ionic conductivity of the gel electrolyte [58]. The TPGE contains gelator and liquid electrolyte, the liquid electrolyte consists of organic solvent, redox couple, additive, or IL electrolyte system. Y. Reng et al. [138] reported the first thermoplastic polymer gel electrolyte used in DSSCs. The electrolyte was composed of poly(acrylonitrile) (PAcN), EC, PC, AcN, and NaI. The light-to-electricity conversion efficiency of this DSSC was lower in comparison with that of the DSSC based on liquid electrolytes, due to the unoptimized components and the difficult penetration of the PAcN network into nanocrystalline TiO_2 film [59, 139]. The high photovoltaic performance and excellent stability of DSSC was obtained by using a TPGE containing poly(vinylidenefluoride-co-hexafluoropropylene) (PVDF–HFP) combined with MePN-based liquid electrolyte containing 1,2-dimethyl-3-propyl imidazolium iodide and iodine [83]. The DSSC showed a similar photovoltaic performance as that of an analogous cell containing the same liquid electrolyte, which means that the polymer matrix has no negative effect on the performance of DSSC.

B. Thermosetting gel electrolytes (TSGEs)

The TPGE is good for fabricating DSSCs. However, there is also a potential venture for actual application of DSSCs, which is the chemical unstability, such as phase separation, crystallization of iodide salts. Therefore, some more environmentally stable electrolytes are still needed. Among those optional methods, the TSGE is one of the good selections for high photovoltaic performance and good long-term stability

of DSSCs. A high stable DSSC based on a TSGE containing ureasil precursors and organic liquid electrolyte containing iodide salts was prepared [123, 140 – 142]. The unique structure of this thermosetting organic–inorganic hybrid gel electrolyte leads to the high quality of DSSC, which maintains 5 – 6% light-to-electricity conversion efficiency even after preserving for several years.

Wu et al. [124, 143 – 145] reported a novel TSGE based on poly(acrylic acid)-poly(ethylene glycol) (PAA–PEG) hybrid and liquid electrolyte for fabricating a high-performance and stable DSSC. It is known that PAA polymer matrix shows excellent hydrogel stability due to the formation of 3D networks structure in hydrogel and the strong interaction between absorbed aqueous solution and hydrophilic groups in PAA [146, 147]. PAA is a kind of oleophobic polymer, which cannot dissolve or swell in organic solvents. By modifying PAA with amphiphilic PEG, the PAA–PEG hybrid shows moderate liquid electrolyte absorbency in some organic Lewis basic liquid electrolytes. The optimized Lewis basic organic mixed solvents for both PAA–PEG hybrid and photovoltaic performance of DSSC was obtained by mixing 30% (v/v) NMP with 70% (v/v) GBL [87]. The TSGE with ionic conductivity of 6.12 mS cm^{-1} was obtained by swelling the PAA–PEG hybrid in the optimized Lewis basic organic mixed solvents containing iodide/triiodide redox couple. Based on the TSGE, a DSSC with light-to-electricity conversion efficiency of 6.10% was attained under AM 1.5 irradiation.

2.4.7. Materials and manufacturing methods for DSSC

A. Substrates

Requirements for a good DSSC substrate are low sheet resistance which should also be independent of temperature up to 450 – 500^{0}C (in case when the electrode post-treatment requires sintering), high transparency, and ability to prevent impurities such as water and oxygen from entering into the cell. The traditional approach is to build the DSSC on transparent conducting oxide (TCO) coated glass sheets. The most often used TCOs are fluorine-doped and indium-doped tin oxides, whose sheet resistances are around 10 Ω/cm^2. Whilst glass is obviously an effective barrier towards water and oxygen penetration into the cell, its disadvantages are fragility, rigidity, heavy weight, and high price. ITO's sheet resistance also increases with temperature so ITO-coated glass is not the best option for cells where high temperature treatments are needed.

Alternative substrate materials such as plastic foils and metal sheets overcome most of the glass' problems. Conductive plastics, like ITO-PET (indium-doped tin oxide coated polyethyleneterphtalate) and ITO-PEN (indium-doped tin oxide coated polyethylenenaphtalate), are light weight and flexible, whereas metals are also mechanically robust, cheap, and their electrical conductivity is superior compared to all other substrate materials. The last factor plays a crucial role in cell size upscaling, since the main part of the total ohmic losses in the cell are due to lateral resistance on the substrate surface. It has also been noticed that substrate-mediated recombination is lower from stainless steel than from glass [148]. Disadvantages of plastics include low temperature tolerance, max. 150 – 160^{0}C, for ITO-PET high sheet resistance, around 60 Ω/cm^2, and uncertainties considering the oxygen and water penetration. For metals, the main problem is the traditionally used, iodine-containing electrolyte.

Triiodide ions are corrosive, and thus far only stainless steel and titanium have shown enough chemical stability in the iodine electrolyte to be successfully employed as DSSC substrates [96, 148 – 155]. Long-term stability of metal-based cells is still unknown, though, and requires further studies before this DSSC type can be transferred to large scale manufacturing. However, the main drive behind the alternative substrate research is the flexibility of both the plastic and metal substrates which enables roll-to-roll type manufacturing of the DSSC, potentially leading to high volume production of low cost solar cells with wide variety of applications.

B. Photoelectrode

The semiconductor material that forms the core of the photoelectrode should be chemically stable and inert towards the electrolyte species, it should have a lattice structure suitable for dye bonding, its conduction band should be located slightly below the LUMO level of the dye in order to facilitate efficient electron injection, and it should be available in nanostructured form to enable high enough dye loading. Titanium dioxide fulfills these requirements – in addition to that, it is also cheap and easily available because of mass production. The material is in wide use for example in pigments and paints and, due to its non-toxicity, even in cosmetic, hygiene and food products. Another semiconductor oxide that has been employed in the DSSC is zinc oxide but there have been problems for example with the dye desorption [156] which is why TiO_2 is still the most widely used DSSC photoelectrode material.

TiO_2 exists in three crystalline forms, anatase, rutile, and brookite, of which the anatase structure is the most suitable for DSSC applications. The typical TiO_2 nanoparticle size in the photoelectrode film is 10 – 30 nm, though larger particles up to 300 – 400 nm are sometimes added to the film to increase the path length of the

absorbed photons by scattering (improved light harvesting efficiency). The optimal photoelectrode film thickness is 10 – 15 μm – if the film is very thin the dye loading remains too low whereas with too thick films, the distance the excited electrons generated on the electrolyte side of the photoelectrode film have to travel before reaching the current collector becomes so long that increased recombination probability starts to decrease the cell efficiency.

Screen-printing is a typical TiO_2 layer deposition method, with which large quantities of even quality films can be prepared with high speed (on laboratory scale, technique called "doctor-blading" depicted in Figure 2.11, in which the TiO_2 precursor is applied through a hand-cut tape mask is often employed). Several research groups prepare their own TiO_2 precursor materials but there exists also commercial titania pastes specifically designed for screen-printing technique – in addition to the TiO_2 nanoparticles they contain some high viscosity organic solvent, binders, pH-adjusting agents, and morphology controlling agents. After the film deposition the solvent and other organic ingredients have to be removed, which is done by sintering the film in 450 – 500^{0}C for half an hour minimum. In this treatment the individual TiO_2 nanoparticles also "neck" together and adhere more tightly to the substrate surface which decreases the interparticle resistance, thus facilitating efficient electron diffusion in the film, and the resistance for the electron transfer from the TiO_2 network to the substrate. Unfortunately, this sintering treatment, which drastically improves the TiO_2 film quality and also its mechanical stability, cannot be employed with plastic substrates, due to their low temperature tolerance. One promising technique for low temperature photoelectrode film preparation is spraying suspension of TiO_2 nanoparticles in high volatility solvent (e.g. ethanol) on heated substrate and then mechanically compressing the resulting powder layer. Titania pastes suitable for

low temperature sintering have also been developed but the problem of inadequate interparticle necking and thus lower cell efficiency, due to slower electron transport in the film and thus higher recombination probability, still remains with these materials too.

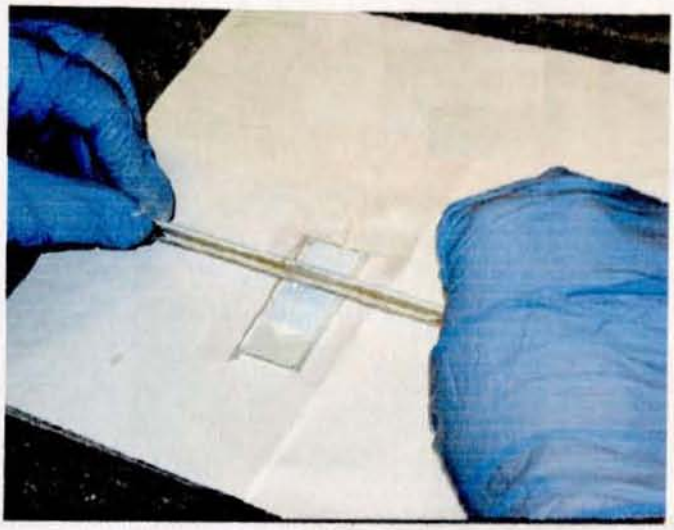

Figure 2. 11: The application process of the TiO_2 to the surface of the conductive glass plate.

Dye sensitization of the photoelectrode is done simply by soaking the TiO_2 film in the dye solution as shown in Figure 2.12 (anhydrous ethanol being the common solvent, though various nitriles have also been used), the soaking time typically being overnight minimum, though the process can be speed up by heating the solution. The dye is one of the most expensive components of the cell, due to the complex structure and demanding, multistep synthesis of the molecule, but since its amount in the solution is very small, typically of the order 10^{-4} M, its effect on the overall manufacturing costs of the cell remains reasonably low. In addition to the ruthenium organometallic complexes mentioned already in Section 2.4, other dyes such as coumarins, eosins, perylenes, and even natural dyes extracted from berries have been employed in the DSSC, though the highest efficiencies have still been obtained with

the Ru-complexes. As a matter of fact, the molecular structure of the dyes and the electron transfer processes in the dye excitation resemble those of the chlorophyll molecule in green plants, which is why the DSSC operating principle has sometimes been called "artificial photosynthesis".

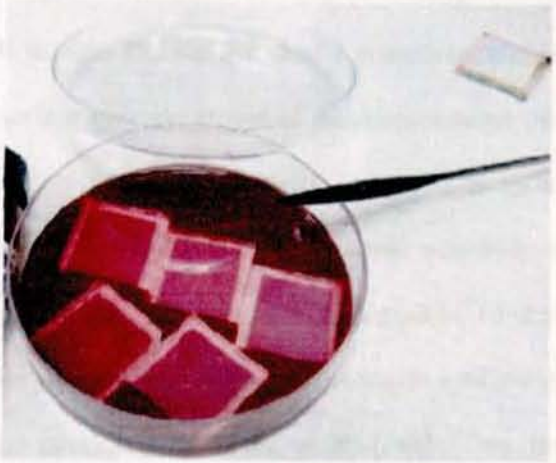

Figure 2. 12: Sintered TiO_2 photoanodes being soaked in dye solution after cooling.

Generally, the molecular adsorption modes on the host surface can be summarized in six different modes:

a) covalent attachment brought about by directly linking groups of interest or *via* linking agents,

b) electrostatic interactions, brought about *via* ion exchange, ion-pairing, or donor-acceptor interactions,

c) hydrogen bonding,

d) hydrophobic interacting-derivatives,

e) van der Waals forces involved in physisorption of molecules on solid surfaces, and

f) physical entrapment inside the pores or cavities of hosts such as cyclodextrins, micelles, etc [157].

The adsorption modes of dyes on semiconductor surfaces are very important for the DSSC efficiency [158]. To construct workable and efficient DSSCs, the dye must be adsorbed on the surface of the semiconductor intimately. Therefore, the first kind provides an approved strategy to accomplish a strong interlinkage between the dye and the semiconductor. It requires that the dye should possess an anchoring group, which should react with surface hydroxyl groups of the semiconductor oxide to form chemical bonds. The standard anchoring group for sensitizers is carboxylic acid (-COOH). Its derivatives, such as ester, acid chloride, acetic anhydride, carboxylate salt, or amide, have also been used. Furthermore, sulfonate ($-SO_3^-$) and silane (SiX_3 or $Si(OX)_3$) have also been adopted [159]. Efficient sensitizers with phosphonic acid binding groups were first developed by Pechy et al. [160]. They found that a ruthenium complex with a single phosphonic acid bound about 80 times stronger to TiO_2 than N3 (which has four carboxylic acid groups) and did not desorb from TiO_2 in the presence of water, in contrast to N3.

Nevertheless, most of the photosensitizers employ the carboxylic acid as anchoring group due to its relative stability and easy synthesis. However, there are different binding modes between the oxide surface and the carboxylic acid (Figure 2.13) [161]. In general, the carboxylic acid group can coordinate to the TiO_2 surface in three ways [162, 163]: unidentate mode, chelating mode, and bridging bidentate mode.

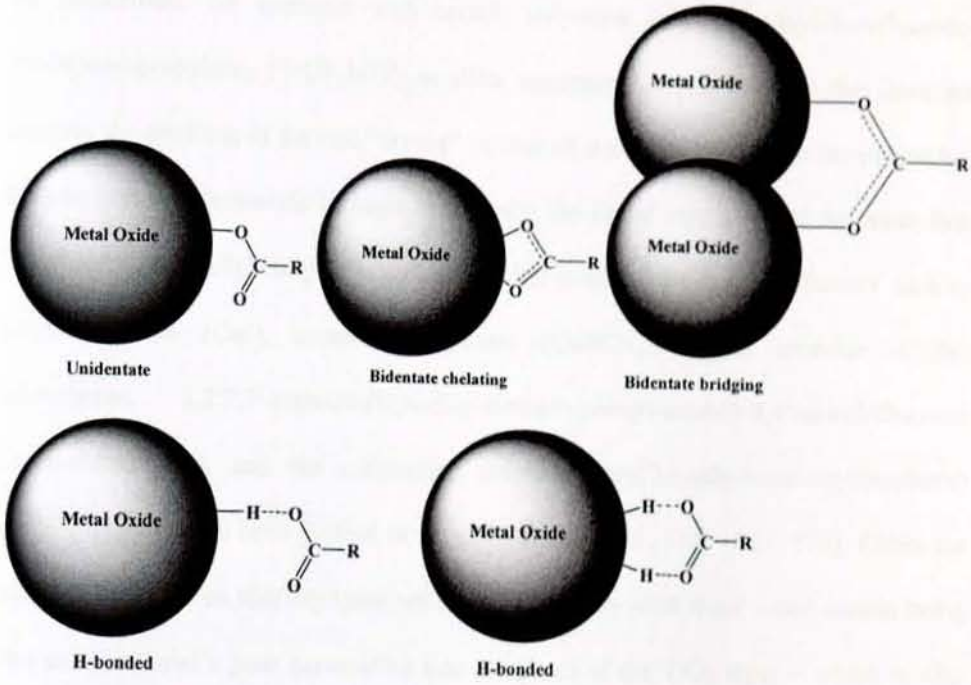

Figure 2. 13: Binding modes for caboxylate unit on TiO_2 surface.

C. Electrolyte

In addition to the redox couple – like the most commonly used iodide/triiodide– the electrolyte usually contains some "blocking agent" that adsorbs on the photoelectrode on those surface sites not occupied by the dye to prevent recombination, i.e. electron leakage from the TiO_2 back to the electrolyte. As it is mentioned earlier additives like 4-*tert*-butylpyridine, guanidinium thiocyanate and 4-guanidinobutyric acid are some molecules used in this purpose [65, 164]. Due to suppressed recombination, the cell open circuit voltage increases. The requirements for the electrolyte solvent are its ability to dissolve the other ingredients and preferably low volatility combined with high viscosity to facilitate fast ionic diffusion between the electrodes. Typical solvents used in the DSSC electrolyte are various nitriles (aceto-, methoxypropio-, valero-, butyro-), carbonates (ethyl-, propyl-), and their mixtures. Liquid electrolyte can also

be gelatinized, for example with certain polymers (e.g. polyvinylidenefluoride-hexafluoropropylene, PVDF-HFP) or silica nanoparticles [165]. While this does not remove the problem of the cell "drying" in case of structural damage to the substrates, it does prevent electrolyte leakage. Obviously, the liquid electrolyte is the weak link considering the cells' long-term stability which is why solid hole conductors such as copper iodide (CuI), copper thiocyanate (CuSCN), copper bromide (CuBr) complexes, 2,2′7,7′-tetrakis-(N,N-di-p-methoxyphenyl-amine)-9,9′-spirobifluorene (spiro-MeOTAD), and the conducting polymer poly(3,4-ethylenedioxythiophene) (PEDOT) have also been studied as its replacement [131, 133, 166 – 174]. Either the cell efficiency or its stability have not been satisfactory with these – one reason being the solid material's poor penetration into the pores of the TiO_2 layer – which is why iodine-based liquid electrolyte is still the most often used alternative in the DSSC. An example of a typical electrolyte composition is 0.5 M lithium iodide (LiI), 0.05 M iodine (I_2), and 0.5 M 4-*tert*-butylpyridine in 3-methoxypropionitrile (triiodide ions are generated in a reaction of molecular iodine with the iodide ions). The amount of iodine may vary according to the electrolyte layer thickness – in cases where the light enters the cell from the counter electrode (CE) side, through the CE and electrolyte (e.g. if the photoelectrode is deposited on opaque metal sheet), the shadowing effect of the dark red triiodide ions in the electrolyte reduces the amount of photons reaching the photoelectrode (iodide ions, on the other hand, are transparent). When the order of the maximum current the cell should be able to generate is known, the triiodide concentration and electrolyte layer thickness can be minimized using the definition for the diffusion-limited current density [175].

$$i_{\text{lim}} = \frac{2nFD_{I_3^-}c_{I_3^-}}{l} \qquad (2.12)$$

where n is the number of electrons transferred in the redox reaction, F the Faraday constant, $D_{I_3^-}$ the triiodide diffusion coefficient, $c_{I_3^-}$ the triiodide concentration, and l the distance between the electrodes.

There is also an interesting, new group of DSSC electrolytes in which so-called ionic liquids, or room temperature molten salts are utilized [176 – 178]. Ionic liquids are fluids with no vapor pressure at all which eliminates the problem of electrolyte drying in case of fractures on the substrate. Typically, ionic liquids are salts of iodine with a large, often imidazole-based cation, for example 1-methyl-3-propylimidazolium iodide (PMImI) or 1, 2-dimethylimidazolium iodide (DMImI). Thus, ionic liquid works as a source of iodide ions and also as a solvent, due to its fluidic nature. The problem of these electrolytes is, however, the high viscosity of many ionic liquids, which slows down the ionic diffusion and tends to keep cell efficiencies down. Some ionic liquids are also hygroscopic which means that special conditions e.g. dry air or nitrogen atmosphere is needed for cell preparation and storage of materials.

D. Counter electrode catalysts

After considering the characteristics of the porous semiconductor oxide, the sensitizer dye and the electrolyte containing the charge mediator, which allows dye regeneration, another essential material for an operative DSSC is the counter-electrode, where the regeneration of the charge mediator takes place. The first requirement for a material to be used as counter-electrode in a DSSC is a low charge transfer resistance and high exchange current densities for the reduction of the oxidized form of the charge mediator. Also, such materials must present chemical and electrochemical stability in the electrolyte medium used in the cell [179]. For

sufficiently fast reaction kinetics for the triiodide reduction reaction at the TCO coated cathode, a catalyst coating is needed.

As already discussed, the best charge mediator for most of the DSSC is the I^-/I_3^- redox couple. Unfortunately however, the iodine (and triiodide) reduction reaction is not reversible in several materials and its kinetics is solvent dependent. For instance, at the surface of transparent glass-ITO or glass-FTO electrodes, the electron-transfer kinetics for reduction of triiodide to iodide is very slow [179].

i. Platinum

The best material that acts as a catalyst and provides high exchange current for this reaction is platinum, particularly as thin films deposited by thermal oxidation of hexachloroplatinate. Pt thin films obtained by sputtering also exhibited good performance as counter electrodes in DSSC, but are more expensive [179]. As a traditional and usually most efficient catalyst, platinum has been used almost exclusively in the literature. However, the performance of the catalyst layer depends on the method by which the Pt is deposited onto the TCO surface. Platinum catalyst coating has been performed for example electrochemically [180, 181], by sputtering [91], pyrolytically or by spin coating [182]. Electrochemically [179] and vapor deposited [183] Pt has been however found unstable in the presence of the iodide electrolyte.

Papageorgiou et al. [179] developed an alternative Pt catalyst coating method called "platinum thermal cluster catalyst". This catalyst provided superior kinetic performance with respect to conventional platinum deposition methods, chemical and electrochemical stability in practical cells, low platinum loading of 5 – 10 mg/cm^2

leading to cost reduction, mechanical stability of the counter-electrode surface and optical transparency of the counter-electrode due to the low platinum content [179].

For DSSCs deposited on glass, thermally deposited or sputtered platinum is the most widely used CE catalyst. The advantages of Pt are its high catalytic activity towards the iodide/triiodide redox reaction which is why only a few nanometer layer of Pt is required – this keeps the cell manufacturing costs low even if Pt is an expensive element, and because the thin Pt layer is almost transparent, platinized counter electrodes can be employed also in cells which require reverse lighting (i.e. lighting from the CE side). Platinum is also chemically stable in the electrolyte, i.e. no remarkable dissolution over time from the CE have been noticed (in case the CE catalyst dissolves and diffuses to the PE, it may act there as recombination centers, thus decreasing the cell efficiency). The usual procedure to prepare the counter-electrode for DSSC consists in spreading a small quantity of a 5 mmol L^{-1} hexachloroplatinic acid solution in isopropanol on the conductive surface of a glass-FTO electrode and heating the coated electrode at 385^0C for 10 minutes. The electrodes prepared by such a procedure remain almost transparent, which can be very useful, since the cell can be irradiated from both sides. Moreover, they present low charge-transfer resistance and high kinetic performance for the I_3^- reduction reaction. This ensures high exchange current densities at the CE, and thus the processes at the CE do not become rate limiting for the processes in solar energy conversion [179]. This results in reduction of metallic platinum as tightly adhered nanoscale clusters on the substrate surface [179]. Due to high temperature involved, this method is naturally not suitable for plastic substrates but sputtering, which is a well known and widely applied method for thin film coatings, can be employed for low temperature tolerance substrates as well.

ii. Carbon

While having excellent catalytic action, platinum has the disadvantage of being very expensive. Kay and Grätzel [184] have developed a cell design, which is very interesting with this respect. The design utilizes a porous carbon counter-electrode as a catalyst layer. This carbon electrode is made from a mixture of carbon black, graphite powder and nanocrystalline TiO_2 particles. A high conductivity (sheet resistance of 5 Ω/cm^2 for a 50 mm thick layer) is obtained due to the carbon black particles connecting together separate graphite flakes, while the TiO_2 particles are used as a binder to the structure. It is claimed that thanks to the very high surface area of these electrodes, caused by the carbon black, these electrodes are as active for triiodide reduction as the conventional Pt electrodes [184].

iii. Conducting polymers

Since platinum is an expensive catalyst, even if the consumption is relatively low, conducting polymers such as poly(3,4-ethylenedioxythiophene) (PEDOT) or polyaniline (PANI) have been studied as its replacement [185]. The main problem with these materials is that often rather thick layers of them are needed in order to reach high enough catalytic activity. This slows down the cell manufacturing process and, as thick catalyst layers also absorb light, these kind of CEs are not suitable for reverse lighting cells.

L. Bay et al. [186] investigated catalytic activity for platinum, PEDOT, polypyrrole (PPy), and PANI-all deposited onto fluorine-doped tin oxide (FTO) glass. Both Pt and PEDOT are found to have sufficiently high catalytic activities for practical use as counter electrodes in DSSC. PEDOT is therefore a good candidate for substituting the expensive platinum. It was also mentioned previously Shibata et al. [187] reported

that the photocurrent for the DSSCs with a PEDOT-PSS electrode was higher than that with a Pt counter electrode when the cells were filled with a gel electrolyte. The charge transfer resistance between the gel film and Pt was 14.1 Ω/cm^2 and that between gel film and PEDOT-PSS decreased to 1.5 Ω/cm^2, which was the reason for the improvement of the photocurrent.

iv. Cobalt Sulfide

Very recently, electrodeposited CoS has been identified as a suitable catalyst for the iodide/triiodide redox couple [188]. Deposited on a flexible substrate polyethylene naphthalate (ITO/PEN) it outperforms Pt on the same substrate, with a charge transfer resistance down to 1.8 Ω/cm^2, while thermal Pt on FTO gave 1.3 Ω/cm^2 using the same ionic liquid electrolyte.

2.4.8. Measurement Process and Characteristic Solar Cell Data

The basis for the characterization of solar cell is the I-V curve (current-voltage curve). The I-V curve of a solar cell can be measured by using a solar simulator or other light sources which provide in combination with filters light according to the international norms. During illumination of the solar cells at 25^0C a voltage is applied and the current is measured, resulting in the I–V curve of that cell which is presented schematically in Figure 2.14.

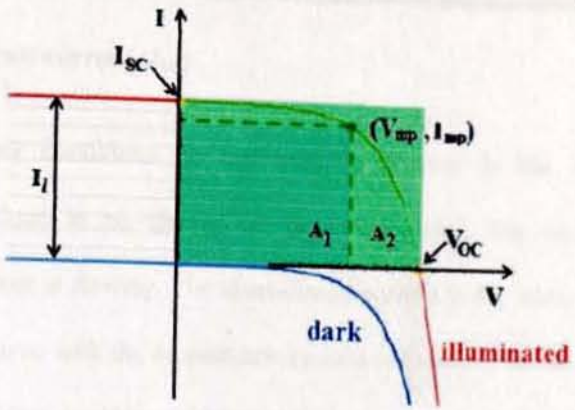

Figure 2. 14: Typical shape of an I-V curve with important values for efficiency determination.

With the help of the I–V curve it is possible to determine important electronic parameters like the open-circuit voltage (V_{OC}), the short circuit current (I_{SC}), and the fill factor (FF).

A. Open-circuit voltage (V_{OC})

Under open-circuit conditions the flow of charges through the illuminated device is interrupted. At these conditions all charge carriers recombine within the photoactive layer. The open-circuit voltage is the intercept point of the illuminated I–V curve with the voltage-axis (x-axis in Figure 2.14) and represents the maximum voltage that the measured solar cell can provide under ideal conditions. The V_{OC} in organic solar cells is predominantly determined by the materials and their frontier orbitals used in the solar cell. However, also other factors connected to the processes in the cell can influence the open-circuit voltage. The V_{OC} can be for example lower due to charge recombination, which cannot be avoided [189].

B. Short-circuit current (I_{SC})

Under short-circuit conditions no resistance is present in the electric circuit. Consequentially there is no change in the voltage and thus no work is done eventhough a current is flowing. The short-circuit current is the intercept point of the illuminated I–V curve with the current-axis (y-axis in Figure 2.14) and represents the maximum current that could be withdrawn from the solar cell if the cell was ideal. Another important value strongly associated with the short-circuit current is the short-circuit current density (J_{SC}). This value reports the short-circuit current per area (Equation 2.13).

$$J_{SC} = \frac{I_{SC}}{A} \tag{2.13}$$

The short-circuit current is directly proportional to the incident photons that can be used by the solar cell as long as no saturation effects occur. I_{SC} is therefore dependent on the surface area of the solar cell, the light intensity, the device thickness, and the absorption range. Also, the charge carrier mobility which depends on the temperature due to a thermally active hopping transport plays an important role [190, 191].

C. Fill Factor (FF)

The fill factor is a measure of the quality of the solar cell and describes the relation between the photogenerated charge carriers and the charge carriers that reach the electrodes. In an ideal solar cell all generated charge carriers reach the electrodes and the FF is 1. Due to charge recombination and resistances within the device not all generated charge carriers reach the electrodes. There are two types of resistance in the solar cell. The serial resistance, R_S, represents the sum of all layer-, contact-, and

current-resistances and is the reciprocal slope of the tangent to the I–V curve under open-circuit conditions (Equation 2.14).

$$R_S = \left(\frac{dV}{dI}\right)_{I=0} \tag{2.14}$$

The shunt (parallel) resistance, R_{SH}, represents the surface recombination losses, which occur at the different interfaces and leakage currents. R_{SH} is the reciprocal slope of the tangent to the I–V curve under short-circuit conditions (Equation 2.15).

$$R_{SH} = \left(\frac{dV}{dI}\right)_{V=0} \tag{2.15}$$

In an ideal solar cell R_S should be minimized ($R_S \rightarrow 0$) and R_{SH} would be maximized ($R_{SH} \rightarrow \infty$). In this case the I–V curve would be rectangular and go along the light-green area in Figure 2.14. In a real solar cell losses cannot be avoided and the I–V curve is bended. The point on the I–V curve where the maximum power of the solar cell can be produced is called maximum power point (mp-point). The mp-point is located on the I–V curve exactly where the product of I and V reaches its maximal value. The area A_1 in Figure 2.14 (dark green color) indicates this maximal power value. The maximum power of an ideal solar cell is represented by area A_2 (light-green). The FF is the relation between those two areas (Equation 2.16).

$$FF = \frac{A_1}{A_2} \tag{2.16}$$

The voltage at the maximum power point is V_{mp} and the current density J_{mp}. The FF can be calculated using these values according to Equation 2.17.

$$FF = \frac{V_{mp} J_{mp}}{V_{OC} J_{SC}} \tag{2.17}$$

D. Solar Cell Efficiency (η)

All the values mentioned above contribute to the overall power conversion efficiency that describes the relation between the electric power that the device produces (P_{out}) and the power of the incident light (P_{in}). The efficiency can be calculated according to Equation 2.18:

$$\eta = \frac{P_{out}}{I_{in}} = \frac{V_{mp} J_{mp}}{I_{in}} = \frac{V_{OC} J_{SC} FF}{I_{in}} \qquad (2.18)$$

E. Incident Photon to Current Efficiency (IPCE)

The incident photon to current conversion efficiency (IPCE) or external quantum efficiency (EQE) describes the relation between the number of the dissipated charges and the number of the incident photons at a certain wavelength (Equation 2.19).

$$\text{IPCE\%} = \frac{1240\ [\text{eVnm}] \times J_{SC}\ [\text{mAcm}^{-2}]}{\lambda\ [\text{nm}]\ I_{in}\ [\text{mAcm}^{-2}]} \times 100 \qquad (2.19)$$

where J_{SC} is the short-circuit photocurrent density for monochromatic irradiation, and λ and I_{in} are the wavelength and the intensity, respectively, of the monochromatic light. If IPCE is 1, every absorbed photon injects an electron into the circuit. IPCE is a measure for the absorption quality of the solar cell at a certain wavelength combined with its charge transport quality. If, e.g., the cell absorbs all incident photons at a certain wavelength but the charges cannot travel to the electrodes due to recombination, the IPCE nevertheless will be zero. Hence, the IPCE correlates often to the absorption spectrum of the active layer but a strong deviation cannot be excluded.

2.5. Natural Dyes as Sensitizer for Photoelectrochemical Cells

2.5.1. Anthocyanins and Anthocyanidins

Flavonoids are sugar bound polyphenols found in all land plants. A class of flavonoids called anthocyanins is responsible for the red and purple coloration of many fruits and flowers. An ample range of colors in the red blue range are available to anthocyanins as a result of their complexation with other polyphenols, pectins, and metal ions [192]. Proposed biological roles of anthocyanins include insect attraction, photoprotection [192], antioxidant activity [193], and photosynthesis enhancement, but the full scope of their abilities has yet to be fully understood.

The various coloured pigments that can easily be extracted from fruits, flowers, and so on, can be employed in DSSCs. Unlike artificial dyes, the natural ones are available, easy to prepare, low in cost, non toxic, environmentally friendly, and fully biodegradable. In most case, their photoactivity belongs to the anthocyanins family. Moreover their absorption spectra have favourable overlap with the solar spectrum. Hara et al. [194] made a remarkable advance in the use of organic dyes for DSSCs. Other groups have obtained good solar electric power conversion efficiencies, testing natural dyes as cheap and environmentally friendly alternatives to artificial sensitizers for DSSCs [195]. The natural dyes that have been employed for this purpose were extracted from red oranges, eggplants, red radicchio, sicilian red wines, blueberry, and mulberry are rich in anthocyanins. The general molecular structure of anthocyanins is shown in Figure 2.15. Red orange juice contains a high concentration of cyanidin-3-glucoside pigment, of citric acid and other antioxidants, such as delphinidin-3-glucoside, flavones (hesperedin and narirutin). The extract from eggplant peels contains nasunin, a mixture of cis-trans isomers of delphinidin-3-(p-

coumaroylrutinoside)-5-glucoside. Delphinidine is the main pigment of the red radicchio too, while, in the extracts of the red wines, the most responsible pigment for their red-violet colour is the malvidine. The main drawback of this component is the presence of OCH_3 groups (in the position of R_1 and R_2 in Figure 2.15) on the phenolic ring. For this reason the phenolic groups is not able to chelate the titanium and most of the sensitization occurs from delphinidine which is the lowest components of these natural compounds in red wines.

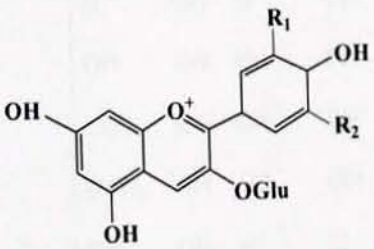

Figure 2. 15: Chemical structures of anthocyanines. R_1 = OH, R_2 = H (Cyanidin-3-glucoside), $R_1 = R_2$ = OH (Delphinidin-3-glucoside), $R_1 = R_2 = OCH_3$ (Malvidin-3-glucoside).

The presence of other additives in the extracted dyes, such as citric acid, which act as co-adsorbers, is responsible for a better sensitization of these solutions onto titanium dioxide film. In fact these compounds, filling the free space between the dye molecules, partially block the physical contact between I_3^- and titanium dioxide semiconductor film surface reducing recombination reactions and inhibiting dye aggregation. Moreover, the presence of 2/3 hydroxyl groups in cyanidine and delphinidine pigments favoures the chelating effect towards titanium, inducing the attachment of Ti(IV) to the hydroxyphenol moiety where the LUMO electron density is located. Hence this leads to an efficient electron injection from the dye to the semiconductor film.

Anthocyanidins is a subgroup of the flavonoids, polyphenolic compounds that are aglycons of corresponding anthocyanins, which are weak acids and occur naturally in many plants. Some selected anthocyanidins with their respective structure are depicted Table 2.1.

Table 2. 1: Selected anthocyanidins and their substitutions.

Anthocyanidin	Basic structure	R_1	R_2	R_3	R_4	R_5	R_6	R_7
Aurantinidin	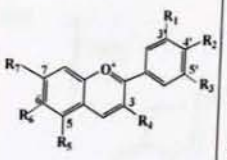	H	OH	H	OH	OH	OH	OH
Cyanidin		OH	OH	H	OH	OH	H	OH
Delphinidin		OH	OH	OH	OH	OH	H	OH
Europinidin		OCH_3	OH	OH	OH	OCH_3	H	OH
Luteolinidin		OH	OH	H	H	OH	H	OH
Pelargonidin		H	OH	H	OH	OH	H	OH
Malvidin		OCH_3	OH	OCH_3	OH	OH	H	OH
Peonidin		OCH_3	OH	H	OH	OH	H	OH
Petunidin		OH	OH	OCH_3	OH	OH	H	OH
Rosinidin		OCH_3	OH	H	OH	OH	H	OCH_3

As of 2003 more than 400 anthocyanins had been reported while in early 2006, puts the number at more than 550 different anthocyanins [196]. The difference in chemical structure that occurs in response to changes in pH is the reason why anthocyanins are often used as pH indicator, as they change red in acids to blue in bases. In aqueous solution anthocyanin species are in equilibrium between a protonated form (flavylium cation) and a quinonoidal form as it is shown in Figure 2.16. In acidic solution they appear red, due to an intense band centred at about 520 nm which is typical of anthocyanins family due to a π–π^* charge transfer transition which results in a shift of the electronic charge density from the chromenium portion to the catechol end of the

anthocyanin molecule. Hence the LUMO presents increased charge density in close proximity to the titanium binding site (Figure 2.16) allowing for good electronic coupling for charge injection. The absorption band of anthocyanins is pH and solvent sensitive, showing the red flavylium form in acidic solution and the purple deprotonated quinonoidal form as pH increases. The visible absorption band also shifts to lower wavelengths upon coordination to metal ions as it is shown in Figure 2.17.

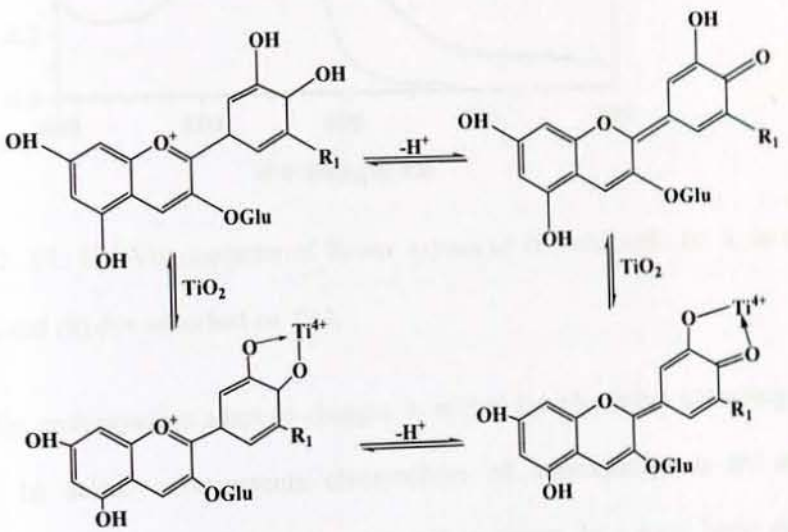

Figure 2. 16: Equilibrium between flavylium and quinonoidal form in anthocyanins in solution and in presence of TiO_2 which is able to bind the anthocyanin.

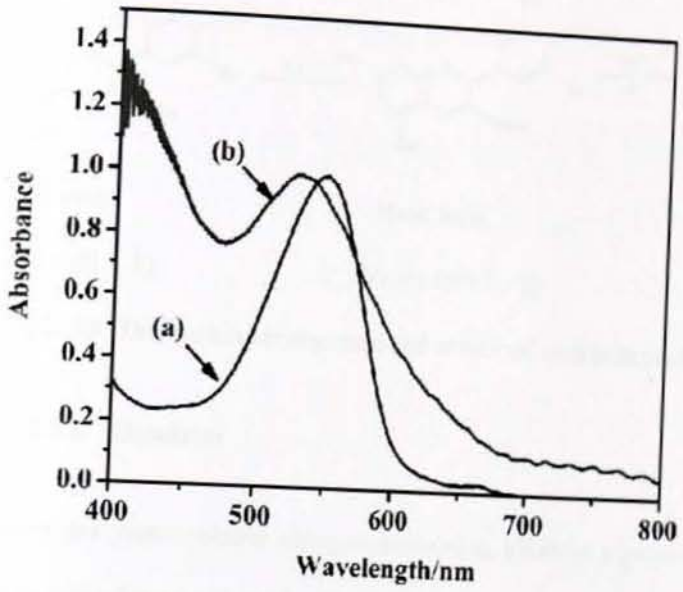

Figure 2. 17: UV-Vis spectrum of flower extract of *H. sabdariffa* (a) in in ethanol solution and (b) dye adsorbed on TiO_2 .

Generally, anthocyanins adapt to changes in acidity (or alkalinity) according to this outline: In acidic environments chromophore of anthocyanins is an aromatic flavylium (2-phenylchromenylium) cation, red in colour. In a more basic condition the double bond of the flavylium cation is disrupted by a water molecule, and the result is a colourless structure. This structure can regain colour under even more alkaline ambient conditions, since dehydroxylation restores a conjugated double bond in the anthocyanin structure. The key to this behaviour lies in the conjugated double bonds. Figure 2.18 shows the change in molecular structure and colour for cyanin for different pH-values. Anthocyanins are not very stable in alkaline environments, or in environments with a high sugar concentration. They are also heat, oxygen and light sensitive.

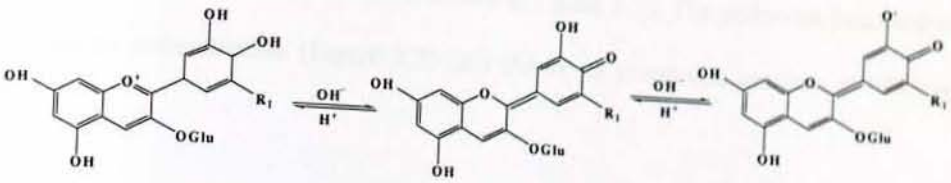

Cation

Red (pH < 3)

Base form

Violet (pH 7 - 8)

Anion

Blue (pH > 11)

Figure 2. 18: The molecular structure and colour of cyanin dependence on pH.

2.5.2. Betalains

Betalains are water-soluble nitrogen-containing alkaloid pigments [197], which are found in vacuoles of cells of families of plants belonging to the order Caryophyllales. Only in this order, and in no other order of plants, betalains are found. Also in some fungi e.g. Fly Agaric (*Amanita muscaria*), betalains exist. A finding, which so far remains unexplained, is why plants containing betalains appear to be void of anthocyanins and *vice versa*. The two pigment groups seem to perfectly exclude each other in the paths of evolution [197].

Betalain pigments represent an additional class of organic natural dyes of potential interest. These pigments have high molar extinction coefficients in the visible region and pH dependent redox properties. The pigments are present in the different parts of the plant including flowers petals, fruits, leaves, stems and roots. There are two categories of betalains, namely betacyanins and betaxanthins. Betacyanins include the reddish to violet betalain pigments. Betaxanthins are those betalain pigments which appear yellow to orange. Among the betaxanthins present in plants include vulgaxanthin, miraxanthin, portulaxanthin, and indicaxanthin. The betalain pigment (Figure 2.19) comprises the red purple betacyanins namely betanin and betanidin. The

chemical structure of betaxanthins is shown in Figure 2.20. The yellowish betaxanthin known as indicaxanthin (Figure 2.20 (a)) shows an absorption maxima at 480 nm [198].

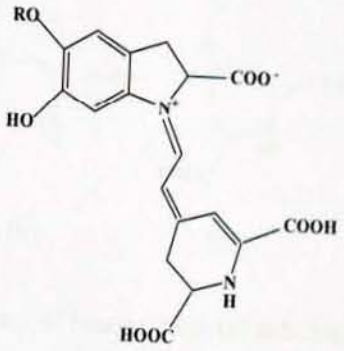

Figure 2. 19:Chemical structure of betacyanins, R = β-D-glucose (Betanin), R = H (Betanidin).

The Eurasian biennial plant beta vulgaris, the common beet root (red beet) is in the family Chenopodiaceae. Its ball-shaped red roots contain a high concentration of betalain pigments, a red-purple pigment, used as a colouring agent in food. Betanin (Figure 2.19 with R = β-D-glucose), makes up 75 – 95% of the total red colouring matter of the beetroot [199]. It is a type of betacyanin, which is a larger group of red-violet pigments. The prickly pear is a member of the Cactaceae family, originating from Mexico and widely distributed in much of Latin America, South Africa, and in the Mediterranean area. Bougainvillea plants (found in the family of Nyctaginaceae) often grow in mild climates and have typically small flowers enclosed by large, brilliant red or purple bracts (modified leaves). The prevailing pigment coloration of the cited plants varies from orange to red, due to the combination of two main dyes: betanin (red-purple) and betaxanthins (yellow-orange) whose chemical structures are shown in Figure 2.19 and Figure 2.20 respectively.

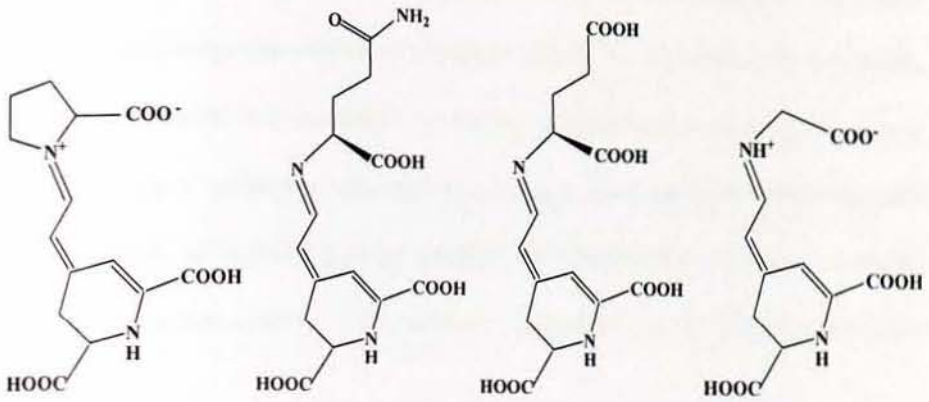

(a) (b) (c) (d)

Figure 2. 20: Chemical structure of betaxanthins, (a) indicaxanthin, (b) vulgaxanthin I (c) Vulgaxanthin II (d) portulaxanthin.

The extracts of red turnips contain pigments that belong to the betalain family. They have been previously studied by Zhang et al. [200] but efficiencies of the devices obtained using these natural pigments are very low. Like anthocyanins, the betalains have favourable light absorbing and antioxidant properties, are capable of complexing metal ions, and exist in nature in association with various copigments which modify their light absorption properties. Betalains possess the functional group –COOH to bind to TiO_2. While the absorption of anthocyanins to titanium dioxide depends on the presence of –OH groups, in betalains the attachment onto TiO_2 film is from carboxylic functions and this should lead to a stronger electronic coupling and rapid forward and reverse electron transfer reactions.

2.5.3. Chlorophyll and its derivatives

Chlorophylls are the key components of natural photosynthetic systems in green plants, bacteria, and algae. In photosynthetic reaction centers, bacteriochlorophylls are organized in a special pair which, upon photoexcitation initiates the charge separation

events leading to the fabrication of NADPH and ultimately of ATP (Figure 2.21), thus converting solar energy into chemical energy for the living organism. It is worthwhile to note that the special pair is excited by energy transfer from antenna systems made of different types of porphyrin and carotenoid arrays, abundantly distributed in grana structures, which effectively harvest sunlight and funnel the electronic excitation energy to the reaction centers. The porphyrin macrocycle is the core of chlorophyll structures.

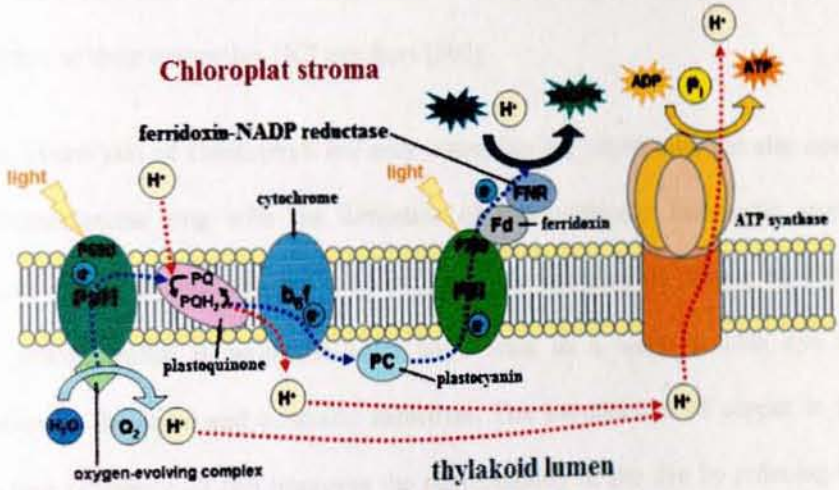

Figure 2. 21: Fabrication of NADPH and ATP (photophosphorylation) through light-dependent reactions of photosynthesis at the thylakoid membrane [201].

There are actually two main types of chlorophyll, named chlorophyll *a* and chlorophyll b (Figure 2.22 (a)). They differ only slightly, in the composition of a side chain R (in chlorophyll *a*, it is $-CH_3$, in chlorophyll b it is CHO). Both of these two chlorophylls are very effective photoreceptors because they contain a network of alternating single and double bonds, and the orbitals can delocalize stabilizing the structure. Such delocalized polyenes have very strong absorption in the visible regions of the spectrum, allowing the plant to absorb the energy from sunlight.

One of the most successful applications of natural chlorophyll derivatives to TiO_2 sensitization dates back to 1993 by Grätzel et al. [202]Chlorophyll *a* (Figure 2.22 (a)) was either used as pure commercial product or extracted with methanol from spinach leaves and partially purified by precipitation in dioxane/water. Treatment of a diethylether solution with dilute HCl gave the magnesium free pheophytin (Figure 2.22 (b)), whereas the acid hydrolysis of the phytyl ester bonds gave pheophorbides *a* (Figure 2.22 (c)) and *b* (not shown) which could be separated by extraction in diethylether at their respective HCl numbers [202].

Alkaline hydrolysis of chlorophyll not only saponifies the phytil ester but also opens the cyclopentanone ring with the formation of two additional carboxylic groups leading to chlorophylline (Figure 2.22 (d)), the Mg complex of chlorin e6 [202]. Copper chlorophyllin is produced on a large scale as a water soluble dye for application in the food and cosmetic industries. The introduction of copper in the chlorin ring (Figure 2.22 (f)) improves the photostability of the dye by reducing the excited state lifetime [202]. However, commercial chlorophyllin contains several degradation products, due to decarboxylation side reactions which lead to the absence of the carboxylic group conjugated to the π–electron system. Thus, to avoid decarboxylation, the carboxylic acid groups of chlorin have been protected as trimethyl esters by treatment with $NaOCH_3$ before the introduction of copper by addition of a saturated solution of cupric acetate in acetic acid. Saponification was carried out afterwards, leading to a good quality Cu chlorin dye (Figure 2.22 (f)) [202].

Chlorophyll *a* (Figure 2.22 (a)) does not adsorb efficiently on TiO_2 from most polar organic solvents, due to the weak interaction of the ester keto and carbonyl groups

with the oxide surface. However the adsorption is carried out quite efficiently from diethyl ether or hexane [202]. The absorption spectrum on TiO_2 film is broadened and red shifted compared to the absorption spectrum in solution, probably due to the interaction with the surface and dye aggregation. The IPCE is low, at 670 nm with an IPCE of 3.5% in the presence of pyridine, which acting as an axial Mg ligand, reduces dye aggregation and excited state quenching. Pheophytin (Figure 2.22 (b)), the free base of chlorophyll, shows a similarly poor photosensitization behavior [202].

The carboxylic group of pheophorbide (Figure 2.22 (c)) allows for a much stronger adsorption onto TiO_2, resulting in an optical density of the electrode in the Q_y band (corresponding to the lowest singlet excited state) at 675 nm, of the order of 0.7. Despite this, the IPCE at 675 nm was only 25%, far behind the unit quantum efficiency for natural photosynthesis. Under the hypothesis that the propionic acid side chain might act as an insulating barrier for charge injection into the conduction band of TiO_2, chlorophyll derivatives with a carboxylic acid conjugated to the π-electron system of the tetrapyrrole macrocycle were investigated ((Figure 2.22 (d)-(g)). The free base chlorin (Figure 2.22 (e)) and Cu chlorin (Figure 2.22 (f)) resulted in good efficiencies in the whole visible region, with an IPCE up to 70% for Cu chlorin at 650 nm [202].

However, the presence of the conjugated carboxylic anchoring group could not be considered entirely responsible for the good quantum efficiencies, since, for example, Cu-2-α-oxymesochlorin (Figure 2.22 (g)) [202], obtained as a major product from saponification of raw chlorophyll in the presence of Cu^{2+}, gave very similar IPCE (up to 70% at 630 nm). Based on this evidence, conjugation of the attaching group with the porphyrin ring does not seem strictly necessary for efficient injection.

Both the photocurrent and the photovoltage generated with chlorophyll derivatives could be significantly improved by addition of relatively high concentration (20 – 100 mM) of cholanic acids to the ethanolic dye solutions [202]. This family of bile acids is characterized by a steroid skeleton with a carboxylic acid side chain and a variable number of OH groups on one side of the steroid backbone. Due to these groups, cholanic acids bind to the TiO_2 surface, and act as spacer preventing dye aggregation and avoiding excited state self quenching. Adsorption of these acidic species also cause a positive shift of the conduction band edge of TiO_2, resulting in a larger driving force for photoinjection from the excited dye. The effect is most prominent with Cu-2-α-oxymesochlorin (Figure 2.22 (g)) which has an excited state oxidation potential barely more negative (-0.5 V vs SCE) than the conduction band edge of TiO_2. Indeed, at 630 nm the IPCE generated by (Figure 2.22 (g)) increases from 25% to 68% in the presence of 20 mM chenodeoxycholic acid [202].

Detailed investigations based on sub-nanosecond laser spectroscopy [203] have demonstrated that non fluorescent chlorophyll derivatives like Cu chlorins have smaller charge injection rate constants ($k_{inj}= 3 \times 10^8\ s^{-1}$) than dyes injecting from singlet states like the free base chlorin e6 ($k_{inj} = 2.2 \times 10^9\ s^{-1}$), however the longer lived triplet state of Cu chlorins still allows for a high electron injection quantum yield. Moreover competitive excited state quenching due to exciton migration and annihilation is reduced with metal porphyrins undergoing efficient intersystem crossing, since long range energy transfer (Forster type) is spin forbidden. Interestingly photon to current conversion yields have been reached in the red part of the spectrum, with overall efficiencies of 2.6% ($J_{SC} = 9.4\ mA/cm^2$, $V_{OC} = 530\ mV$ for (Figure 2.22 (g)) under full sunlight ($100\ mW/cm^2$) [202].

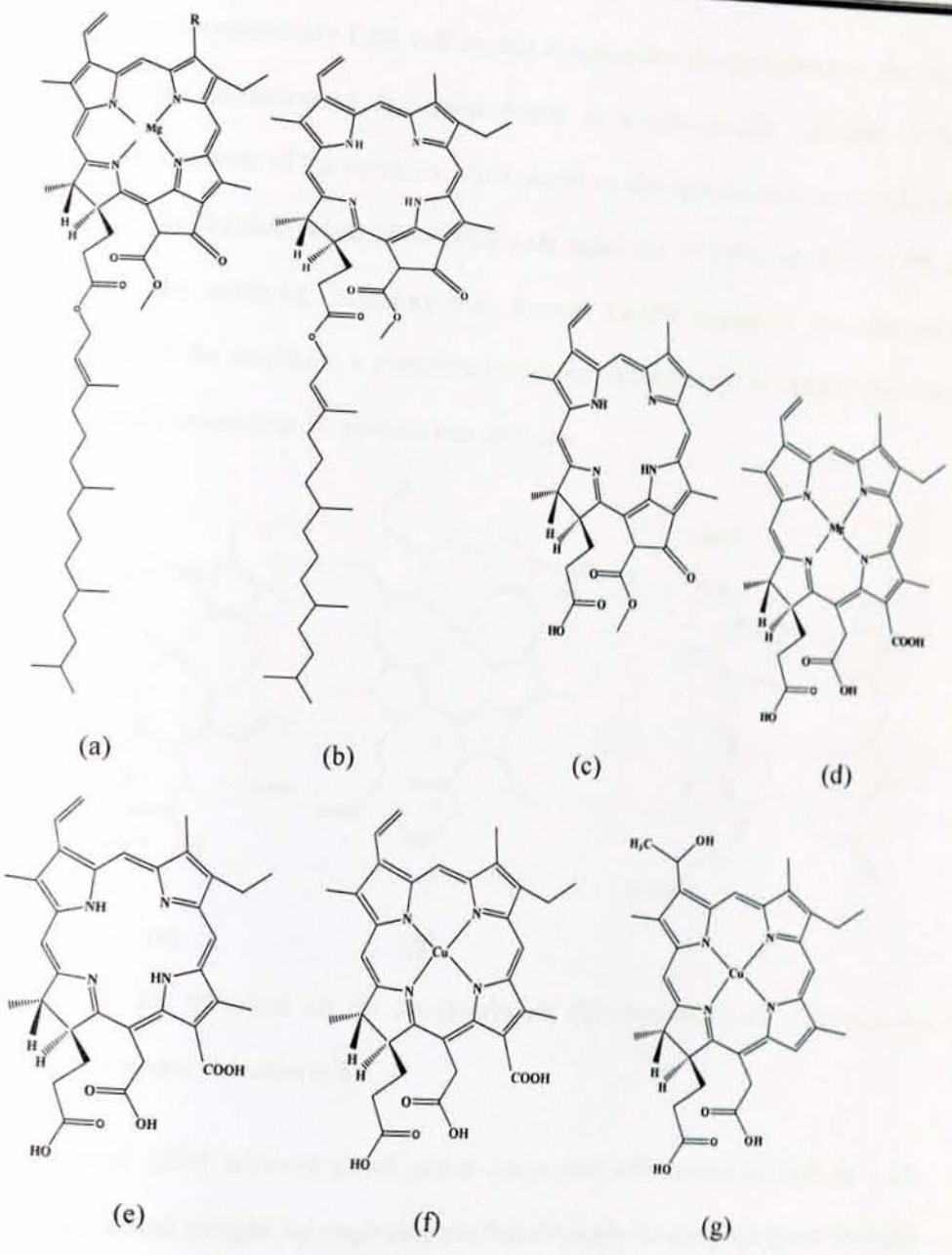

Figure 2. 22: Structure of natural chlorophyll derivatives: (a) R = CH_3, chlorophyll *a*; R = CHO, chlorophyll *b* (b) pheophytin; (c) pheophorbide *a*; (d) Mg chlorin e_6; (e) chlorin e_6; (f) Cu chlorine e_6; (g) Cu-2-α-oxymesochlorin.

Researchers have pursued efficient TiO_2 sensitization exploiting natural pyrrole macrocycles. Interestingly, Amao et al. [204] have used Zn chlorine e6 (Figure

2.23(a)) to spontaneously form side-to-side π–aggregates (J-aggregates) on the TiO_2 surface. The formation of aggregates results in a considerable red shift of the electronic spectrum of the sensitizer which shows an absorption maximum at 800 nm. Although the absolute values of the IPCE were rather low (< 10%), an IPCE of 7% at 800 nm was achieved, indicating that, through careful tuning of the electronic properties of the sensitizer, a photoelectrochemical device based on natural dyes can absorb and convert near IR photons into electrons.

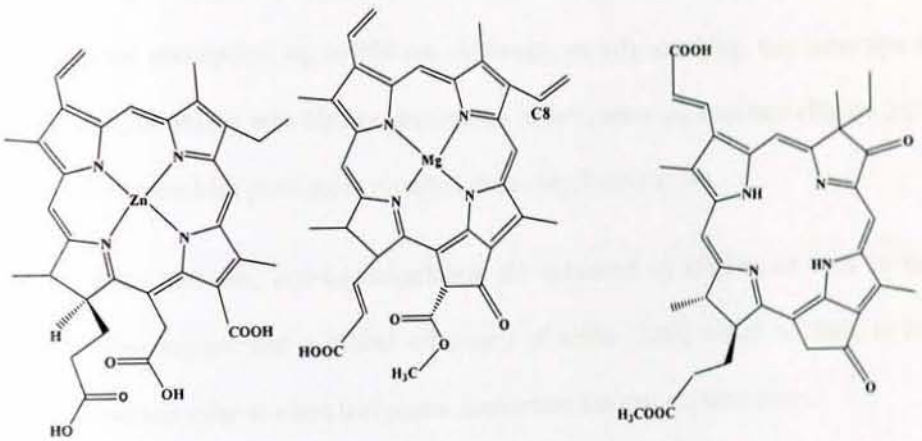

(a) (b) (c)

Figure 2. 23: Structure of: (a) Zn chlorin e6; (b) chlorophyll c2 (Chl–c2); (c) synthetic oxo-bacteriochlorin B1.

Wang et al. [205] achieved global power conversion efficiencies as high as 4.6% under simulated sunlight, by employing purified chlorophylls extracted from Wakame brown seaweed (*Undaria pinnatifida*), of which the most effective was chlorophyll c2, probably due to the presence of the vinyl group in the C8 position (see Figure 2.23 (b)) which, acting as an electron donor, increases the electronic density of the chlorophyill ring. This results in a slight red shift of the absorption spectrum of the dye and, more importantly, in an improvement of the electron donating capabilities of its excited state, thanks to a less positive ground state oxidation potential (1.06 V vs

NHE with respect to 1.13 V vs NHE measured for the saturated Chl–c2 with the ethyl group in the C8 position).

By using TiO_2 photoelectrodes equipped with a light scattering layer, Chl–c2 generated IPCE% ranging from 80 to 60% in the 380 – 700 nm range, and correspondingly displayed a relevant performance under AM 1.5 conditions, with $J_{SC} \approx 14$ mA/cm^2 and $V_{OC} = 0.58$ V. These performances have been very recently surpassed by an entirely synthetic bacteriochlorin sensitizer [206] capable of a panchromatic absorption, up to 800 nm. Although, strictly speaking, this latter dye is not natural, its design was clearly inspired by nature, since its structure (Figure 2.23 (c)) closely resembles previously reported chlorophyll derivatives.

Starting from 800 nm, oxo-bacteriochlorin B1 achieved an IPCE% of 70% in the whole visible region and a global efficiency of 6.6% [206], which to date, is the highest reported solar to electrical power conversion for chlorin sensitizers.

3. EXPERIMENTAL: MATERIALS AND METHODS

3.1. Preparation of Photoelectrochemical cell based on Blend of Poly(3-hexylthiophene) (P3HT) and [6,6]-phenyl-C61-butyricacid methyl ester (PCBM)

3.1.1. Coating of ITO with the photoactive material

In this study a blend of P3HT (Aldrich) and PCBM (Merk) was used as a photoactive electrode. Both P3HT and PCBM were used without any pre-treatment. ITO-coated glass having transmittance above 80% in the visible region of the solar spectrum was employed as a substrate for the photoactive materials and counter electrodes. It was cleaned successively with acetone (Aldrich), 2-propanol (Riedel-de Haen), and ethanol (BDH) and dried with an air gun. A solution of the photoactive electrode was prepared by dissolving a mixture of 2.5 mg P3HT and 2.5 mg PCBM in 1 ml of 1, 2-dichlorobenzene (Riedel-de Haen). The photoactive film was formed by drop casting a solution of P3HT and PCBM on a pre-cleaned ITO-coated glass.

3.1.2. Preparation of the counter electrode

The polymer film for the counter electrode was formed by electrochemical polymerization of 3, 4-ethylenedioxythiophene (EDOT) (Bayer), in a three electrode one-compartment electrochemical cell. The electrochemical cell consisted of a pre-cleaned ITO-coated glass working electrode, platinum foil counter electrode, and quasi-Ag/AgCl reference electrode dipped in $LiClO_4$ (Aldrich) acetonitrile (Sigma-Aldrich) solution. The solution used for the polymerization contained 0.1 M EDOT and 0.1 M $LiClO_4$ in acetonitrile. The monomer was used as received. The polymerization was carried out potentiostatically at +1.8 V. At this potential, the

electrode surface becomes covered with blue-doped PEDOT film. The cell was then rinsed with acetonitrile and dried in air.

3.1.3. Preparation of the solid state electrolyte PEC assembly and measurement

The polymer electrolyte was prepared by dissolving 309 mg of POMOE in 25 ml of methanol (Fluka). The redox couple I_3^-/I^- was prepared by dissolving 48.13 mg KI (BDH) and 7.36 mg I_2 (Aldrich) separately in 25 ml of methanol (Fluka). Finally, 2 ml of each of the above three solutions were mixed to produce the polymer electrolyte complexed with a redox couple. The mole ratio of oxygen to potassium as calculated by taking into account both the oxymethylene and oxyethylene oxygen atoms was 25 and the mole ratio of KI to I_2 was 10, i.e., the concentration of I_2 is one-tenth the concentration of KI. The ionic conductivity of POMOE is known to be high at room temperature when the oxygen to cation (potassium) mole ratio is 25 [207].

Finally, the polymer electrolyte complexed with I_3^-/I^- was deposited in the form of thin film by solvent casting on top of P3HT:PCBM coated ITO-glass and allowed to dry in a laboratory atmosphere. The PEC was completed by pressing against PEDOT-coated ITO-glass counter electrode. Figure 3.1 shows the chemical structures of P3HT, PCBM, and PEDOT, and the device structure of the solid-state PEC used in this study. The PEC was then mounted in a sample holder inside a metal box with 1 cm^2 opening to allow light from the source. All experiments were carried out at room temperature.

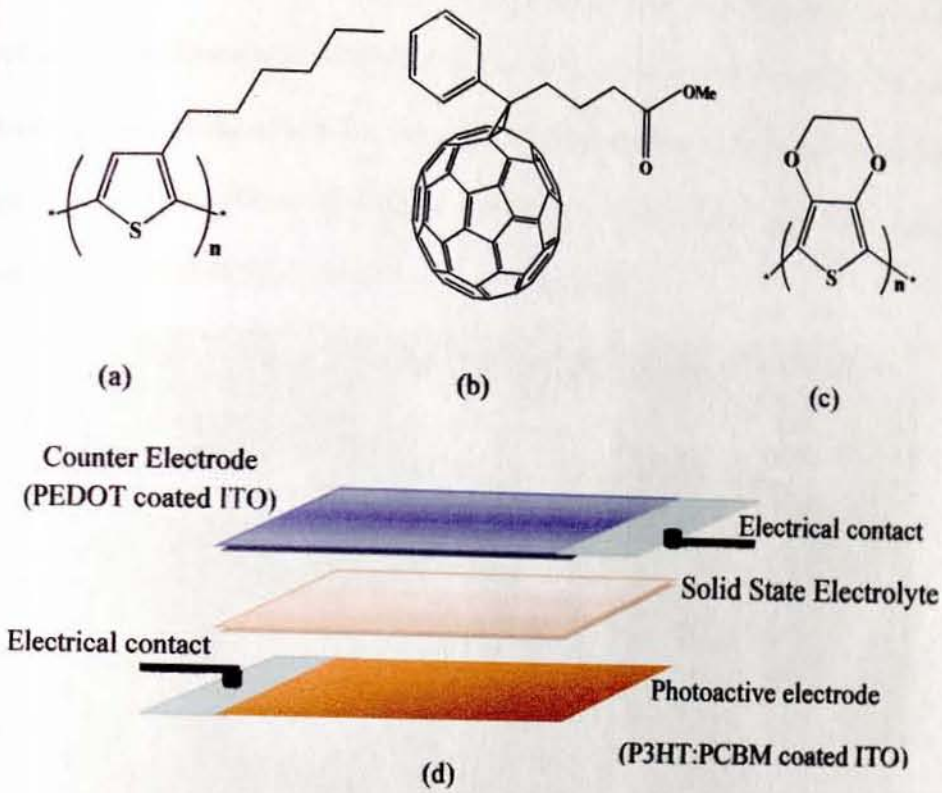

Figure 3. 1: The Chemical structure of (a) poly(3-hexylthiophene), P3HT, (b) 1-(3-methoxycarbonyl)propyl-1-phenyl [6,6]C_{61}, PCBM, (c) poly(3,4-ethylenedioxy thiophene), PEDOT, and (d) the basic structure of the solid-state PEC.

The photoelectrochemical measurements of the cell were performed using a computer-controlled CHI630A Electrochemical Analyzer. A 250-W tungsten–halogen lamp regulated by an Oriel power supply (Model 68830) was used to illuminate the PEC. A grating monochromator (Model 77250) placed into the light path was used to select a wavelength between 300 and 800 nm. The measured photocurrent spectra were corrected for the spectral response of the lamp and the monochromator by normalization to the response of a calibrated silicon photodiode (Hamamatsu, Model S1336-8BK) whose sensitivity spectrum was known. No correction was made for the reflection from the surface of the sample. The white light intensity was measured in

the position of the sample cell with Gigahertz-Optik $X1_1$ Optometer. A series of neutral density filters were used to vary the light intensity incident on the sample. The general experimental set-up for the photoelectrochemical measurements is shown in Figure 3.2. The optical absorption spectrum of the film was measured using Spectroscopic GENESYS 2PC UV–Vis spectrometer.

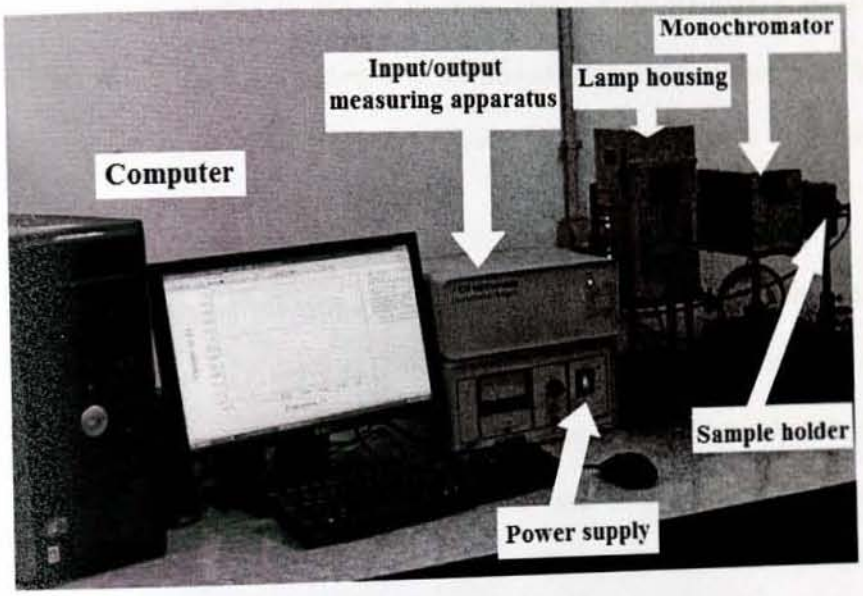

Figure 3. 2: General experimental set-up for the photoelectrochemical measurements.

3.2. Preparation of Solid State Photoelectrochemical Cell based on Dye Sensitized TiO_2

3.2.1. Preparation of the photoanode

Preparation of mesoporous TiO_2 film was done with the method described in reference [53]. Nanocrystalline TiO_2 films were prepared by spreading a viscous dispersion of colloidal TiO_2 particles on ITO with heating under air for 30 min at 450^0C. The method for preparation of nanocrystalline films employed commercial TiO_2 (P25, Degussa). 3 g powder was ground in a porcelain mortar with 1 ml water containing 0.1 ml acetylacetone to prevent reaggregation of the particles. After the powder had been dispersed by the high shear forces in the viscous paste, it was diluted

by slow addition of 4 ml water under continued grinding. Finally, a detergent 0.05 ml Triton X-100, (Aldrich) was added to facilitate the spreading of the colloid on the substrate. The ITO was covered on two parallel edges with adhesive tape to control the thickness of the TiO_2 film and to provide noncoated areas for electrical contact. The colloid was applied to one of the free edges of the conducting glass and distributed with a glass rod sliding over the tape-covered edges as shown in Figure 2.11. After air drying, the electrode was fired for 30 min at 450^0C in a furnace (Carbolite Model ELF 11/14B).

Coating of the TiO_2 surface with dye was carried out by soaking the film for 2 h in a 0.3 mM solution of N-719 dye (Aldrich) in dry ethanol. The dye coating was done immediately after the high temperature annealing in order to avoid rehydration of the TiO_2 surface or capillary condensation of water vapor from ambient air inside the nanopores of the film. The presence of water in the pores decreases the injection efficiency of the dye. The electrode was dipped into the dye solution while it was still hot. After completion of the dye adsorption, the electrode was withdrawn from the solution under a stream of dry air. It was stored in dry ethanol or immediately wetted with redox electrolyte solution for testing.

3.2.2. Preparation of the solid state electrolyte, PEC assembly and measurement

The polymer electrolyte was prepared by dissolving 311 mg of POMOE in 25 ml of methanol. The redox couple I_3^-/I^- was prepared by dissolving 48.47 mg KI in 25 ml of methanol and 7.41 mg I_2 in 25 ml of methanol. Finally, 1ml of each of the above three solutions were mixed to produce the polymer electrolyte complexed with a redox couple. The mole ratio of oxygen to potassium as calculated by taking into account both the oxymethylene and oxyethylene oxygen atoms was 25 and the mole ratio of

KI to I_2 was 10. Finally, the polymer electrolyte complexed with I_3^-/I^- was deposited in the form of thin film by solvent casting on top of the dye coated TiO_2 electrode and allowed to dry in a laboratory atmosphere. The PEC was completed by pressing against PEDOT-coated ITO glass counter electrode which was prepared using a procedure mentioned in section 3.1.2. The PEC was then mounted in a sample holder inside a metal box with 1 cm^2 opening to allow light from the source. All experiments were carried out at room temperature. The photoelectrochemical measurements of the cell were performed using a procedure described in section 3.1.3 using an experimental setup shown in Figure 3.2. The basic structure of the device is shown in Figure 3.3.

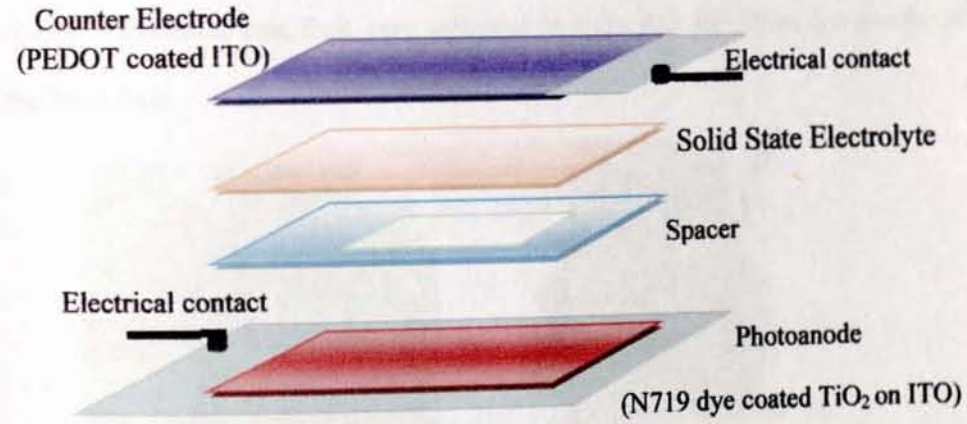

Figure 3. 3: The device structure of the solid-state PEC based on dye coated nc-TiO_2 photoanode.

3.3. Preparation of natural dye sensitized solar cell from *Syzygium guineense* Extracts

3.3.1. Preparation of the photoanode

Natural dyes were extracted from fruits of *Syzygium guineense* with different solvents namely water, methanol, and ethanol. The dyes extracted with these solvents were

obtained using the following steps: fruits of *Syzygium guineense* were washed with water, separated from the seed, cut with knife into smaller pieces and dried in open air for two weeks. The dried materials of the fruit were made into powder with an electrical blender. The powder of the plant material was soaked in three different solvents (water, ethanol and methanol) in three 250 ml brown colored bottles. All the samples were kept with stirring for 12 hours and the solid material was allowed to settle down overnight. Then the solids were filtered out. Filtrates were used as sensitizer without further purification and concentration. Further purification through solvent-solvent extraction of the ethanol extract was done with different solvents. The further purified solutions also were used as sensitizer. Figure 3.4 depicts a picture of *Syzygim Guineense* tree, fruit, seed separated from the fruit for drying and powder of the dried fruit.

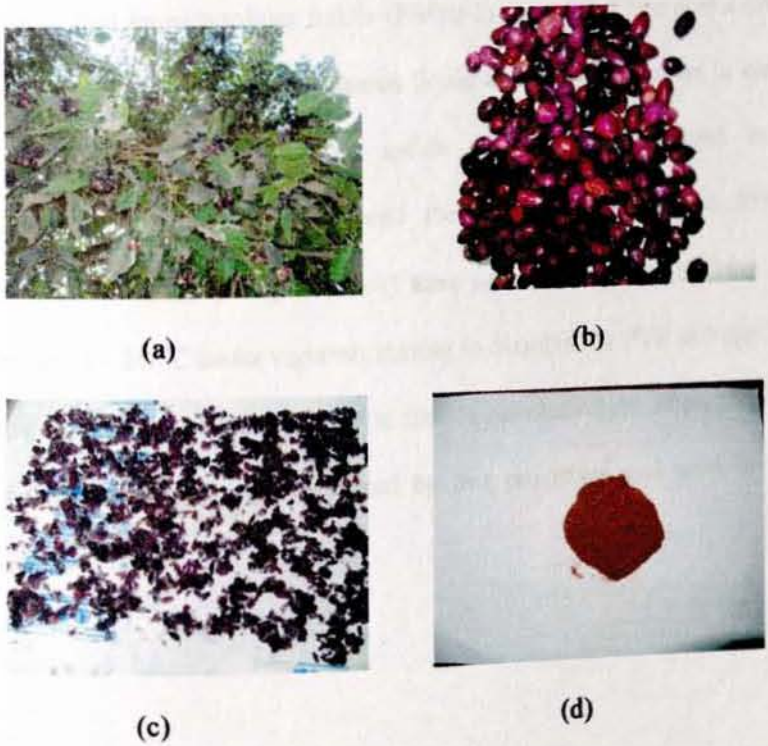

Figure 3. 4: *Syzygim Guineense* (a) tree (b) fruit (c) seed separated from the fruit for drying (d) powder of the dried fruit.

Precleaned ITO conductive glass sheets (2.5 cm × 1.5 cm) were used for the preparation of the photoanode. Preparation of mesoporous TiO_2 paste and TiO_2 coated photoanode film was done with the method described earlier in Section 3.2.1.

Coating of the TiO_2 surface with dye was carried out by soaking the film for 2 h in the extracted dyes. After completion of the dye adsorption, the electrode was withdrawn from the solution under a stream of dry air and was immediately wetted with redox electrolyte solution for testing.

3.3.2. Preparation of the Quasi-Solid state electrolyte, PEC assembly and measurement

The polymer gel electrolyte was prepared as reported in reference [208]. 0.9 M of 1-ethyl-3-methyl immidazolium iodide (EMIm-I) was added into acetonitrile (Aldrich) under stirring to form a homogeneous liquid electrolyte. In order to obtain a better conductivity, 0.5 M of sodium iodide (BDH) was dissolved in the above homogeneous liquid electrolyte, and then 0.12 M iodine and 35% (w/w) of polyvinylpyrrolidone (PVP) (Aldrich) were added. Then, the resulting mixture was heated at 70 – 80 ^{0}C under vigorous stirring to dissolve the PVP polymer, followed by cooling down to room temperature to form a gel electrolyte. Photographic picture of the polymer gel electrolyte prepared by this procedure and used in this study is depicted in Figure 3.5.

Figure 3. 5: Polymer gel electrolyte composed of polymer PVP, EMIm-I, NaI, and I_2 as quasi-solid state electrolyte.

Finally, the gel electrolyte was deposited in the form of thin film on top of the dye coated TiO_2 electrode. The photoelectrochemical cell (PEC) was completed by pressing against PEDOT-coated ITO glass counter electrode which was prepared electrochemically with a procedure described in Section 3.1.2. The PEC was then mounted in a sample holder inside a metal box with an area of 1 cm^2 opening to allow light from the source. All experiments were carried out at ambient temperature. Absorption spectra measurement of the extracted dyes and photoelectrochemical measurements of the DSSCs were performed using a procedure described in Section 3.1.3. Figure 3.6 shows the chemical structure of 1-ethyl-3-methylimmidazolium iodide (EMIm-I) and polyvinylpyrrolidone (PVP).

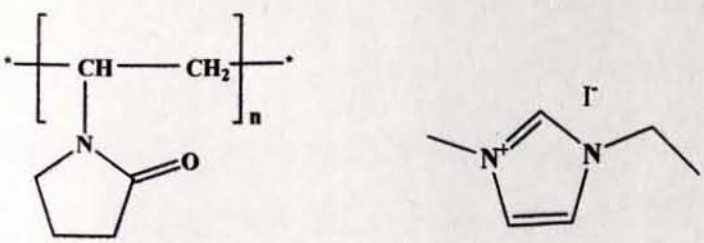

(a) (b)

Figure 3. 6: The Chemical structure of (a) Polyvinylpyrrolidone (PVP) (b) 1-ethyl-3-methyl immidazolium iodide.

Figure 3.7 shows the device structure of quasi-solid state dye sensitized PEC.

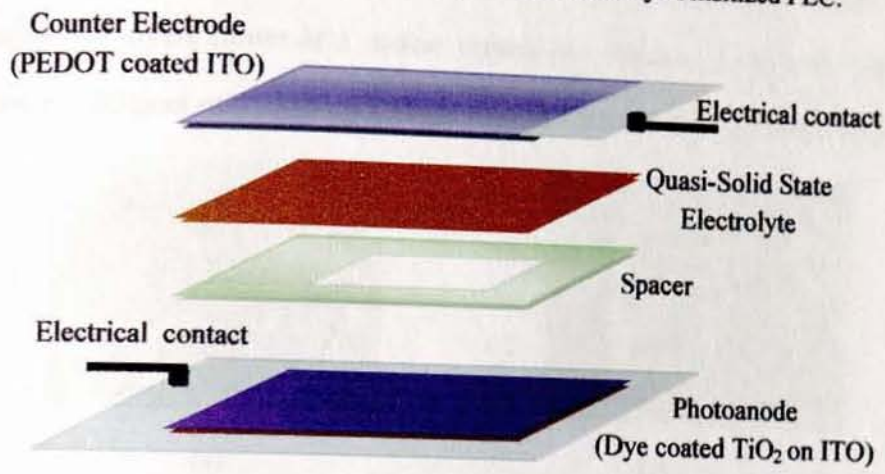

Figure 3. 7: The device structure of quasi-solid state dye sensitized PEC.

3.4. Preparation of Quasi-Solid State Dye-Sensitized Solar Cells from Leaf and flower Extracts as Sensitizers

3.4.1. Preparation of the photoanode

A 0.5 mM solution of commercial ruthenium dye [Ru(II)(2,2'-bipyridyl-4,4'-dicarboxylic-acid)(2,2'-bipyridyl-4,4'-ditetrabutylammonium-carboxylate) $(NCS)_2$] called N719 (Aldrich) was prepared in dry ethanol. Fresh leafs of *A. caudatus* and *I. herbstii*, flowers of *I. indica* and *Hibiscus sabdariffa* were air dried for two weeks and made into powder form with an electric blender. The powder of the plant material was soaked in 0.1M HCl solution and ethanol in two 250 ml brown colored bottles for each plant materials. All the samples were kept with stirring for 12 hours and the solid material was allowed to settle down overnight. Then the solids were filtered out. Filtrates were used as sensitizer without further purification and concentration. If properly stored, protected from direct sunlight and refrigerated at about $+4^0$C, the acidic natural dye solutions (pH = 5.0) are usually stable, with a deactivation half-time of more than 12 months [209]. Figure 3.6(a) and (b) depicts a picture of leaf of *I.*

herbstii, and *A. caudatus*, respectively. Figures 3.6 (c) and (d) show flower of *I. indica* and drying flower of *I. indica*, respectively. Figures 3.6 (e) and (f) depict flower of *Hbiscus sabdariffa* and drying flower of *Hbiscus sabdariffa*, respctively.

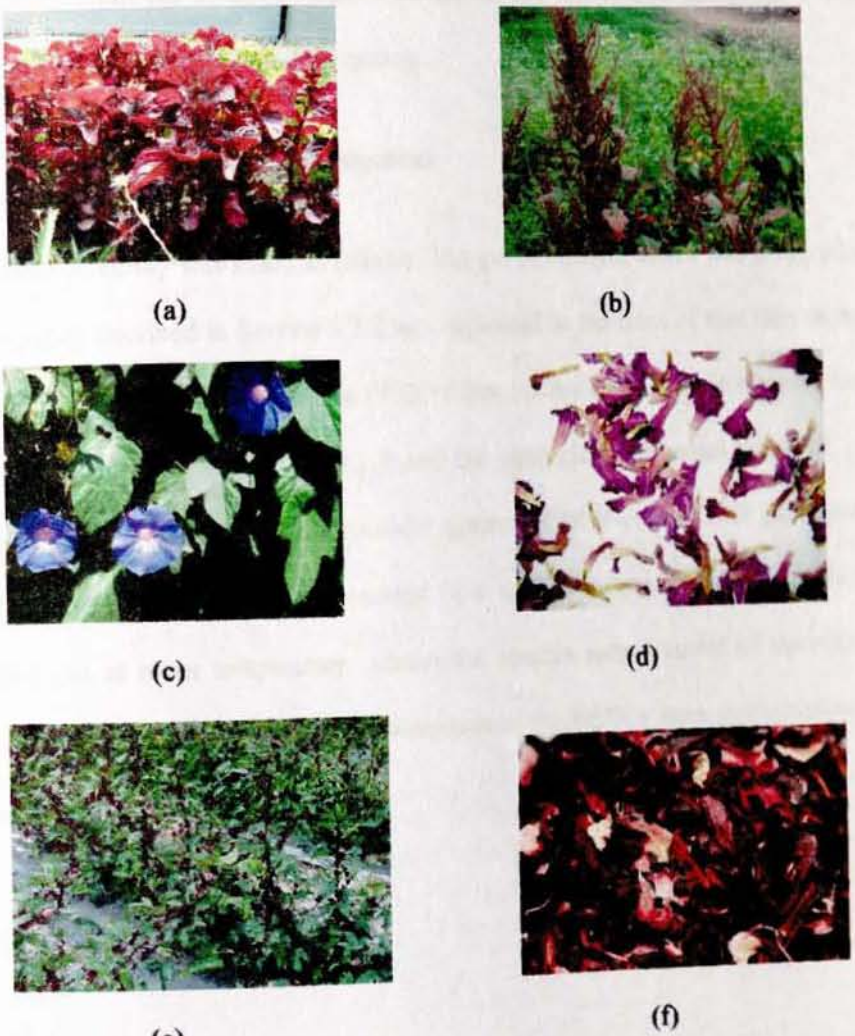

Figure 3. 8: Leafs of and flowers of the investigated plants (a) Leaf of *I. herbstii* (b) Leaf of *A. caudatus* (c) Flower of *I. indica* (d) Drying flower of *I. indica* (e) Flower of *Hbiscus sabdariffa* (f) Drying flower of *Hbiscus sabdariffa*.

Precleaned ITO conductive glass sheets (2.5 cm × 1.5 cm) were used for the preparation of the photoanode. Preparation of mesoporous TiO_2 paste and TiO_2 coated photoanode film was done with the method described earlier in Section 3.2.1.

Coating of the TiO_2 surface with dye was carried out by soaking the film overnight in the extracted dyes. After completion of the dye adsorption, the electrode was withdrawn from the solution under a stream of dry air. It was immediately wetted with redox electrolyte solution for testing.

3.4.2. PEC assembly and measurement

The PEC assembly was made as follows. The gel electrolyte which was prepared with a procedure decribed in Section 3.3.2 was deposited in the form of thin film on top of the dye coated TiO_2 electrode. The PEDOT film for the counter electrode was formed as it was described in Section 3.1.2 and the photoelectrochemical cell (PEC) was completed by pressing the photoanode against PEDOT-coated ITO glass counter electrode. The PEC was then mounted in a sample holder. All experiments were carried out at room temperature. Absorption spectra measurement of the extracted dyes and photoelectrochemical measurements of the DSSCs were performed using a procedure described in Section 3.1.3.

4. RESULTS AND DISCUSSION

4.1. Photoelectrochemical Solar Energy Conversion based on Blend of Poly(3-hexylthiophene) (P3HT) and [6,6]-phenyl-C61-butyricacid methyl ester (PCBM)

4.1.1. Background

Organic photovoltaic (OPV) devices based on π-conjugated polymers have been intensively studied following the discovery of fast charge transfer between polymer and C_{60} [35, 210 – 217]. The photovoltaic process in OPV first starts from the absorption of light mainly by the polymer, followed by the formation of excitons. The exciton then migrates to and dissociates at the interface of donor (polymer)/acceptor (fullerene). Separated electrons and holes travel to opposite electrodes and are collected at the electrodes, resulting in an open circuit voltage (V_{OC}). Upon connection of electrodes, a photocurrent (short circuit current, I_{SC}) is generated.

Regioregular polythiophene derivatives have been widely investigated for bulk heterojunctions (BHJs) because of their highly crystallizable state, leading to good light harvesting in the visible spectrum and excellent carrier mobility. Power conversion efficiencies (PCEs) of up to 5% have been achieved using poly(3-hexylthiophene)|[6,6]-phenyl-C_{61}-butyric acid methylester (P3HT|PCBM) composites as the photoactive layer [215, 218 – 220]. More recently, the PCE of BHJ polymer solar cells (PSCs) has been increased to around 6.0 – 7.4% by using low bandgap conjugated polymers as electron donors and PCBM or [6,6]-phenyl C_{70} butyric acid methyl ester ($PC_{70}BM$) as electron acceptor [221 – 224]. However, the efficiency of device based on P3HT, is difficult to improve because of its limited absorption range, which absorbs photons only at wavelengths less than 650 nm and merely about 22%

of the absorbed photons from sun light [225]. Moreover, its high lying highest occupied molecular orbital (HOMO) also limits the V_{OC} for the devices based on P3HT:PCBM blend. V_{OC} of P3HT:PCBM cells is limited around 0.6 V due to the relatively small energy difference between the highest occupied molecular orbital (HOMO) of P3HT and the lowest unoccupied molecular orbital (LUMO) of PCBM [226]. With a bandgap of 1.9 eV of P3HT, this system is still limited by the mismatch of the absorption to the terrestrial solar spectrum [223]. A bandgap of 1.3 – 1.5 eV is regarded as ideal for polymer–fullerene BHJ solar cells [227].

Previously the use of substituted polythiophenes as photoactive electrodes in solid-state photoelectrochemical cells (PECs) have been reported [38, 39, 43, 228, 229]. Mengesha et al. [230] also made the first report on solid-state photoelectrochemical energy conversion using conducting polymer and fullerene mixtures. In this work experimental results on the behaviour of a solid-state PEC containing a mixture of poly(3-hexylthiophene) (P3HT) and PCBM coated on indium-doped tin oxide (ITO) used as a photoactive electrode; amorphous polyethylene oxide complexed with the I_3^-/I^- redox couple used as an electrolyte; and a thin transparent layer of poly(3,4-ethylenedioxythiophene), PEDOT, electrochemically coated on ITO as a counter electrode is presented. P3HT combines commercial availability with sufficient solubility, a low bandgap relative to the most conjugated polymers and a high degree of intermolecular order leading to high-charge carrier mobility [231].

Unlike classical solid electrolytes, both the anions and the cations are mobile in polymer electrolytes. The stronger cation bonding to the polymer chain liberates anions from cation association and thus results in higher anion mobility and conductivity. Cation mobility depends on the strength of the cation-polymer

interactions; if these are strong, cation transport is suppressed. The criteria for the development of polymer electrolyte systems that can achieve good working conductivity, in the range 10^{-3}-10^{-6} S/cm, are established. The low ionic conductivity can be compensated by forming very thin films with large surface area. The polymer must be capable of dissolving the salt and ionizing it to produce sufficient number of charge carrying species. It must also be amorphous to allow easy movement of ions, and must have a flexible chain to assist the ion transport. In PEO the ionic conductivity was found to increase on departing from the stoichiometric ether oxygen to cation ratio (O:M), as the number of vacant sites would increase on increasing the O:M ratio. Here the polymer electrolyte, amorphous poly(ethylene oxide) (POMOE) with the redox couple is used as an electrolyte. POMOE has a melting point below room temperature and a glass transition temperature of 209 K [232 – 236]. At room temperature it will not crystallize or form crystalline polymer-salt complexes with moderate salt concentrations. Figure 4.1 shows the simplified schematic representation of cation movements in a polymer electrolyte [237].

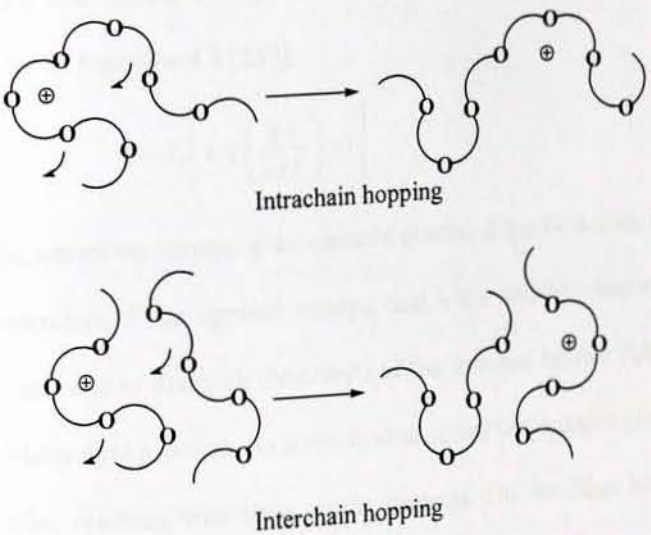

Figure 4. 1: Schematic representation of cation motion in a polymer electrolyte.

Electrochemically oxidized PEDOT was required on ITO because it improved charge transfer between ITO and the iodide/triiodide redox couple through its catalytic behaviour [228]. It is known that bare ITO is irreversible for the I_3^-/I^- redox reaction [238].

4.1.2. Current density– voltage characteristics

The current from the PEC is measured as a function of the applied voltage, both in the dark, and under illumination. This data allows the J_{SC}, the V_{OC}, and the rectifying properties of the devices to be determined, and enables to calculate the fill factor. Figure 4.2 show the current-voltage curves of the PECs based on a blend of P3HT:PCBM, in the dark and under white light illumination at 100 mW/cm^2, respectively. The devices were illuminated from their front sides (ITO|PEDOT).

In the dark, the current was negligible and remained relatively constant in the negative potential range while a larger anodic current was observed in the larger positive potential range. The current-voltage characteristic of the cell in the dark is described mathematically by Equation 4.1 [239]:

$$I = I_0\left[\exp\left(\frac{qV}{nkT}\right)-1\right] \qquad (4.1)$$

where I_0 is the saturation current, q the electron charge, k the Boltzman constant, T the absolute temperature, V the applied voltage, and n the ideality factor. The positive applied potential acts to diminish the effects of the internal barrier field that is set at the polymer/electrolyte junction. As a result, charge carriers acquire enough energy to cross the barrier, resulting with large anodic currents. On the other hand, applying a negative potential enhances the barrier potential and only a small current flows. The current response of the devices to the applied potentials in the dark indicates that the

devices exhibit the desirable photoelectrochemical properties. Under illumination, cathodic photocurrents were observed that extend from a negative potential range up to a positive potential range, which is expressed as the open-circuit voltage (the voltage where the current is zero). This indicates that the direction of the photoinduced charge separation is the same as that of the charge separation by the applied potential. The current-voltage characteristic under illumination can be described by Equation 4.2 [239]:

$$I = I_{ph} - I_0\left[\exp\left(\frac{qV}{nkT}\right) - 1\right] \qquad (4.2)$$

where I_{ph} is the photogenerated minority carrier current (which is opposite in sign to the dark current) and is equal to the product of the absorbed photon flux and the charge on an electron. The V_{OC} of BHJ based solar cells is strongly correlated to inherent material properties. It was demonstrated that the open circuit voltage of polymer/fullerene BHJ based solar cells is correlated to the reduction potential of the fullerene molecule [240]. A reduction potential defines the LUMO level of the molecule. Moreover, the V_{OC} of polymer/fullerene based solar cells is affected by the morphology of the active layer [241]. From Table 4.1, it can be seen that the P3HT:PCBM based device exhibits many fold improvement in the short-circuit current density, higher V_{OC} when compared with the P3HT:C_{60} [230] based device. Higher V_{OC} and the several fold enhancement in the short circuit current density of P3HT:PCBM based device most likely originates from the enhanced charge carrier separation and improved charge carrier mobility [35] due to better solubility of mixture of P3HT with PCBM in an organic solvent which also results in better morphology compared with mixture of P3HT with C_{60} in the same organic solvent.

Table 4. 1: Typical photoelectrochemical parameters calculated from J–V characteristics for P3HT:PCBM PEC compared with P3HT:C_{60} PEC [230].

Photoactive material	V_{OC}(mV)	J_{SC}(μA/cm^2)	Reference
P3HT:C_{60} (1:1)	97.8	7.28	[230]
P3HT:PCBM (1:1)	140.0	28.4	This work

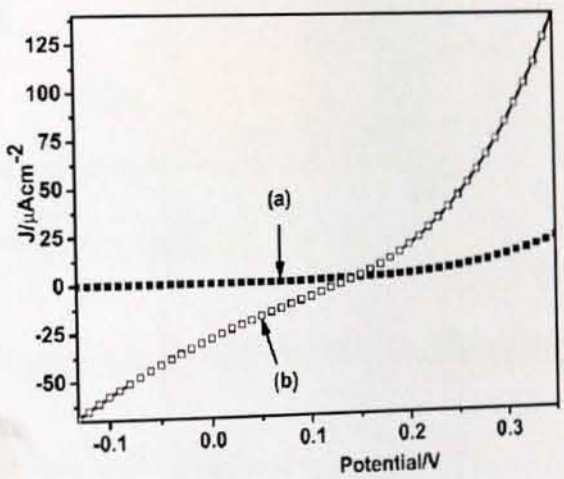

Figure 4. 2: Current density-voltage characteristics of ITO|P3HT:PCBM |POMOE:I_3^-/I^- |PEDOT|ITO cell (a) in the dark and (b) under illumination through front side with light intensity of 100 mWcm^{-2}.

Figure 4. 3 illustrates the schematic of operation of the P3HT:PCBM based solid-state PECs. The energy levels of the LUMO and the HOMO of P3HT are at -3.53 eV and -5.2 eV, respectively [242] while those of PCBM are at -3.75 eV and -6.1 eV, respectively [36]. Thus, photogenerated free electrons can be transferred from the LUMO of P3HT directly to the electrolyte or to the LUMO of PCBM and then to the electrolyte where they reduce I_3^- to I^-, E_{redox} (I_3^-/I^-) = -4.9 eV [76]. I_3^- is regenerated when I^- is oxidized at the counter electrode (anode). In the mean time, the

photogenerated holes move to the back contact (ITO) of the PEC through the polymer network. Thus, light energy is converted to electrical energy without net chemical change.

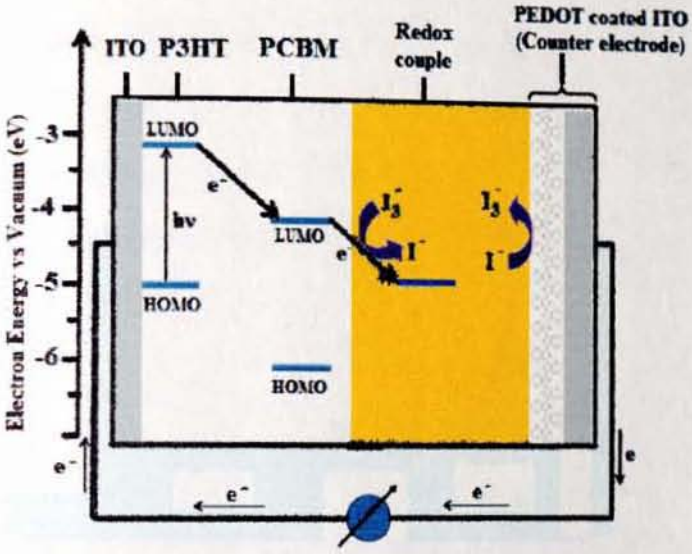

Figure 4. 3: Schematic of operation of the P3HT:PCBM-based solid-state PEC.

4.1.3. The dependence of J_{SC} and V_{OC} on time

The parameters that are used to describe solar cells are short-circuit current density (J_{SC}) and open-circuit voltage (V_{OC}). These parameters determine the efficiency and are the key parameters in experimental investigation of solar cells. Steady state and transient measurements of J_{SC} and V_{OC}, established during long and short period of irradiation, are used to characterize the stability of the PECs towards illumination. Figure 4.4 shows photocurrent response to continuous illumination with light intensity of 100 $mWcm^{-2}$ for the ITO|P3HT:PCBM|POMOE:I_3^-/I^-|PEDOT|ITO solid-state PEC. The inset in Figure 4.4 and Figure 4.5 show the short-circuit current density and open circuit voltage, respectively, as a function of time for the ITO|P3HT:PCBM |POMOE:I_3^-/I^-|PEDOT|ITO solid-state PEC. The illumination was made from the

PEDOT|ITO side (front side) with a white light intensity of 100 $mWcm^{-2}$. The generation of photovoltage and photocurrent were characterized by a rise to a steady state value when the light is switched on and decay at approximately the same rate when the light is switched off. The stability of the photocurrent was very good. The short-circuit photocurrent density and open-circuit voltage obtained from the transient measurements were 26.28 $\mu A/cm^2$ and 142.5 mV, respectively. The results of time dependence study show that the steady state J_{SC} and V_{OC} values are consistent with those obtained from the J–V curve.

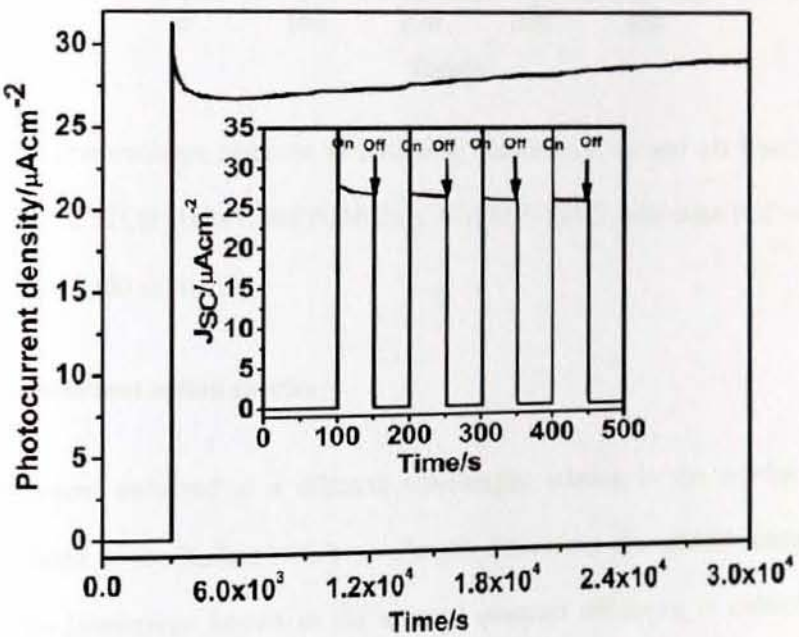

Figure 4. 4: Photocurrent response to continuous illumination with light intensity of 100 $mWcm^{-2}$ for the ITO|P3HT:PCBM|POMOE:I_3^-/I^-|PEDOT|ITO solid-state PEC from the front side. The inset shows the photocurrent response to switching illumination on and off.

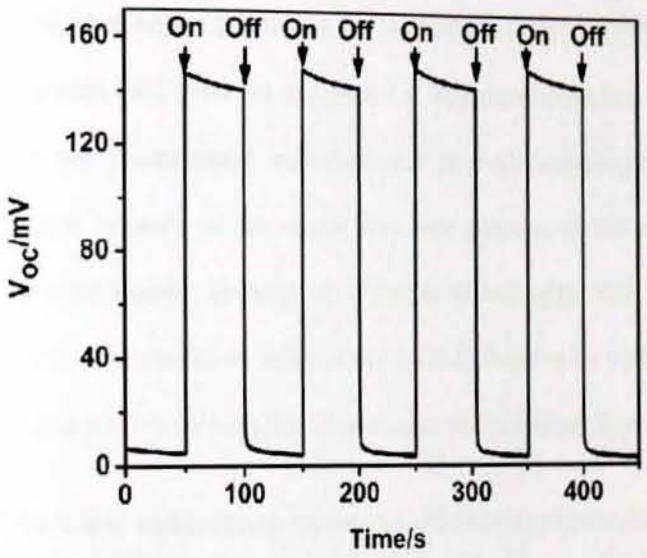

Figure 4. 5: Photovoltage response to switching illumination on and off from the front side of the ITO|P3HT:PCBM|POMOE:I_3^-/I^-|PEDOT|ITO solid-state PEC with light intensity of 100 $mWcm^{-2}$.

4.1.4. Photocurrent action spectra

The photocurrent collected at a different wavelength, relative to the number of photons incident on the surface at that wavelength, determines the spectral response of the device (sometimes known as the external quantum efficiency or collection efficiency at each wavelength). Light of different wavelengths is absorbed at different depths in the conjugated polymer film. The ability of a solar cell to generate photocurrent at a given wavelength of the incident light is measured by the incident monochromatic photon to current conversion efficiency (IPCE), defined as the number of electrons generated per number of incident photons. It can be calculated using Equation 2.19.

The photocurrent action spectrum plotted in terms of IPCE% *versus* wavelength under front- and backside illumination conditions for the ITO|P3HT:PCBM|POMOE:I_3^-/I^-|PEDOT|ITO solid-state PEC is shown in Figure 4.6. The wavelength was varied at 10 nm intervals and the photocurrent was measured at each wavelength. For each wavelength, the light intensity of the source was kept constant at 100 mW/cm^2 but correction for monochromatic intensity at different wavelengths was made when calculating the IPCE. The maximum value of the IPCE is found to be 1.52 % for front side illumination and 0.17 % for backside illumination at a wavelength of 510 nm.

Comparison of front side and backside conversion efficiencies showed that front side illumination resulted in higher conversion efficiency than backside illumination at the maximum absorbance. The reason behind this difference lies on the optical filtering effect of the P3HT:PCBM composite film. When light is illuminated from the backside, only a small fraction of the excitons (bound electron–hole pairs) produced by light absorption reach the interface to dissociate into carriers. Moreover, the presence of a high density of the traps in the film reduces the number of carriers for the photocurrent generation. The greater the distance from the surface, the smaller is the probability for an exciton to reach the interface and dissociate into carriers.

The IPCE% values at the maximum absorbance for pure P3HT-based PEC is 0.024% under front side and 0.003% under backside illumination conditions [229], and for P3HT:C_{60} composite based PEC is 0.43% under front side and 0.01% under backside [230] which is smaller than what has been presented here for the P3HT:PCBM-based PEC.

Comparison of the optical absorption spectrum and spectral photoresponse can be used to identify the active junction responsible for the photoelectrochemical

phenomena. If illumination through the front side of the PEC produces a spectral response that corresponds to the absorption spectrum of the P3HT:PCBM composite film, then P3HT:PCBM|electrolyte junction is responsible for the photoelectrochemical phenomena. If illumination from backside produces a matching spectrum, then it is the P3HT:PCBM|ITO junction that is active.

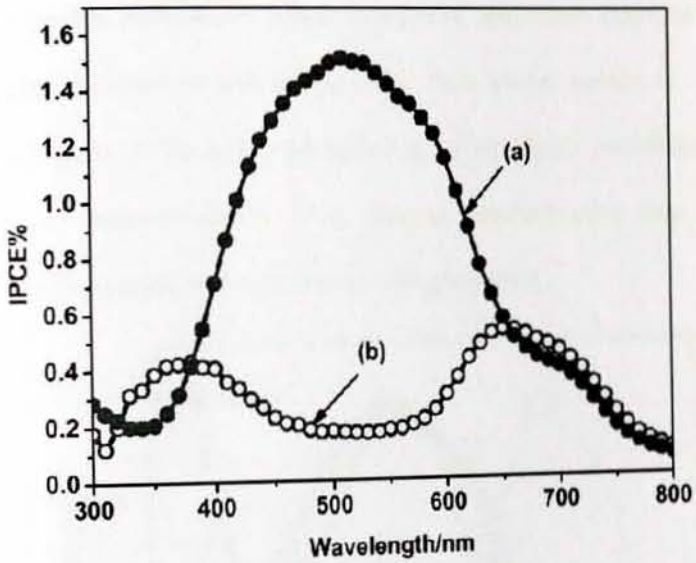

Figure 4. 6: Photocurrent action spectra for ITO|P3HT:PCBM|POMOE:I_3^-/I^- |PEDOT|ITO solid-state PEC illuminated through (a) front side and (b) backside.

The normalized absorption spectrum of the P3HT:PCBM composite film as compared to normalized photocurrent action spectra of ITO|P3HT:PCBM|POMOE:I_3^-/I^-| PEDOT| ITO solid-state PEC for front side and backside illumination conditions are shown in Figure 4.7. The wavelength dependence of the IPCE% obtained from front side illumination closely resembles the absorption spectrum of P3HT:PCBM film, indicating that the photoactive junction is the P3HT:PCBM|electrolyte interface. When illuminated through the backside, there is a mismatch between the action spectrum and the optical absorption spectrum. This can be explained as follows.

When the absorption constant is high, excitons are created very close to the ITO|photoactive layer (backside). Therefore, only a small fraction of the light reaches the barrier regions and as a result charge carriers are lost due to recombination or trapping, which decreases the photocurrent. However, at wavelengths where the absorption constant is low, light penetrates deeper and the excitons will be created much closer to the photoactive electrode/polymer electrolyte interface so that a relatively large photocurrent will be measured. Only charge carriers in or near the space charge region of the active junction have a significant probability of being collected by the external circuit. Thus, photons absorbed away from the active junction generally have no effect on photocurrent generation.

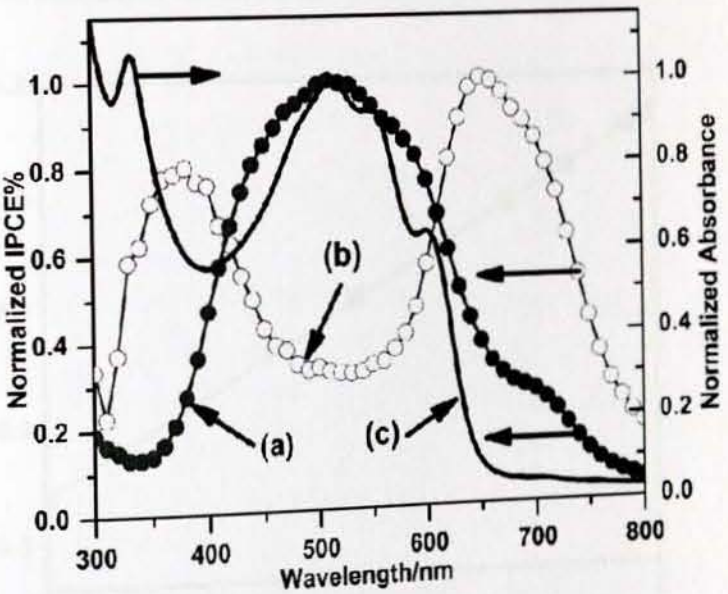

Figure 4. 7: Normalized photocurrent action spectrum of ITO|P3HT:PCBM|POMOE: I_3^-/I^-|PEDOT|ITO for illumination through (a) front side, (b) backside, and (c) normalized optical absorption spectrum of P3HT:PCBM blend deposited on glass.

4.1.5. The dependence of J_{SC} and V_{OC} on light intensity

For organic and some inorganic solar cells, the J_{SC} increases with increasing light intensity (I_{in}) and is proportional to I^{α}_{in} [243]. Thus, a plot of $\log J_{SC}$ versus $\log I_{in}$ yields a straight line whose slope is characteristic of the photoactive material. The plot of $\log J_{SC}$ versus $\log I_{in}$ of the ITO|P3HT:PCBM|POMOE:I_3^-/I^-|PEDOT|ITO solid-state PEC is shown in Figure 4.8. The illumination intensity was varied from 0.01 to 100 mWcm^{-2}. The J_{SC} increases with illumination intensity and is proportional to I_{in}^{α}, where α is the power factor and I_{in} is the incident light intensity. The plot of $\log J_{SC}$ versus $\log I_{in}$ yielded a straight line with $\alpha = 0.94$ which is close to 1. Such dependence implies there is no bimolecular recombination of excitons [243 – 246].

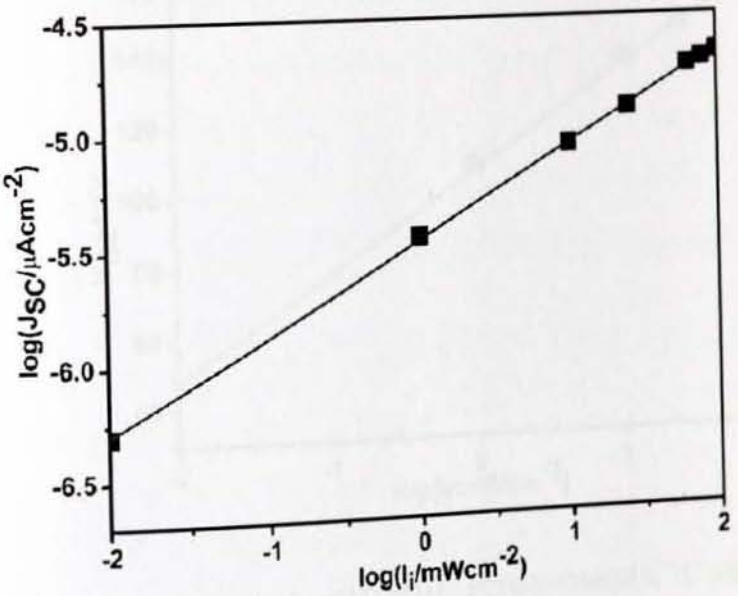

Figure 4. 8: Plot of $\log J_{sc}$ *versus* $\log I_{in}$ of ITO|P3HT:PCBM|POMOE:I_3^-/I^-|PEDOT|ITO solid-state PEC.

For Schottky junction solar cells under open-circuit conditions, no net current will flow through the junction. Thus, Equation 4.2 can be rearranged to yield the following relationship:

$$V_{OC} = \frac{nkT}{q}\ln\left[\left(\frac{I_{ph}}{I_o}\right)+1\right] \approx \frac{nkT}{q}\ln\left(\frac{I_{ph}}{I_o}\right), \text{ for } I_{ph}>>I_0 \qquad (4.3)$$

As can be seen from Equation 4.3, V_{OC} increases logarithmically with the light intensity because I_{ph} is linearly proportional to the incident light intensity. The plot of V_{OC} versus $\log I_{in}$ of the ITO|P3HT:PCBM|POMOE:I_3^-/I^-|PEDOT|ITO solid-state PEC is shown in Figure 4.9. V_{OC} increases logarithmically with the light intensity, in agreement with the projected behaviour of Schottky barrier solar cells [247].

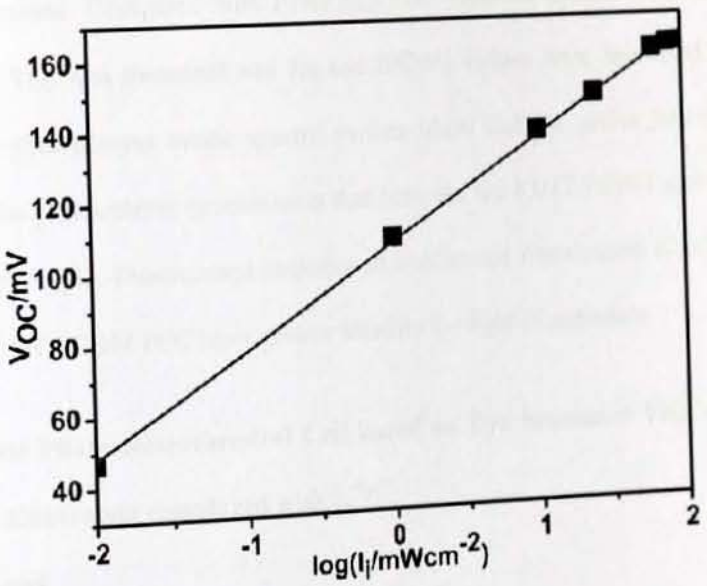

Figure 4. 9: Plot of V_{OC} versus $\log I_{in}$ of ITO|P3HT:PCBM|POMOE:I_3^-/I^-|PEDOT| ITO solid-state PEC.

4.1.6. Conclusion

In this study, a solid-state PEC was constructed from mixtures of P3HT and PCBM, in bulk heterojunction structure. Photoelectrochemical and optical properties of this organic device was studied together with the dependence of J_{SC} and V_{OC} on illumination intensity. The photoelectrochemical properties of a solid-state PEC based on blends of P3HT and PCBM were compared with the corresponding blends of P3HT and C_{60} PECs. An open-circuit voltage of 140 mV and a short- circuit current density of 28.4 $\mu A/cm^2$ at light intensity of 100 mW/cm^2; IPCE% of 1.52% for front side illumination and IPCE% of 0.17% for backside illumination at a wavelength of 510 nm were obtained. Compared with P3HT:C_{60} PEC reported earlier the results show that higher V_{OC} was measured and J_{SC} and IPCE% values were increased by many folds. The photocurrent action spectra studies show that the active junction responsible for the photocurrent generation is that between the P3HT:PCBM and the solid polymer electrolyte. Photocurrent response to continuous illumination also has shown that the P3HT:PCBM PEC has a greater stability for light illumination.

4.2. Solid State Photoelectrochemical Cell based on Dye Sensitized TiO_2 and Polymer Electrolyte complexed with I_3^-/I^-

4.2.1. Background

So far, the most successful DSSC was obtained on TiO_2 nanocrystalline film combined with a ruthenium–polypyridine complex dye, as first reported by O'Regan and Grätzel [33]. Overall conversion efficiency of 10.4% was achieved on a TiO_2–RuL'$(NCS)_3$ (black dye) system, in which the spectral response of the complex dye was extended into the near-infrared region so as to absorb far more of the incident light [7, 248, 249]. The porous nature of nanocrystalline TiO_2 films drives their use in

DSSCs due to the large surface area available for dye-molecule adsorption. Moreover, the suitable relative energy levels at the semiconductor–sensitizer interface (i.e., the position of the conduction-band edge of TiO_2 being lower than the excited-state energy level of the dye) allow for the effective injection of electrons from the dye molecules to the semiconductor [250].

Eventhough the light-to-electrical energy conversion efficiencies of DSSCs based on liquid electrolytes have reached over 10% under AM 1.5 (100 $mWcm^{-2}$) [53], there are some problems such as leakage of the electrolytes, evaporation of the solvent, and high temperature instability, which cause difficulties in sealing and performance degradation of DSSCs [251]. Enormous efforts have been devoted to solve these problems by employing solid or quasi-solid-state electrolytes that substituted the conventional volatile organic solvent-based electrolytes to fabricate DSSCs [58, 130, 169, 252]. The polymer electrolyte is an important class of the solid or quasi solid-state electrolytes for DSSCs because it has the advantages of relatively high ionic conductivity and easy solidification [79].

Previously Sergawie *et al.* [253] reported a work on regenerative type PEC based on emeraldine base form of polyaniline as a sensitizer. Here the studies made on an all-solid-state PEC constructed with nc-TiO_2 coated onto indium tin-oxide (ITO), covered with N-719 dye and used as a photoactive electrode, the ion conducting polymer poly[oxymethylene-oligo(oxyethylene)], POMOE, complexed with redox couple as a solid polymer electrolyte, and a PEDOT coated on ITO as counter electrode is presented. The polymer electrolyte POMOE, having a repeating unit of $CH_2O(CH_2CH_2O)_9$, was used since it is a good ionic conductor at room temperature [232, 234 – 236].

4.2.2. Current– voltage characteristics

The current density–voltage characteristics of the ITO|PEDOT|POMOE:I_3^-/I^-|TiO_2:Dye|ITO PEC in the dark and under illumination are shown in Figure 4.10. The device was illuminated through the ITO|TiO_2:Dye side using white light the intensity of which is approximately 100 mW/cm^2. The current density–voltage characteristic of the polymer electrolyte/TiO_2:Dye interface in the dark obeys the diode equation as depicted in Equation 4.1. The forward current corresponds to a positive bias where the barrier height is lowered, whereas in reverse polarization the increased barrier prevents the passage of a current.

Under illumination, absorption of photons initially creates excitons, and later both the majority and the minority carriers. The concentration of photogenerated majority carriers is usually small. This implies that illumination does not significantly perturb the majority carrier. Because the majority carrier concentrations are essentially unchanged, the majority charge flow is also unchanged. Majority carriers should thus exhibit the J–V characteristics that is well described by the diode equation, regardless of whether it is in the dark or under illumination. The current under illumination can generally be described by adding the current from photogenerated carriers to the dark current (Equation 4.2).

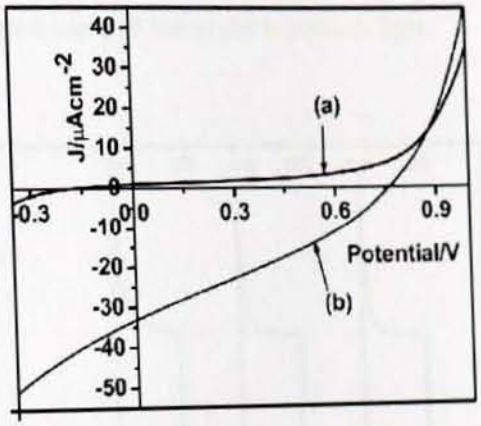

Figure 4. 10: Current density-voltage characteristics of ITO|PEDOT|POMOE:I_3^-/I^- |TiO_2:N719|ITO cell (a) in the dark and (b) under illumination through front side with light intensity of 100 $mWcm^{-2}$.

As it is depicted in Figure 4.10. the short circuit current density (J_{SC}) and the open circuit voltage were measured to be 33.2 $\mu A/cm^{-2}$ and 762 mV, respectively. The fill factor which is the measure of the squareness of the output characteristics was calculated to be 0.32.

4.2.3. The dependence of J_{SC} and V_{OC} on illumination time

Time dependence of short-circuit current density (J_{SC}) and open circuit voltage (V_{OC}) was studied for the hybrid PEC through illumination with a white light intensity of 100 $mWcm^{-2}$. The short circuit current density and open circuit voltage induced by periodically blocking the light path to the sample are shown in Figures 4.11 and 4.12, respectively. When the light is switched on, the photocurrent rises to a steady-state value of about 35 μAcm^{-2} and decays at approximately the same rate to zero current

when the light is switched off. As can be seen from changes in photocurrent with time of illumination, the photoactive material seems stable towards light.

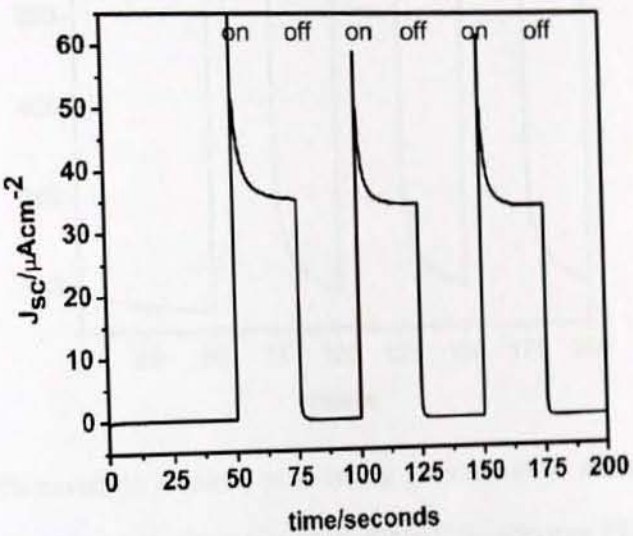

Figure 4. 11: Photocurrent response to transient illumination with light intensity of 100 $mWcm^{-2}$ for the ITO|PEDOT|POMOE:I_3^-/I^-|TiO_2:N719|ITO solid-state PEC from the front side.

The photovoltage, on the other hand, increased immediately (Figure 4.12) when the cell was illuminated and remained steady during illumination; it decayed slowly after stopping the illumination. Open-circuit voltage obtained from the transient measurements was 771 mV. The results of time dependence study show that the steady state J_{SC} and V_{OC} values are consistent with those obtained from the current density–voltage curve.

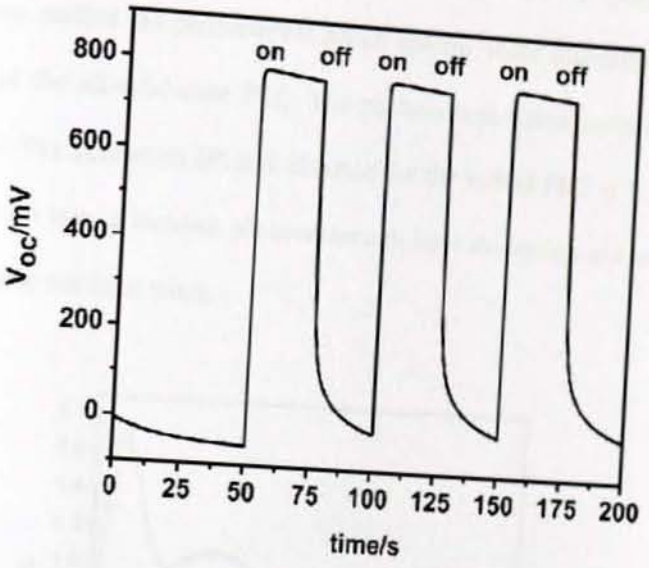

Figure 4. 12: Photovoltage response to switching illumination on and off from the front side of ITO|PEDOT|POMOE:I_3^-/I^-|TiO_2:N719|ITO solid-state PEC with light intensity of 100 mWcm^{-2}.

4.2.4. Photocurrent Action Spectra

In conventional inorganic semiconductor solar cells, the absorption with a photon of energy greater than the bandgap leads to a direct generation of an electron-hole pair that is separated by the built-in electric field; the charges are transported to opposite electrodes and produce a photocurrent. However, in molecular semiconductors [254-259], the absorption of a photon creates an exciton rather than free charge carriers. To generate photocurrent, these excitons must dissociate into free carriers either in the bulk or at the interface. Based on experimental results obtained from many molecular semiconductor solar cells, only those excitons that reach the active junction produced free charge carriers. The excitons reach this interface by diffusion, then dissociate into carriers that are transported to opposite electrodes for collection.

To verify the generation of charge carriers at the ITO|TiO_2:N719 polymer electrolyte interface, we studied the photocurrent action spectra under illumination through the front side of the all-solid-state PEC. The photocurrent action spectra are shown in Figure 4.13. The maximum IPCE% obtained for the hybrid PEC is 1.7% at 330 nm. Corrections for loss of incident photons through light absorption and reflection of the electrodes have not been made.

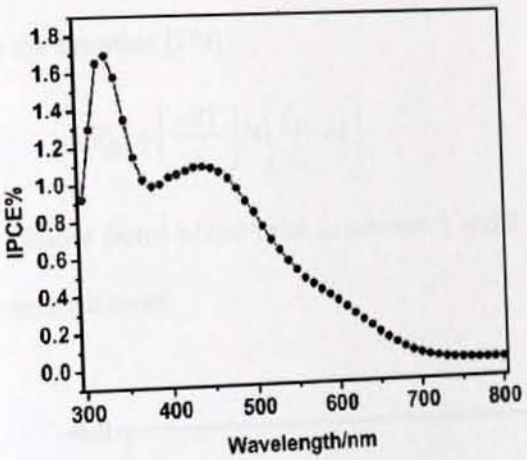

Figure 4. 13: Photocurrent action spectra for ITO|PEDOT|POMOE:I_3^-/I^-|TiO_2:N719 |ITO solid-state PEC.

4.2.5. The dependence of J_{SC} and V_{OC} on light intensity

The maximum open-circuit photovoltage attainable in the dye sensitized solar cell is the difference between the Fermi level of the solid under illumination and the Nernst potential of the redox couple in the electrolyte. However, for these devices this limitation has not been realized and V_{OC} is in general much smaller. It appears that V_{OC} is kinetically limited and for an n-type semiconductor in a regenerative cell the diode Equation 2.10 can be applied [260].

The plot of $\log J_{SC}$ versus $\log I_{in}$ of the ITO|PEDOT|POMOE:I_3^-/I^-|TiO_2:Dye|ITO PEC is shown in Figure 4.14. The illumination intensity was varied from 0.01 to 100 $mWcm^{-2}$. The J_{SC} increases with illumination intensity and is proportional to I^{α}_{in}, where α is the power factor and I_{in} is the incident light intensity. The plot of $\log J_{SC}$ *versus* $\log I_{in}$ yielded a straight line with $\alpha = 0.98$ indicating that recombination traps are absent. For Schottky junction solar cells under open-circuit conditions, no net current will flow through the junction. The gain in open circuit voltage can be calculated from the Equation [249]:

$$V_{OC} = \left(\frac{nRT}{F}\right) \ln\left[\frac{I_{SC}}{I_0} - 1\right] \qquad (4.4)$$

where n is the ideality factor whose value is between 1 and 2 for the DSSC and I_0 is the reverse saturation current.

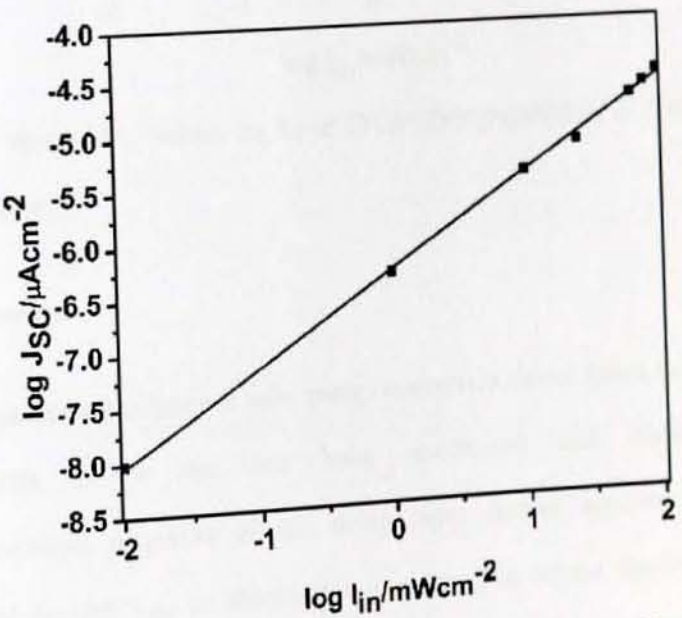

Figure 4. 14: Plot of $\log J_{sc}$ *versus* $\log I_{in}$ of ITO|PEDOT|POMOE:I_3^-/I^-|TiO_2:N719 |ITO solid-state PEC.

As can be seen from Equation 4.4, V_{OC} increases logarithmically with the light intensity because J_{SC} is linearly proportional to the incident light intensity. The plot of V_{OC} *versus* $\log I_{in}$ of the ITO|PEDOT|POMOE:I_3^-/I^-|TiO_2:Dye|ITO PEC is shown in Figure 4.15. V_{OC} increases logarithmically with the light intensity.

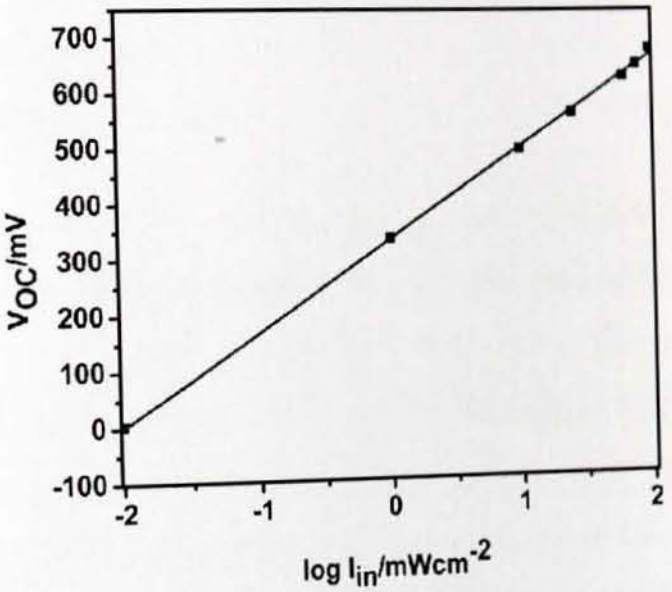

Figure 4. 15: Plot of V_{oc} versus log I_{in} of ITO|PEDOT|POMOE:I_3^-/I^-|TiO_2:N719 |ITO solid-state PEC.

4.2.6. Conclusions

A solid-state photoelectrochemical solar energy conversion device based on nc-TiO_2 sensitized with N-719 dye has been constructed and characterized. Photoelectrochemical properties of this device were studied together with the dependence of J_{SC} and V_{OC} on illumination intensity. The current density–voltage characteristics in the dark and under white light illumination and action spectra under monochromatic illuminations have been studied. The following device parameters were obtained: an open-circuit voltage of 762.5 mV and a short circuit current of 33.2

$\mu A/cm^2$ at light intensity of 100 mW/cm^2; the IPCE% obtained was 1.7% at 330 nm. The dependence of the short-circuit current density and an open-circuit voltage on the incident light intensity and illumination time have also been studied. The dependence of J_{SC} on intensity indicated that there are no traps.

4.3. Natural Dye sensitized Solar Cells using Pigments Extracted from *Syzygium guineense*

4.3.1. Background

Synthetic organic dyes [261 – 263] and transition metal coordination compounds, mostly ruthenium polypyridil complexes [53, 248], have been used as effective sensitizers, since they couple broad and intense charge transfer bands to favorable ground and excited state energies for the electron injection reactions from the excited dye to TiO_2 and the regeneration of the oxidized dye with iodide. However, the preparation routes for metal complexes are often based on multi-step procedures involving tedious and expensive chromatographic purification procedures. In order to replace the rare and expensive Ru(II) compounds many kinds of organic synthetic dyes have been actively studied and tested as low-cost materials: chlorophyll derivatives [203], porphyrins [264], phtalocyanines [73], carboxylated derivatives of anthracene [265], and coupled semiconductors with lower energy band-gaps, among others.

Natural dyes are substances that can easily be obtained from fruit, vegetable, leaves, and flowers through solvent extraction and can be employed in dye sensitized photoelectrochemical cells. To date, selected chlorophyll derivatives, raw anthocyanin, and betalain extracts are the most successful natural sensitizers, resulting in the generation of monochromatic photon to current conversion efficiency

exceeding 60% for liquid state photoelectrochemical cell. Maximum overall conversion efficiencies above 2% under simulated sunlight have been achieved, which is comparable to that of natural photosynthesis [203, 198].

Fruit, vegetable, leaves, and flowers contain several dyes which can easily be extracted and employed in dye sensitized solar cells. For instance, Tennakone et al. [266] investigated the use of tannins and related phenolic substances extracted from black tea, nuts, and pomegranate, as well as anthocyanins from flowers and leaves. The pigments contained in the flowers of Hibiscus species are anthocyanins such as cyanidin-3-glucoside and delphinidine-3-glucoside [267]. Recently Zhou et al. [268] also investigated 20 natural dyes extracted from natural materials such as flowers, leaves, fruits, traditional Chinese medicines, and beverages as sensitizers. Among the 20 natural dyes an ethanol extract of mangosteen pericarp without further purification gave a power conversion efficiency of 1.17%.

In this work natural pigment was extracted from fruits of Dokma (*Syzygium guineense*). To the best of our knowledge dye from fruits of *Syzygium guineense* are not reported as sensitizers of DSSCs. The extracted dye was characterized by UV-vis absorption spectra. The photoelectrochemical properties of the quasi–solid–state DSSCs using these extracts as sensitizer and polymer polyvinylpyrrolidone (PVP) mixed with 1-ethyl-3-methylimmidazolium iodide (EMIm-I), sodium iodide and iodine as quasi–solid–state electrolyte were investigated. Additionally, stepwise purification of the extract was performed and the photovoltaic properties of DSSCs sensitized with purified products were studied.

Polyvinyl pyrrolidone (PVP) deserve a special attention among the polymers because of good environmental stability, easy processability, moderate electrical conductivity,

and rich information in charge transport mechanism [269]. PVP is a nitrogen-containing heterocyclic polymer, which can form PVP-I_2 by reaction with I_2 (Equation (4.5)) [270].

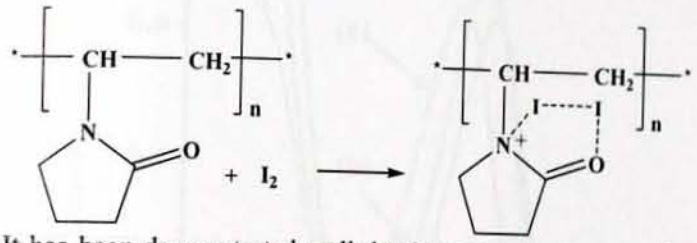

(4.5)

It has been demonstrated well that N-containing heterocycles can enhance the open-circuit photovoltage (V_{OC}) of the solar cell [113].

4.3.2. Absorption of the natural dyes

We attempted to use the extracted colorful natural dye as sensitizers for DSSCs. Figure 4.16 shows the representative UV–vis absorption spectra for the ethanol, methanol, and water extracted fruits of *Syzygium guineense*. As shown in Figure 4.16, the absorption peak show negative solvatochromism, resulting in a blue-shift as the solvent polarity increases. Such solvent-induced shifts are usually interpreted in terms of the different solvation interactions between the polar groups of the dye molecule and the solvent, and mainly depend on solvent polarity and hydrogen-bond [271]. The ethanol, methanol, and water extracts exhibit an absorption peak of about 540 nm, 530 nm, and 520 nm, respectively. These absorption peaks indicate that anthocyanins are present, a group of natural phenolic compounds. The chemical adsorption of these dyes on the surface of nanostructured TiO_2 is generally accepted to occur because of the condensation of alcoholic-bound protons with the hydroxyl groups [272].

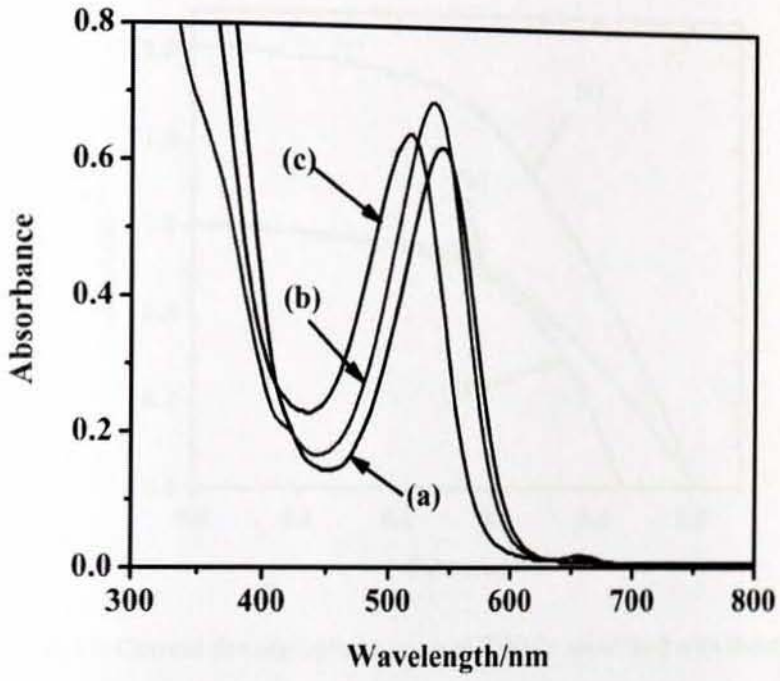

Figure 4. 16: Light Absorption spectra of dye solution of fruits of *Syzygium guineense* extracted from (a) ethanol (b) methanol and (c) water.

4.3.3. Effect of extracting solvent on DSSC's efficiency

Effect of extracting solvent on DSSC performance was studied by varying the solvent. Three different solvents; water, methanol, and ethanol were used as extracting solvent. The typical J–V curves of the DSSCs fabricated with the dyes extracted from *Syzygium guineense* using methanol, ethanol, and water as extracting solvent are shown in Figure 4.17. The PEC parameters obtained are given in Table 4.2. The respective photocurrent action spectra are given in Figure 4.18.

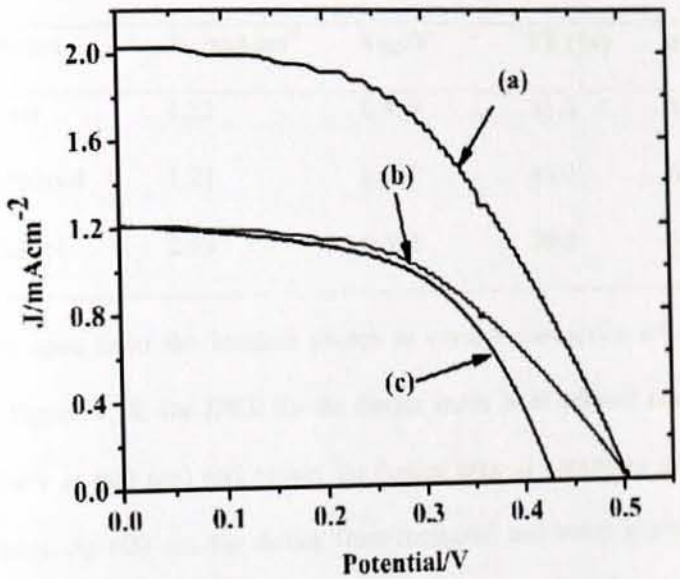

Figure 4. 17: Current density-voltage curve of DSSCs sensitized with the dye of fruits of *Syzygium guineense* extracted with (a) ethanol (b) methanol and (c) water.

It was reported that the extracting solvent has an effect on the efficiency of DSSCs [273]. The efficiency of the DSSCs was found to increase immensely when ethanol was used for extracting anthocyanin from aged Jaboticaba skin [273]. In this study, similar finding was also obtained. As shown in Table 4.2, the DSSC fabricated from extract obtained using ethanol as a solvent shows the highest power conversion efficiency than using water and methanol. This might owe to the fact that anthocyanin is more soluble in ethanol [274], and hence, the aggregation of dye molecules is less as expected. A good dispersion of dye molecules on the oxide surface could in fact improve the efficiency of the system.

Table 4. 2: Effect of extracting solvent on DSSC efficiency of *Syzygium guineense*.

Solvent	J_{SC}/mAcm^{-2}	V_{OC}/V	FF (%)	η (%)
Water	1.22	0.430	55.0	0.30
Methanol	1.21	0.507	49.0	0.30
Ethanol	2.03	0.506	50.0	0.51

As can be seen from the incident photon to current conversion efficiency (IPCE) curves in Figure 4.18, the IPCE for the device made from ethanol extract dye is the highest (24% at 600 nm) and covers the largest area as compared to methanol and water extract. At 600 nm the device from methanol and water extract dye showed IPCE values of 14.4% and 12%, respectively. The IPCE onset of the device from ethanol extract dye starts at the longest wavelength as compared to methanol and water extract. The difference in the IPCE values between the devices is consistent with their difference in short circuit current values.

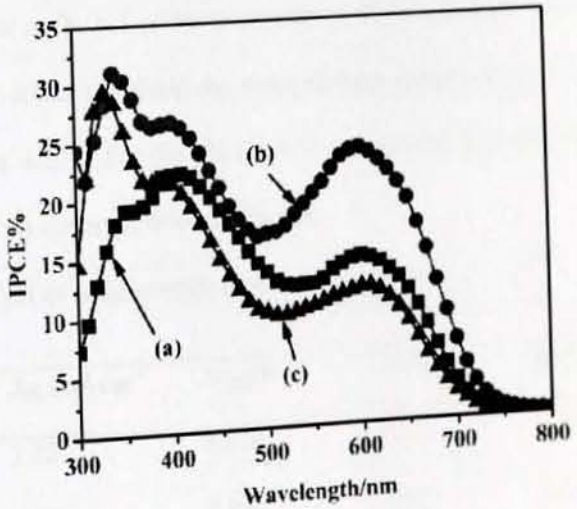

Figure 4. 18: IPCE spectra of the dye fruits of *Syzygium guineense* extracted from (a) methanol (b) ethanol and (c) water.

4.3.4. Effect of pH of extract solutions on DSSC's efficiency

The chemical structure of anthocyanin is shown in Figure 2.15 (Chapter 2). Equilibrium between flavylium and quinonoidal form of anthocyanins in solution and in presence of TiO_2 to bind with the anthocyanin is shown in Figure 2.16 (Chapter 2). Irrespective of the kind of solvent, upon changing the pH the relative amounts of the flavylium and quinonoidal forms of the dye will be affected shifting the equilibrium to either side. For this reason the effect of pH investigated in this study was for water extract of fruits of *Syzygium guineense*. The original pH of this extract was found to be 3.3. As shown in Table 4.3, the pH of the extract solution has a significant effect on the performance of DSSCs. The efficiency was found to increase with decreasing pH and reached a maximum at the optimum pH 1.0. The reason for this is at pH below 2.0 anthocyanin exists as flavylium ion (Figure 2.16 (a)), which is stable form of anthocyanin [275]. The pH dependence of absorption spectra also shows that the peak intensity first increases with pH and then decreases as shown in Figure 4.19. It has been observed that as the pH of the water extract of *Syzygium guineense* fruit dye decreases from 3.3 to lower pH value, the color changes progressively from light red to intense red (Figure 4.20). For the pH below 1.0 the color gradually disappeared. This might be due to the decomposition of the dye.

Table 4. 3: Effect of pH of water extract on DSSC parameters.

pH	J_{SC}/mAcm^{-2}	V_{OC}/V	FF (%)	η (%)
3.3	1.22	0.430	55.0	0.30
2.0	1.58	0.401	49.4	0.32
1.0	2.20	0.404	40.0	0.35
0.5	1.20	0.397	48.0	0.23

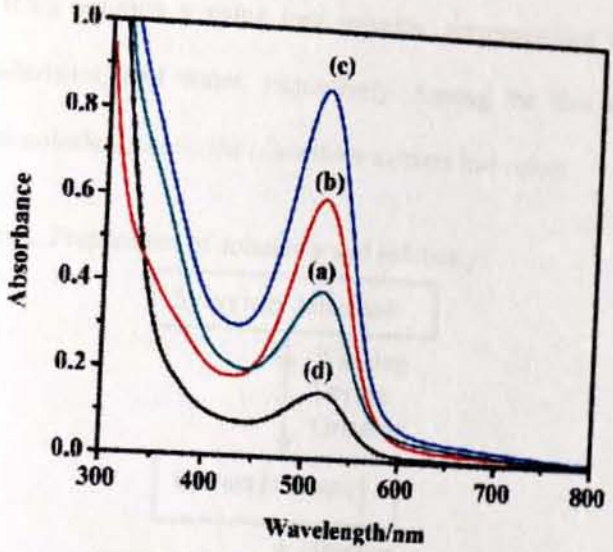

Figure 4. 19: Light absorption spectra for the water extract of the dye solution of *Syzygium guineense* at (a) pH of 3.3 (b) pH of 2.0 (c) pH of 1.0 and (d) pH of 0.5.

Figure 4. 20: Aqueous extract of *Syzygium guineense* at different pH values.

4.3.5. Purification and characterization of extracts from fruits of *Syzygium guineense*

Flow chart I and II presents the whole purification process of the extract from fruits of *Syzygium guineense*. As shown in Flowchart I, two kinds of extracts were obtained from *Syzygium guineense*, denoted as solution x and solution y, respectively. Solution y was further purified, as displayed in Flowchart II. Four kinds of extracts were

obtained from solution y using four solvents, corresponding to chloroform, ethyl acetate, n-butanol, and water, respectively. Among the four extracts, chloroform extract was colorless, while the other three extracts had colors.

Flow chart I: Preparation of solution x and solution y.

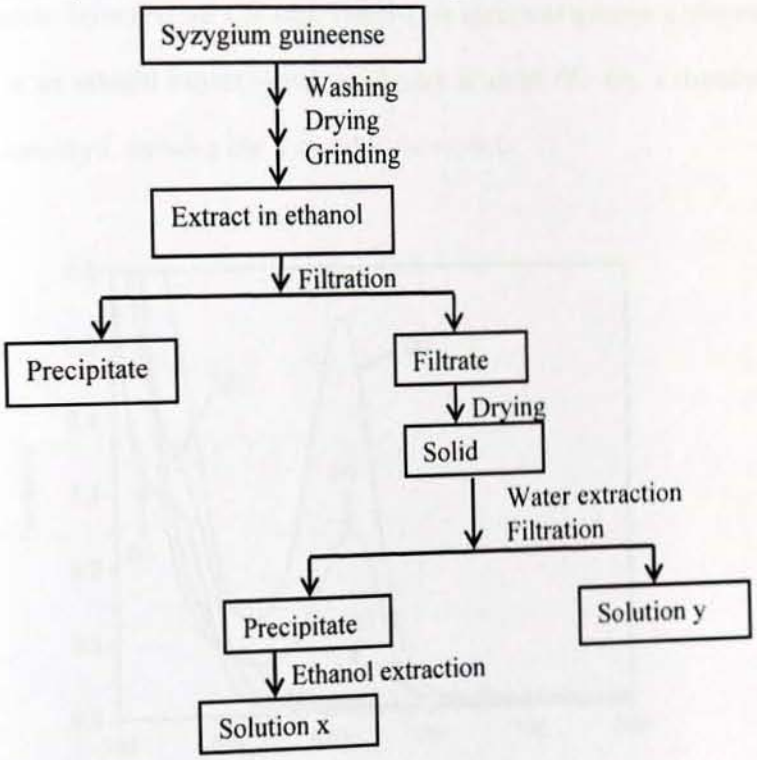

Flow chart II: Solvent-solvent extraction from solution y.

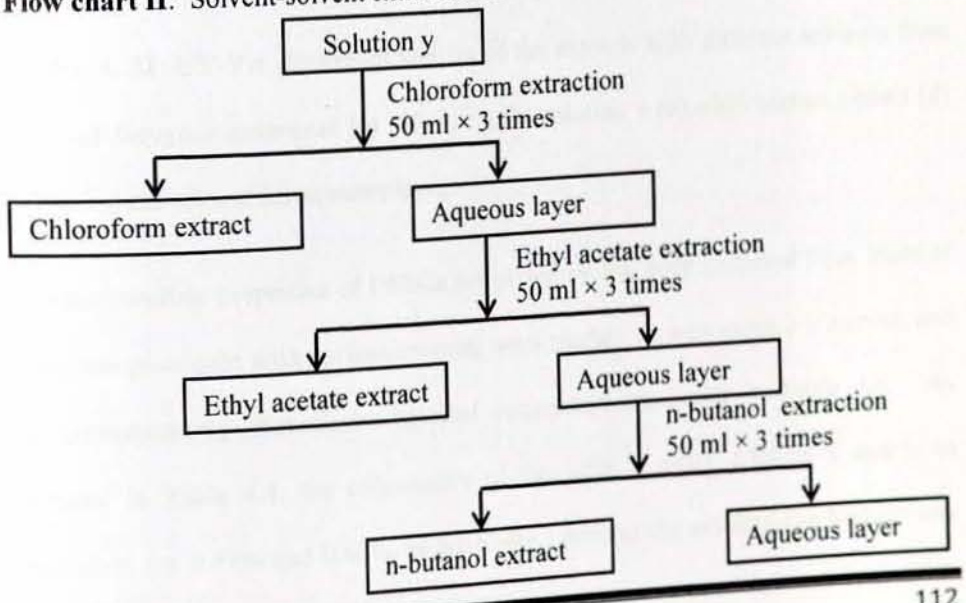

The UV-vis spectra of solution x and solution y and the remaining three extracts displayed in Figure 4.21 were investigated; the extracts with different solvents exhibit different absorption peaks, and the absorption of solution y (Figure 4.21 (b)) is the superposition of the ethyl acetate (Figure 4.21 (c)), n-butanol (Figure 4.21 (d)) extract and the aqueous layer (Figure 4.21 (e)). The UV-vis spectra of solution x (Figure 4.21 (a)) which is an ethanol extract shows small peak at about 665 nm, a characteristic peak for chlorophyll, showing that it contains chlorophyll.

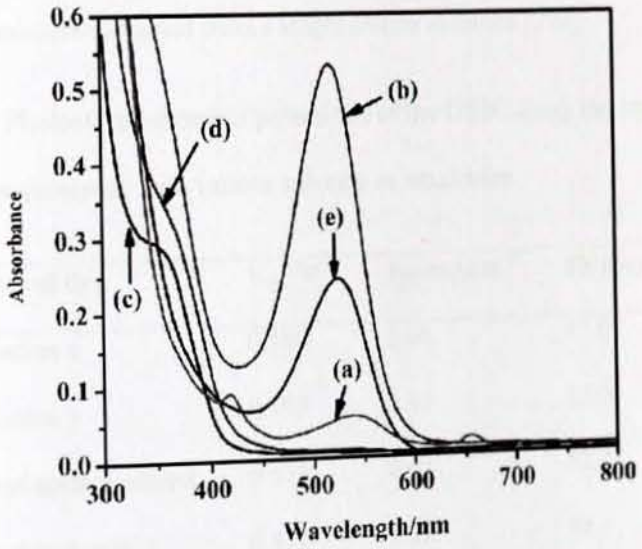

Figure 4. 21: UV-Vis absorption spectra of the extracts with different solvents from fruits of *Syzygium guineense* (a) solution x (b) solution y (c) ethyl acetate extract (d) n-butanol extract and (e) aqueous layer.

The photovoltaic properties of DSSCs sensitized by the dyes extracted from fruits of *Syzygium guineense* with various solvents were studied by measuring J-V curves, and the corresponding photoelectrochemical parameters are listed in Table 4.4. As depicted in Table 4.4, the efficiencies of the DSSCs using solution x and y as sensitizers are 0.49% and 0.40%, respectively. Among the extracts, the highest was

obtained with aqueous layer. The efficiency of DSSC with y as sensitizer is more or less comparable with the sum of the efficiencies of DSSCs sensitized with ethyl acetate, n-butanol extracts, and aqueous layer. This result indicates that the mixed extract adsorbed on TiO_2 shows synergistic photosensitization compared with individual extracts. Such behavior was also reported by Kumara et al. [276]. The efficiency of the DSSC sensitized with the extract containing shisonin and chlorophyll was 1.31%, which was about the sum of the efficiencies of DSSCs sensitized with shisonin (1.01%) and chlorophyll (0.58%). This was due to synergistic sensitization by the dye mixture extracted from a single natural resource [276].

Table 4. 4: Photoelectrochemical parameters of the DSSC using the extracts of fruits of *Syzygium guineense* with various solvents as sensitizers.

Natural dye	**V_{OC}/V**	**J_{SC}/mAcm^{-2}**	**FF (%)**	**η (%)**
Solution x	0.500	2.08	47.0	0.49
Solution y	0.395	2.92	35.0	0.40
Ethyl acetate extract	0.475	0.63	52.2	0.16
n-butanol extract	0.412	0.29	49.1	0.06
Aqueous layer	0.437	1.12	44.0	0.22

4.3.6. Conclusions

Dyes obtained from nature, i.e. from fruits *Syzygium guineense* were used as sensitizers in DSSCs. The dyes extracted from this material contained anthocyanin, carotene, chlorophyll, etc. The highest photoelectrochemical performance of the quasi-solid state DSSCs based on these dyes was observed for ethanol extract with V_{OC} of 0.506 V, J_{SC} of 2.03 mAcm^{-2}, and power conversion efficiency of 0.51%.

Furthermore, the ethanol extract was further purified stepwise. The photoelectrochemical performance for the extracts with different solvents indicated that the individual components have synergistic effect in the performance of the DSSC. Overall, natural dyes as sensitizers of DSSCs are promising because of their simple preparation technique, wide availability, environmental friendliness, and low-cost production.

4.4. Solar Energy Conversion based on Quasi-Solid State Dye-Sensitized Solar Cells using Leaf and flower Extracts as Sensitizers

4.4.1. Background

Natural dyes containing anthocyanins [273, 277 – 280] and carotenoids [281] have shown overall solar energy conversion efficiencies below 1%. Betalain pigments represent an additional class of dyes of potential interest and purified extracts from commercial sources have been subjected to a detailed photoelectrochemical study [200]. These dyes are present in plants of Amaranthaceae family and have high molar extinction coefficients in the visible region. The pigments are present in the different part of the plant including flowers, fruits, leaves, stems, and roots.

Natural dyes, such as chlorophyll derivatives, have previously been used to sensitize TiO_2 nanocrystalline solar cells, achieving efficiencies of 2.6% and short circuit current density of 9.4 mA/cm^2, but these dyes still require involved pigment purification and the coadsorption of other compounds on the TiO_2 surface [202]. Tennakone and co-workers[125] have used cyanidin (cyanin without the sugar moiety) in a dye sensitized nanocrystalline solar cell. However, cyanidin is harder to isolate and less photostable than cyanin [266].

Here the results of a series of experiments carried out on raw extracts of the following species: leafs of *Amaranthus caudatus* and *Iresine herbstii*, and flower of morning glory (*Ipomoea indica*) and Karkade (*Hbiscus sabdariffa*) are presented. *A. caudatus*, as with many others of the amaranths, are originally from the American tropics. The exact origin is unknown, as it is believed to be a wild *Amaranthus hybridus* aggregate. The red color of the inflorescences is due to a high content of betacyanins, like in the related species known as "Hopi red dye" amaranth. *I. herbstii* also consists of a high content of betacyanins. The prevailing pigment coloration of *A. caudatus* and *I. herbstii* varies form orange to red, due to the combination of two main dyes: betacyanin (red-purple) and indicaxanthin (yellow-orange) whose schematic structures are reported in Figure 2.19 and Figure 2.20 (Chapter 2) [282]. As shown in these figures, these dyes contain carboxylic functions which facilitate TiO_2 surface binding. The main component of the 0.1 M HCl extract of *A. caudatus* and *Iresine herbstii* is betalains.Whereas the respective ethanol extract is chlorophyll (Figure 2.22 shows these families of compounds). The main component of the ethanol and 0.1 M HCl extracted dye from flower of *Ipomoea indica* and *Hibiscus sabdariffa* is anthocyanin (Figure 2.15 in Chapter 2).

In this work natural pigment was extracted using 0.1 M HCl and ethanol. The extracted dye was characterized by UV-vis absorption spectra. The photoelectrochemical properties of the quasi–solid–state DSSCs using these extracts as sensitizer and polymer polyvinylpyrrolidone (PVP) mixed with 1-ethyl-3-methylimmidazolium iodide (EMIm-I), sodium iodide and iodine, as quasi-solid state electrolyte were investigated [208].

4.4.2. Absorption Spectra of Raw Natural Dye Extract

Betalain extracted from Leafs of *A. caudatus* and *I. herbstii* in 0.1 M HCl solution displayed an intense absorption in the 400 – 600 nm region due to the presence of the red-purple betacyanines (Figure 4.22). These absorption bands originate from $\pi-\pi^*$ transitions and DFT calculations carried out on betanidin [283] have pointed out its essential charge transfer character, with the LUMO centered on the dihydropyridine portion of the molecule. Compared to neutral extracts, dyes extracted in acidic conditions present a stronger absorption contribution at lower wavelengths, indicating an increase of the indicaxanthin concentration [284]. This is consistent with the fact that indicaxanthin is mainly contained in vacuoles whose membranes are lysed in acidic conditions.

As previously observed by other authors [200], the acidic environment was essential for obtaining betalain sensitized photo-electrodes characterized by high optical densities, capable of an almost complete absorption of visible photons in the 400 – 600 nm range. The reason is most probably related to protonation of betalainic carboxylic groups which are otherwise unable, in their anionic form to bind to the TiO_2 surface. The conditions of dye extraction have also an effect on the light harvesting efficiency of the sensitized photoanodes [284]. It was found that the absorption peak of 0.1 M HCl extract for both *A. caudatus* and *I. herbstii* is about 530 nm and 536 nm, respectively and the absorption band from 400 nm to 600 nm.

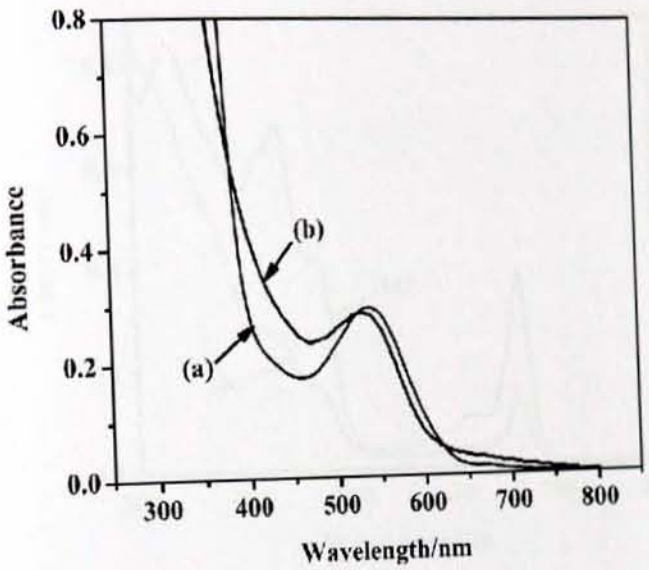

Figure 4. 22: UV-Vis spectrum of leaf extracts in 0.1 M HCl solution (a) of *I. herbstii* showing betanin (536 nm) and (b) of *A. caudatus* showing betanin (530 nm) visible absorption.

The ethanol extracts of *A. caudatus* and *I. herbstii* leaf, whose colors are green, reach a maximum absorption peak of 433 nm and 664 nm which is a characteristic peak of chlorophyll a. It also shows absorption maxima at 466 nm and small peak at 618 nm showing the presence of chlorophyll b. Figure 4.23 shows the representative UV-vis absorption spectra of ethanol extracts of these plant materials.

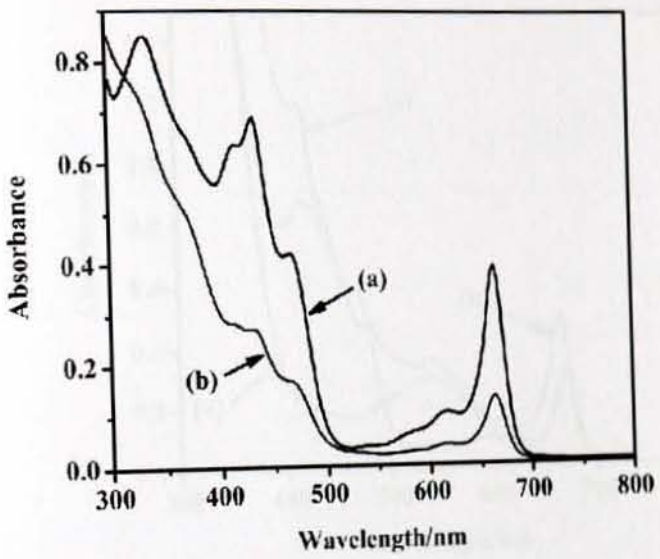

Figure 4. 23: UV-Vis spectrum of leaf extracts in ethanol for (a) *I. herbstii* and (b) *A. caudatus*

Figure 4.24 shows the UV–vis absorption spectra of the dyes extracted from ethanol and 0.1 M HCl for *I. herbstii,* and their mixtures. It was found that the absorption peak of 0.1 M HCl extract for *I. herbstii* is about 536 nm and the absorption band from 400 nm to 600 nm while those of ethanol extract show absorption peak at 433 nm, 466 nm, 618 nm, and 664 nm and absorption band from 400 nm to 500 nm and from 600 nm to700 nm. The difference in the absorption characteristics of the dyes extracted in these two solvents is due to the different types of pigments namely betalains and chlorophylls, respectively. The combination of the ethanol and 0.1 M HCl extracts of *I. herbstii* did not affect the absorption peaks, the distinct peaks were detected, corresponding to the absorption nature of both extracts.

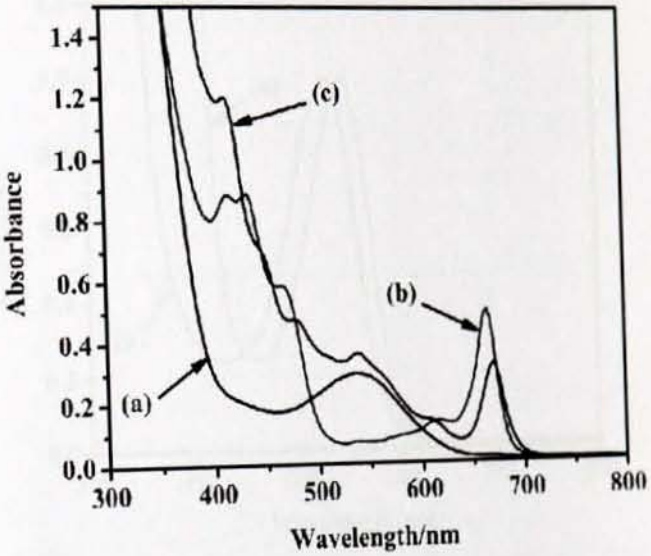

Figure 4. 24: UV-Vis spectrum of leaf extracts for *I. herbstii* (a) in 0.1 M HCl (b) in ethanol and (c) mixture of dyes extracted in ethanol and 0.1 M HCl.

Figure 4.25 shows the representative UV–vis absorption spectra for the ethanol and 0.1 M HCl solution extracted from flowers of of *I. indica* and Figure 4.26 shows the representative UV–vis absorption spectra for the ethanol and 0.1 M HCl solution extracted from flowers of *H. sabdariffa*. The ethanol and 0.1 M HCl extracts of *I. indica* exhibit an absorption peak of about 550 nm and 530 nm respectively whereas the ethanol and 0.1 M HCl solution extracts of *H. sabdariffa* exhibit an absorption peak of about 550 nm and 520 nm, respectively. These absorption peaks indicate the presence of anthocyanins. The chemical adsorption of these dyes on the surface of nanostructured TiO_2 is generally accepted to occur because of the condensation of alcoholic-bound protons with the hydroxyl groups [272].

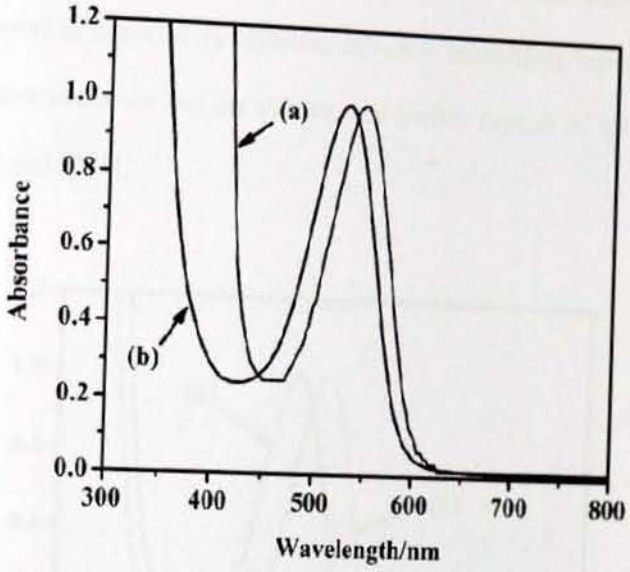

Figure 4. 25: UV-Vis spectrum of leaf extracts solution of *I. indica* (a) in ethanol showing anthocyanin (550 nm) visible absorption and (b) in 0.1 M HCl showing anthocyanin (530 nm).

Solvatochromic properties of squaraine dyes have been extensively investigated. As studies on solvatochromic and molecular hyperpolarizability studies of unsymmetrical squaraine dyes have indicated that these dyes possess large dipole in the ground state compared to their excited state [285], which would result in a very large solvent reorganization following the excitation process. This is the reason why unsymmetrical squarine dyes become solvent polarity sensitive showing solvatochromism. S. Alex et al. [286] studied the dependence of absorption maxima of unsymmetrical squaraine dyes as well as that of two representative symmetrical squaraines in common solvents. This study indicated that the unsymmetrical squaraine dyes showed hypsochromic shift with increasing solvent polarity.

Similarly, anthocyanins, being unsymmetrical molecules, are expected to show solvatochromism. As shown in Figure 4.25 and Figure 4.26, the absorption peaks

show a blue-shift as the solvent polarity increases. Such solvent-induced shifts are usually interpreted in terms of the different solvation interactions between the polar groups of the dye molecule and the solvent, and mainly depend on solvent polarity and hydrogen-bond [271].

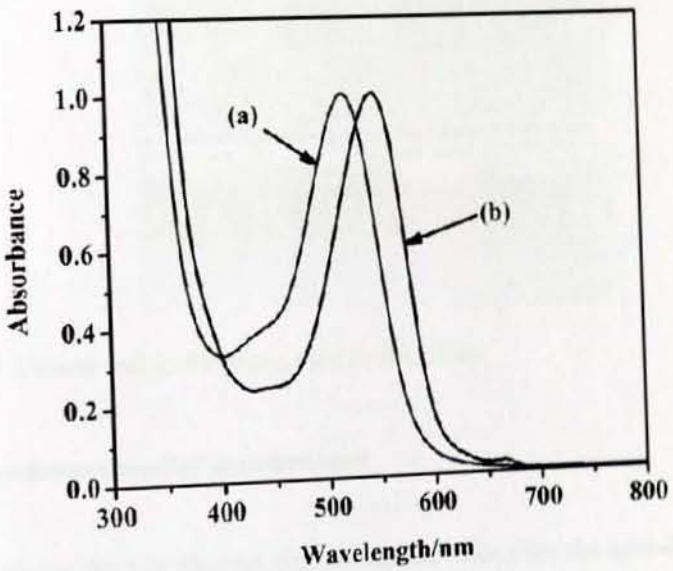

Figure 4. 26: UV-Vis spectrum of leaf extracts solution of *H. sabdariffa* (a) in 0.1 M HCl showing anthocyanin (520 nm) and (b) in ethanol showing anthocyanin (550 nm).

Figure 4.27 depicts the ethanol and 0.1 M HCl extract dye solutions of flower and leaf used in this study.

Figure 4. 27: Flower and leaf extracts used in this study.

4.4.3. Photoelectrochemical measurement

Figure 4.28 shows the J–V (current density–voltage) curve for the light-illuminated *I. herbstii* extract sensitized solar cell. A DSSC sensitized by a mixed extract had efficiency below value of those sensitized with purely ethanol and 0.1 M HCl extracts. However, this is rather different from the result by Kumara et al. [276], in which a DSSC fabricated using chlorophyll and shisonin dyes showed synergistic effect of both dyes. Although the mixture of 0.1 M HCl and ethanol extract of *I. herbstii* absorbs wider range of the visible spectrum compared with the individual dye's absorption spectra, the mixed dye does not show synergistic characteristics (Figure 4.24). We hypothesize two possible reasons for this phenomenon in which the mixed extract of *I. herbstii* did not show synergistic photosensitization. First, the coadsorption suppresses electron injection possibly due to the increase in concentration quenching. Second, the strong steric hinderance of basic molecular

structures for the main components of the extracts of *I. herbstii* with various solvents prevents the dye molecules from effectively arraying on the TiO_2 film. Hence, this leads to a deficiency of electron transfer from dye molecules to conduction band of TiO_2.

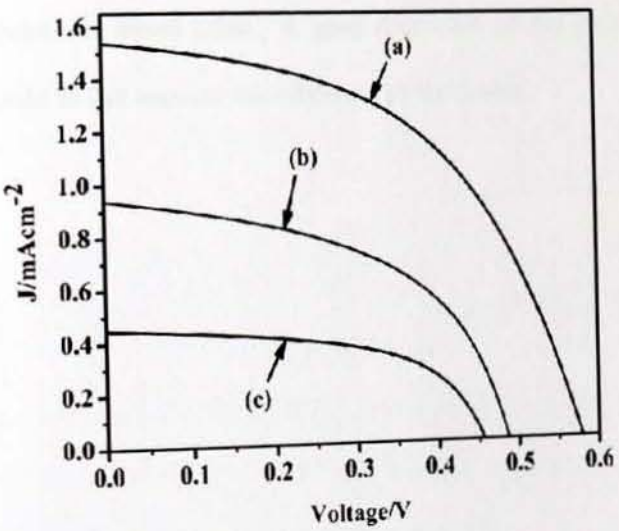

Figure 4. 28: J-V curve for DSSC sensitized by the extract of *I. herbstii* extracted from (a) ethanol (b) 0.1 M HCl (c) mixture of dyes extracted in ethanol and 0.1 M HCl.

Table 4.5 presents the performance of the DSSCs in terms of short circuit current density (J_{SC}), open-circuit voltage (V_{OC}), fill factor (FF), and energy conversion efficiency (η) of ethanol solution of standard N719 dye based DSSC, 0.1 M HCl and ethanol extract dyes based DSSC of the plant materials studied in this work. Obviously, the efficiency of cell sensitized by plant extracts from ethanol was significantly higher than those sensitized by the 0.1 M HCl extracts. This is due to the difference in the kinds of dyes extracted using ethanol and 0.1 M HCl as a solvent for *I. herbstii* and *A. caudatus*. For these materials the ethanol extract mainly contains

chlorophyll where as the 0.1 M HCl extract mainly contains betalains. For flower extracts of *H. sabdariffa* and *I. indica* based DSSC in which both of them contain anthocyanin, here also ethanol extract dye performs better than 0.1 M HCl extract. This might owe to the fact that anthocyanin is more soluble in ethanol, and hence, the aggregation of dye molecules is less as expected as it was explained in Section 4.3.3 for *Syzygium guineense* based DSSC. A good dispersion of dye molecules on the oxide surface could in fact improve the efficiency of the device.

Table 4. 5: The photoelectrochemical performance of the DSSCs based on a dye extracted from *I. herbstii* using different solvents.

Dye source	J_{SC}/mAcm^{-2}	V_{OC} /V	FF (%)	η (%)	Reference
N719	15.74	0.590	58.30	5.41	
	15.72	0.626	55.00	5.41	[208]
I. herbstii in ethanol	1.54	0.580	51.00	0.45	
I. herbstii in 0.1M HCl	0.94	0.490	50.00	0.23	
Mixture [a]	0.45	0.460	56.00	0.12	
A. caudatus in ethanol	3.44	0.570	50.00	1.00	
A. caudatus in 0.1M HCl	1.00	0.470	55.40	0.26	
I. indica in ethanol	3.11	0.550	55.10	0.94	
I. indica in 0.1M HCl	1.56	0.490	57.00	0.43	
H. sabdariffa in ethanol	3.21	0.490	62.30	1.00	
H. sabdariffa in ethanol[b]	2.51	0.488	58.00	0.72	[287]
H. sabdariffa in 0.1M HCl	1.83	0.470	57.80	0.50	
H. sabdariffa in water at pH=1.0 [b]	2.72	0.408	63.00	0.70	[287]

Mixture[a]: mixture of extract of *I. herbstii* in ethanol and *I. herbstii* in 0.1 M HCl

[b]: liquid state electrolyte (0.5 M KI mixed with 0.05 M I_2 in water – free ethylene glycol).

Figure 4.29 shows the action spectra of the monochromatic incident photon-to-current conversion efficiency (IPCE) for the DSSC sensitized with *I. herbstii* dye extracted from ethanol, 0.1 M HCl and a mixed dye extracted from ethanol and 0.1 M HCl. The IPCE for the DSSC of ethanol and 0.1 M HCl extract reached about 56% at 410 nm and about 43% at 350 nm, respectively. For mixed dye the IPCE reached about 32% at 330 nm. The result from the action spectra was also observed to be consistent and similar to that of the current density-voltage measurement.

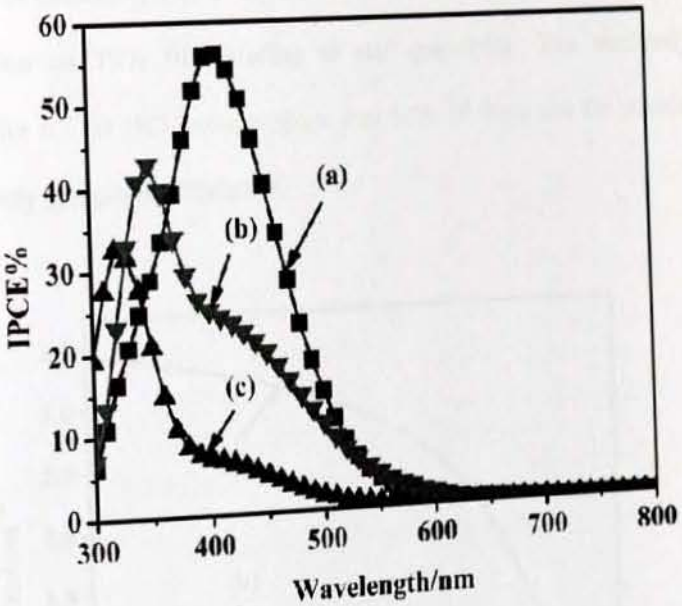

Figure 4. 29: Photocurrent action spectrum of DSSC sensitized by the extract of *I. herbstii* extracted from (a) ethanol (b) 0.1 M HCl and (c) mixture of dyes extracted in ethanol and 0.1 M HCl.

Figure 4.30 shows the J–V curve for DSSC based on *A. caudatus* extract and Figure 4.31, the respective IPCE. The IPCE for the DSSC of ethanol extract reached about 80% at 410 nm that of 0.1 M HCl extract it reached about 55% at 340 nm. The result

from the action spectra was also observed to be consistent and similar to that of the current density-voltage measurement.

DSSCs based on ethanol extract of *A. caudatus* dyes show higher performances than *I. herbstii* whereas more or less similar result was obtained from 0.1 M HCl extract (Table 4.5). Eventhough their ethanol extracts contain the same dye namely chlorophyll, the decreased performance for ethanol extract of *I. herbstii* compared with the respective ethanol extract of *A. caudatus* might be due to a higher concentration of chlorophyll in *I. herbstii* ethanol extract which might also result in dye aggregation on TiO_2 film leading to self quenching. The similarity in the performance for 0.1 M HCl extracts show that both of them are the sources of the same dye mainly composed of betalain.

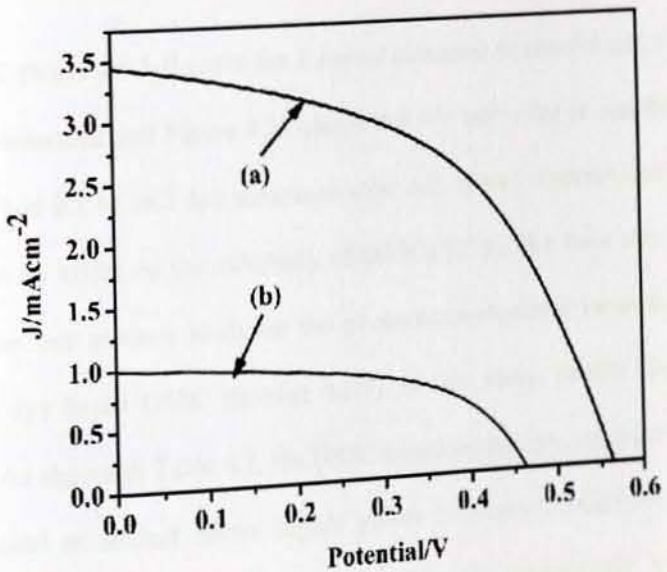

Figure 4. 30: J–V curve for DSSC sensitized by the extract of *A. caudatus* extracted from (a) ethanol and (b) 0.1 M HCl.

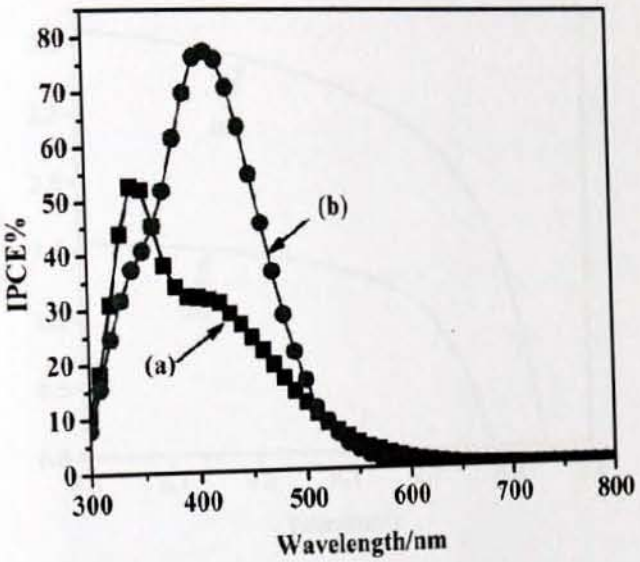

Figure 4. 31: Photocurrent action spectrum of a DSSC sensitized by the extract of *A. caudatus* extracted from (a) 0.1 M HCl and (b) ethanol.

Figure 4.32 shows the J-V curve for *I. indica* extracted in ethanol and 0.1 M HCl dye sensitized solar cell and Figure 4.33 shows the J-V curve for *H. sabdariffa* extracted in ethanol and 0.1 M HCl dye sensitized solar cell. It was reported that the extracting solvent has an effect on the efficiency of DSSCs [273]. We have also found similar results from our pevious study on the photoelectrochemical behavior of *Syzygium guineense* dye based DSSC (Section 4.3.3). In this study, similar finding was also obtained. As shown in Table 4.5, the DSSC based on the dye extracted from *I. indica* using ethanol as solvent shows higher power conversion efficiency than the one extracted from 0.1 M HCl, which is 0.94% and 0.43%, respectively. Similarly, for *H. sabdariffa*, ethanol and 0.1 M HCl extract dyes used as sensitizer shown a power conversion efficiency of 1.00% and 0.50%, respectively. The IPCE also shows the same trend (Figure 4.34 and Figure 4.35).

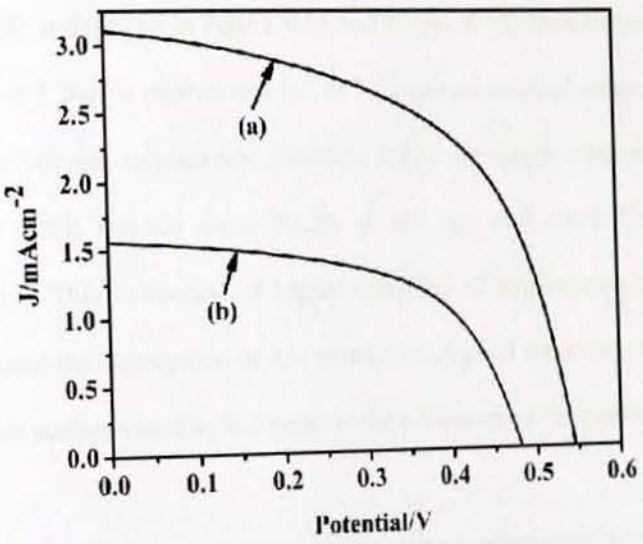

Figure 4. 32: J–V curve of DSSC sensitized by flower extract of *I. indica* extracted from (a) ethanol and (b) 0.1 M HCl.

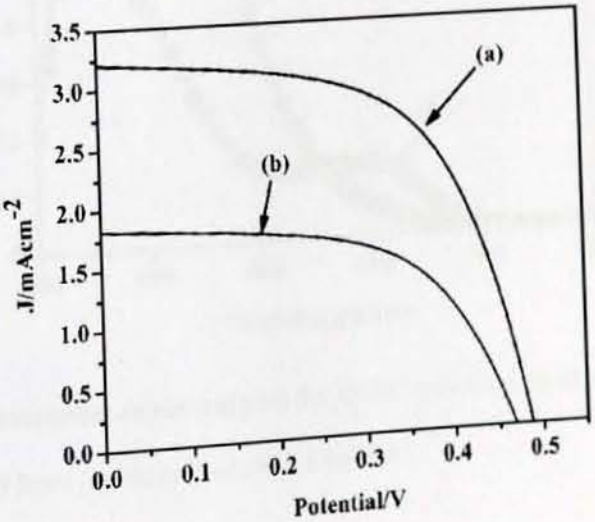

Figure 4. 33: J–V curve for DSSC sensitized by flower extract of *H. sabdariffa* extracted from (a) ethanol and (b) 0.1 M HCl.

The IPCE curve of DSSC based on ethanol and 0.1 M HCl extract from *I. indica* and *H. sabdariffa* is depicted in Figure 4.34 and Figure 4.35, respectively. The IPCE for the DSSC of *I. indica* ethanol and 0.1 M HCl extract reached about 75% at 420 nm and 56% at 340 nm, respectively. Similarly for *H. sabdariffa* ethanol and 0.1 M HCl extract the IPCE reached about 50.2% at 600 nm, and about 33.8% at 590 nm respectively. This is because of higher solubility of anthocyanin in ethanol [274], which reduces the aggregation of dye molecules. A good dispersion of dye molecules on the oxide surface could in fact improve the efficiency of the system.

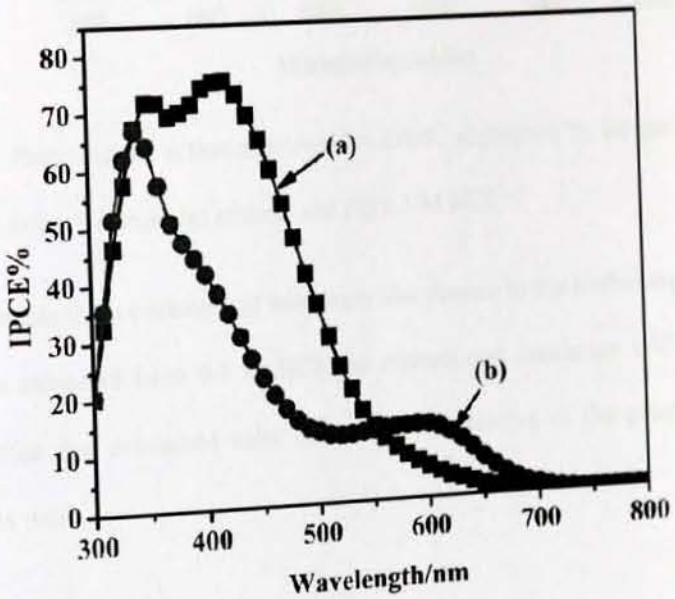

Figure 4. 34: Photocurrent action spectrum for DSSC sensitized by flower extract of *I. indica* extracted from (a) ethanol and (b) 0.1 M HCl.

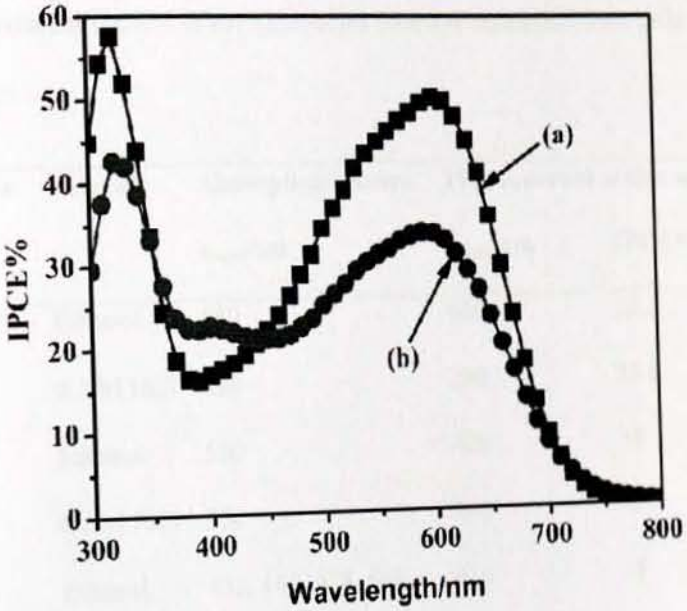

Figure 4. 35: Photocurrent action spectrum for DSSC sensitized by flower extract of *H. sabdariffa* extracted from (a) ethanol and (b) 0.1 M HCl.

Table 4.6 presents the wavelength at maximum absorbance in the visible region of the dye solutions extracted from 0.1 M HCl and ethanol and maximum IPCE% of the quasi-solid state dye sensitized solar cells of the respective of the plant materials studied in this work.

Table 4. 6: Wavelength at maximum absorbance of the dye solutions in the visible region and maximum IPCE% of the quasi-solid state dye sensitized solar cells of the respective dyes.

Natural Dye	Solvent	Absorption spectra	Photocurrent action spectra	
		λ_{max}/nm	λ_{max}/nm	IPCE%
H. sabdariffa	Ethanol	550	600	50.2
	0.1 M HCl	520	590	33.8
I. indica	Ethanol	550	420	75
	0.1 M HCl	530	340	56
I. herbstii	Ethanol	433, 466, 618, 664	410	56
	0.1 M HCl	536	350	43
A. caudatus	Ethanol	433, 466, 618, 664	410	80
	0.1 M HCl	530	340	55

4.4.4. Conclusions

In this work dyes obtained from nature, mainly flowers and leaves of plants, were used as sensitizers in DSSCs. The dyes extracted from leafs of *A. caudatus* and *I. herbstii*, and flower of *I indica* contained betalain, chlorophyll, and anthocyanin. We have reported an investigation on these pigments as natural photosensitizers, describing and comparing their sensitization activity with respect to one of the best ruthenium dyes (N719). Betalain raw pigments simply extracted in 0.1 M HCl from *A. caudatus* and *I. herbstii* achieved IPCEs higher than 50% and solar energy conversion efficiency of 0.26% and 0.23%, respectively. Whereas the pigments extracted in ethanol which contains mainly chlorophyll achieved the highest solar energy

conversion efficiency of 1.00%. Mixing of 0.1 M HCl extract and ethanol extract of *I. herbstii* didn't show any synergistic effect. Anthocyanin pigments extracted in 0.1 M HCl and in ethanol from *I. indica* also gave IPCE higher than 55% and power conversion efficiency of 0.43% and 0.94%, respectively and similarly those of *H. sabdariffa* extracted in ethanol gave IPCE higher than 50% at 600 nm whereas the one extracted in 0.1 M HCl gave about 34% at the same wavelength and the power conversion efficiency are 1.00% and 0.50%, respectively. Although the efficiencies obtained with these natural dyes are still below the current requirements for large scale practical application, the results are encouraging and may boost additional studies oriented to the search of new natural sensitizers and to the optimization of solar cell components compatible with such dyes.

References

1. Grätzel, M. *Acc. Chem. Res.* **2009,** *42* , 1788.
2. Eisenberg, R.; Nocera, D. G. *Inorganic Chemistry.* **2005,** 44, 6799.
3. Kudo, A.; Miseki, Y. *Chem. Soc. Rev.* **2009,** 38, 253.
4. Osterloh, F. E. *Chem. Mater.* **2008,** 20, 35.
5. Lewis, N. S.; Nocera, D. G. *Proc. Natl. Acad. Sci.* **2006,** *103*, 15729.
6. Boyle, G. *Renewable energy: power for a sustainable future*. Oxford University Press in association with the Open University: Oxford, **1996**.
7. Grätzel, M. *Phil. Trans. R. Soc. London, A* **2007,** *365*, 993.
8. Hagfeldt, A.; Boschloo, G.; Sun, L. C.; Kloo, L.; Pettersson, H.; *Chem. Rev.* **2010,** *110*, 6595.
9. Chapin, D. M.; Fuller, C. S.; Pearson, G. L. *J. Appl. Phys.* **1954,** *25*, 676.
10. Becquerel.; A. E. *C. R. Acad. Sci.* **1839**, 9, 145.
11. West, W. *Proc. VogelCent. Symp. Photogr. Sci. Eng.* **1974**, 18, 35.
12. Gerischer, H.; Tributsch, H. *Ber. Bunsenges. Phys. Chem.* **1968**, 72, 437.
13. Hauffe, K.; Danzmann, H. J.; Pusch, H.; Range, J.; Volz, H. *J. Electrochem. Soc*. **1970**,117, 993.
14. Myamlin, V. A.; Pleskov, Y. V. *Electrochemistry of Semiconductors*, Plenum Press, New York, **1967**.
15. Ellis, A. B.; Kaiser, S. W.; Wrighton, M. S. *J. Am. Chem. Soc*. **1976**, 98, 1635.
16. Ellis, A. B.; Bolts, J. M.; Wrighton, M. S. *J. Electrochem. Soc*. **1977**,124, 1603.
17. Hodes, G.; Manassen, J.; Cahen, D. *Nature* **1976**, 261, 403.
18. Miller, B.; Heller, A. *Nature* **1976**, 262, 680.
19. Fujishima A.; Honda, K.; *Nature*, **1972,** 238, 37.

20. Fujishima A.; Honda, K. *Bull. Chem. Soc.* Jpn., **1971**, 44, 1148.

21. Daniel D.; Gutz, I. G. R. *Electrochem. Commun.* **2007**, 9, 522.

22. Gerischer, H. *J. Electrochem. Soc.* **1966**, 113, 1174.

23. Gerischer, H. *J. Electroanal. Chem. Interfacial Electrochem.* **1975**, 58, 263.

24. Shirakawa, H.; Louis, E.J.; MacDiarmid, A.G.; Chiang, C.K.; Heeger, A.J. *J. Chem. Soc.Chem. Comm* **1977**, 578.

25. Chiang, C. K.; Fincher Jr, C. R.; Park, Y. W.; Heeger, A. J.; Shirakawa, H.; Louis, E. J.; Gau, S. C.; MacDiarmid, A. G. *Phys. Rev. Lett.* **1977**, 39, 1098.

26. Chiang, C.K.; Druy, M.A.; Gau, S.C.; Heeger, A.J.; Louis, E.J.; MacDiarmid, A.G.; Park, Y.W.; Shirakawa, H. *J. Am. Chem. Soc.* **1978**, 100, 1013.

27. Brabec, C.J.; Padinger, F.; Sariciftci, N.S.; Hummelen, J.C. *J. Appl. Phys.* **1999**, 85, 6866.

28. Arbizzani, C.; Mastragostini, M.; Scrosati B. *In Handbook of Organic Conductive Molecules and Polymers*, Vol. 4, Ed. Nalwa, H.S. (John Wiley & Sons, New York,**1997**.

29. Yang, Y.; Heeger, A.J. *Nature* **1994**, 372, 344.

30. Halls, J.J.M.; Walsh, C.A.; Greenham, N.C.; Marseglia, E.A.; Friend, R.H.; Moratti, S.C.; Holmes, A.B. *Nature* **1995**, 376, 498.

31. Hide, F.; Diaz-Garcia, M.; Schwartz, D.; Andersson, M.; Pie, Q.; Heeger, A.J. *Science* **1996**, 273, 1833.

32. Sariciftci, N.S.; Heeger A.J. *In*: *Handbook of Organic Conductive Molecules and Polymers*, Vol. 1, Ed. Nalwa, H.S. John Wiley & Sons, New York, **1997**.

33. O' Reagan, B.; Graetzel, M. *Nature* **1991**, 353, 737.

34. Wöhrle, D.; Meissner, D. *Adv. Mat.* **1991**, 3, 129.

35. Shaheen, S.E.; Brabec, C.J.; Sariciftci, N.S.; Padinger, F.; Fromherz, T.; Hummelen, J.C. *Appl. Phys. Lett.* **2001**, 78, 841.

36. Brabec, C.J.; Sariciftci, N.S.; Hummelen, J.C. *Adv. Funct. Mater.* **2001**, 11, 15.

37. Burroughes, J.H.; Bradley, D.C.C.; Brown, A.R.; Marks, R.N.; Mackay, K.; Friend, R.H.; Burns, P.L.; Holmes, A.B. *Nature* **1990**, 372, 539.

38. Yohannes, T.; Inganäs, O. *J. Electrochem. Soc.* **1996**, 143, 87.

39. Yohannes, T.; Solomon, T.; Inganäs, O. *Synth. Met.* **1996**, 82, 215.

40. Yohannes, T.; Carlberg, J.C.; Inganäs, O.; Solomon, T. *Synth. Met.* **1997**, 88, 15.

41. Too, C. O.; Wallace, G. G.; Burrell, A. K. ; Collis, G. E.; Officier, D.L.; Boge, E.W.; Brodie, S. G.; Evans, E.J. *Synth. Met.* **2001**, 123, 53.

42. Cutler, C. A.; Burrell, A. K.; Officier, D. L.; Too, C. O.; Wallace, G.G. *Synth. Met.* **2002**, 128, 35.

43. Yohannes, T.; Inganäs, O. *Synth. Met.* **1999**, 107, 97.

44. Grätzel, M. *Nature* **2001**, 414, 338.

45. Liang,Y.;Xu, Z.; Xia, J.; Tsai,S.T.; Wu,Y.; Li,G.; Ray,C.; Yu,L. *Adv. Mater.* **2010**, 22, E135.

46. Kamat, P.V.; Barazzouk,S.; Thomas, K.G.; Hotchandani, S. *J.Phys.Chem.B* **2000**, 104, 4014.

47. Hara, K.; Arakawa H., *Handbook of Photovoltaic Science and Engineering*, Ed. Luque, A.; Hegedus, S., John Wiley & Sons, Inc., England, **2003**.

48. O'Regan, B.; Durrant, J.; *J. Phys. Chem. B.* **2006**, 110, 8544.

49. Bisquert, J., *J. Phys. Chem. B.* **2004**, 108, 2323.

50. Kern, R.; Sastrawan, R.; Ferber, J.; Stangl, R.; Luther, J. *Electrochimica Acta.* **2002**, 47, 4213.

51. Peter, L.; Duffy, N.; Wang, R.; Wijayantha, K., *J. Electroanal. Chem.* **2002**, 524-525,127.

52. Murakami, T.; Grätzel, M., *Inorganica Chimica Acta* **2008**, 361, 572.

53. Nazeeruddin, M. K.; Kay, A.; Rodicio, I.; Humphry-Baker, R.; Muller, E.; Liska, P.; Vlachopoulos, N.; Grätzel, M. *J. Am. Chem. Soc.* **1993**, 115, 6382.

54. Bechinger, C.; Ferrere, S.; Zaban, A.; Sprague, J.; Gregg, B. *Nature* **1996**, *383*, 608.

55. Hagfeldt, A.; Gratzel, M. *Chem. Rev.* **1995**, *95*, 49.

56. Huang, S. Y.; Schlichtho¨rl, G.; Gra¨tzel, M.; Frank, A. J. *J. Phys. Chem. B* **1997**, *101*, 2576.

57. Argazzi, R.; Bignozzi, C.; Heimer, T.; Castellano, F.; Meyer, G. *Inorg. Chem.* **1994**, *33*, 5741.

58. Cao, F.; Oskam, G.; Searson, P.; Stipkala, J. M.; Heimer, T. A.; Farzad, F.; Meyer, G. J. *J. Phys. Chem.* **1995**, *99*, 17071.

59. Matsumoto, M.; Miyazaki, H.; Matsuhiro, K.; Kumashiro, Y.; Takaoka, Y. *Solid State Ionics* **1996**, *89*, 263.

60. Lanzafame, J. M.; Miller, R. J. D.; Muenter, A. A.; Parkinson, B. A. *J. Phys. Chem.* **1992**, 96, 2820.

61. Burfeindt, B.; Hannappel, T.; Storck, W.; Willig, F. *J. Phys. Chem.* **1996**, *100*, 16463.

62. Rehm, J. M.; McLendon, G. L.; Nagasawa, Y.; Yoshihara, K.; Gra¨tzel, M. *J. Phys. Chem.* **1996**, *100*, 9577.

63. Tachibana, Y.; Moser, J. E.; Gra¨tzel, M.; Klug, D. R.; Durrant, J. R. *J. Phys. Chem.* **1996**, 100, 20056.

64. Grätzel, M. *Inorganic Chem.* **2005**, 44, 20.

65. Grätzel, M. *J. Photochem. Photobiol A*, **2004**, 164, 3.

66. Halme, J. *PhD Thesis*, TKK Dissertations 167, **2009**, Espoo, Finland.

67. Polo, A.S.; Itokazu, M.K.; Iha, N. Y. M. *Coord. Chem. Rev.* **2004**, 248, 1343.

68. Kalyanasundaram, K.; Vlachopoulos, N.; Krishnan, V.; Monnier, A.; Grätzel, M. *J. Phys. Chem.* **1987**, 91, 2342.

69. Mao, H.; Deng, H.; Li, H.; Shen, Y.; Lu, Z.; Xu, H. *J. Photochem. Photobiol. A. Chem.* **1998**, 114, 209.

70. Kay A. ; Grätzel, M. *J. Phys. Chem.* **1993**, 97, 6272.

71. Fang, J.; Wu, J.; Lu, X.; Shen Y.; Lu, Z. *Chem. Phys. Lett.* **1997**, 270, 145.

72. Nazeeruddin, M. K.; Humphry Baker, R.;Grätzel, M.;Murrer, B.A. *Chem.Commun.* **1998**, 719.

73. Nazeeruddin, M. K.; Humphry-Baker, R.; Graetzel, M.; Wohrle, D.; Schnurpfeil, G.; Schneider, A.; Hirth, N.; Trombach, J. *Porphyrins Phthalocyanines* **1999**, 3, 230.

74. Kalyanasundaram, K.; Grätzel, M. *Coord. Chem. Rev.* **1998**, 177, 347.

75. Alibabaei, L.; Wang, M.; Giovannetti, R.; Teuscher, J.; Censo, D. D.; Moser, J.-E.; Comte, P.; Pucciarelli, F.; Zakeeruddin, S. M.; Gratzel M. *Energy Environ. Sci.* **2010**, 3, 956.

76. Hagfeldt, A.; Grätzel, M. *Acc. Chem. Res.* **2000**, 33, 269.

77. Sauve', G.; Cass, M. E.; Coia, G.; Doig, S. J.; Lauermann, I.; Pomykal, K. E.; Lewis, N. S. *J. Phys. Chem. B*, **2000**, 104, 6821.

78. Nogueira, A. F.; Longo, C.; De Paoli, M. A. *Coord. Chem.* Rev. **2004**, 248, 1455.

79. Li, B.;Wang, L. D.; Kang, B.; Wang, P.; Qiu. Y. *Sol. Energy Mater. Sol. Cells.* **2006**, 90, 549.

80. Papageorgiou, N.; Athanassov, Y.; Armand, M.; Bonhote, P.; Pettersson, H.; Azam, A.; Grätzel, M. *J. Electrochem. Soc.* **1996**, *143*, 3099.

81. Hauch, A.; Georg, A. *Electrochim. Acta* **2001**, *46*, 3457.

82. Han, L.; Koide, N.; Chiba, Y.; Islam, A.; Komiya, R.; Nobuhiro, F.; Fukui, A.; Yamanaka, R. *Appl. Phys. Lett.* **2005**, *86*, 213501.

83. Wang, P.;Zakeeruddin, S. M.; Moser, J. E.; Sekiguchi, T.; Grätzel, M. *Nat. Mater.* **2003**, 2, 402.

84. Kebede, Z.; Lindquist., S. E. *Sol. Energy Mater. Sol. Cells.* **1999**, 57, 259.

85. Fukui, A.; Komiya, R.; Yamanaka, R.; Islam. A. *Sol. Energy Mater. Sol. Cells.* **2006,** 90, 649.

86. Hao, S. C.; Wu, J. H.; Fan, L. Q.; Huang, Y. F.; Lin, J.M.; Wei, Y.L. *Sol. Energy.* **2004,** 76, 745.

87. Wu, J. H.; Lan, Z.; Lin, J. M.; Huang, M. L. *J. Power Sources.* **2007**, 173, 585.

88. Cahen, D.; Hodes, G.; Grätzel, M.; Guillemoles, J. F.; Riess, I. *J. Phys. Chem. B* **2000**,104, 2053.

89. Schlichthorl, G.; Huang, S. Y.; Sprague, J.; Frank, A. J. *J. Phys. Chem. B.* **1997**, 101, 8141.

90. Kang, T. S.; Chun, K. H.; Hong, J. S.; Moon, S. H.; Kim. K. J. *J. Electrochem. Soc.* **2000**, 147, 3049.

91. Hong, J. S.; Joo, M.; Vittal, R.; Kim, K. J. *J. Electrochem. Soc. E* **2002**, 149, 493.

92. Alexander, I. P.; Geske., D. H. *J. Am. Chem. Soc.* **1958**, 80, 1340.

93. Toivola, M.; Ahlskog, F.; Lund. P. *Sol. Energy Mater. Sol. Cells.* **2006**, 90, 2881.

94. Wang, Z. S.; Sayama, K.; Sugihara, H. *J. Phys. Chem. B.* **2005**, 109, 22449.

95. Bergeron, B. V.; Marton, A.; Oskam, G. *J. Phys. Chem. B* **2005**, 109, 937.

96. Oskam, G.; Bergeron, B. V.; Meyer, G. J. *J. Phys. Chem. B* **2001**, 105, 6867.

97. Sapp, S. A.; Elliott, C. M.; Contado, C. *J. Am. Chem. Soc.* **2002**, 124, 11215.

98. Nusbaumer, H.; Moser, J. E.; Zakeeruddin, S. M. *J. Phys. Chem. B* **2001**, 105, 10461.

99. Grätzel, M.; Frank, A. J. *J. Phys. Chem.* **1982**, 86, 2964.

100. Lagemaat, J. V. D.; Park, N. G.; Frank, A. J. *J. Phys. Chem. B* **2000**, 104, 2044.

101. Kopidakis, N.; Schiff, E. A.; Park, N. G.; Frank, A. J. *J. Phys. Chem. B* **2000**, 104, 3930.

102. Solbrand, A.; Lindstrom, H.; Hagfeldt, A.; Lindquist, S.E. *J. Phys. Chem. B* **1997**, 101, 2514.

103. Zaban, A.; Meier, A.; Gregg, B. *J. Phys. Chem. B* **1997**, 101, 7985.

104. Nister, D.; Keis, K.; Lindquist, S.E.; Hagfeldt, A. *Sol. Energy Mater. Sol. Cells.* **2002**, 73, 411.

105. Frank, A. J.; Kopidakis, N.; Lagemaat, J. V. D. *Coord. Chem. Rev.* **2004**, 248, 1165.

106. Olson, C. L. *J. Phys. Chem. B* **2006**, 110, 9619.

107. Liu,Y.; Hagfeldt,A.; Xiao, X.R.; Lindquist, S.E. *Sol. Energy Mater. Sol. Cells* **1998**, 55, 267.

108. Watson, D. F.; Meyer, G. J. *Coord. Chem. Rev.* **2004**, 248, 139.

109. Kusama, H.; Arakawa, H. *Sol. Energy Mater. Sol. Cells.* **2004**, 81, 87.

110. Kusama, H.; Arakawa, H. *Sol. Energy Mater. Sol. Cells.* **2004**, 82, 457.

111. Kusama, H.; Arakawa, H. *J. Photochem. Photobiol A.* **2004**, 164, 103.

112. Kusama, H.; Arakawa, H. *J. Photochem. Photobiol A.* **2004**, 162, 441.

113. Kusama, H.; Kurashige, M.; Arakawa. H. *J. Photochem. Photobiol.* A **2005**, 169, 169.

114. Kusama, H.; Arakawa, H. *Sol. Energy Mater. Sol. Cells.* **2005**, 85, 333.

115. Kusama, H.; Arakawa, H. *J. Photochem. Photobiol A.* **2004**, 165, 157.

116. Lan, Z.; Wu, J.; Lin, J.; Huang, M.; Li, P.; Li, Q. *Electrochim. Acta.* **2008**, 53, 2296.

117. Matsumoto, H.; Matsuda, T.; Tsuda, T.; Hagiwara, R.; Ito, Y.; Miyazaki ;Y. *Chem. Lett.* **2001**, 26.

118. Wang, P.; Zakeeruddin, S.M.; Moser, J. E.; Grätzel, M. *J. Phys. Chem. B* **2003**, 107, 13280.

119. Kitamura, T.; Maitani, M.; Matsuda, M.; Wada, Y.; Yanagida, S. *Chem. Lett.* **2001**, 1054.

120. Papageorgiou, N.; Athanassov, Y.; Armand, M.; Bonhote, P.; Pettersson, H.; Azam, A.; Grätzel, M. *J. Electrochem. Soc.* **1996**, 143, 3099.

121. Wang, P.; Zakeeruddin, S. M.; Moser, J. E.; Baker, R. H.; Grätzel, M. *J. Am. Chem. Soc.* **2004**, 126, 7164.

122. Wu, J. H.; Hao, S. C.; Lan, Z.; Lin, J. M.; Huang, M. L.; Huang, Y. F. *Adv. Funct. Mater.* **2007**, 17, 2645.

123. Stathatos, E.; Lianos, P.; Lavrencic-Stangar, U.; Orel, B. *Adv. Mater.* **2002**, 14, 354.

124. Lan, Z.; Wu, J. H.; Lin, J. M.; Huang, M. L. *J. Power Sources* **2007**, 164, 921.

125. Tennakone, K.; Kumara, G.; Kumarasinghe, A. R.; Wijayantha, K. G. U.; Sirimanne, P. M. *Semicond. Sci. Technol.* **1995**, 10, 1689.

126. Kumara, G.; Konno, A.; Senadeera, G.K.R.; Jayaweera, P.V.V.; Silva, D.D.; Tennakone, K. *Sol. Energy Mater. Sol. Cells.* **2001**, 69, 195.

127. O'Regan, B.; Schwartz, D. T. *Chem. Mater.* **1998**, 10, 1501.

128. Tennakone, K.; Senadeera, G. K. R.; Silva, D. D.; Kottegoda, I. R. M.. *Appl. Phys. Lett.* **2000**, 77, 2367.

129. Tennakone, K.; Perera, V. P. S.; Kottegoda, I. R. M.; Kumara, G. *J. Phys. D* **1999**, 32, 374.

130. Bach, U.; Lupo, D.; Comte, P.; Moser, J. E.; Weissortel, F.; Salbeck, J.; Spreitzer, H.; Grätzel, M. *Nature* **1998**, 395, 583.

131. Stergiopoulos, T.; Arabatzis, L. M.; Katsaros, G. *Nano Lett.* **2002**, 2, 1259.

132. Wang, P. ; Dai, Q.; Zakeeruddin, S. M. *J. Am. Chem. Soc.* **2004**, 126, 13590.

133. Wang, H.; Li, H.; Meng, Q. *J. Am. Chem. Soc.* **2005**, 127, 6394.

134. Murphy, S. B. R. *In: Polymer Networks—Principles of Their Formation, Structure and Properties*, Stepto, R. F. T. (Ed.), Blackie Academic, London **1998**.

135. Megahed, S.; Scrosati, B. *Interface* **1995**, 4, 34.

136. Abraham, K. M. *In: Application of Electroactive Polymer*, Scrosati, B. (Ed.), Chapman & Hall, London **1993**.

137. Mohmeyer, N.; Wang, P.; Schmidt, H. W.; Zakeeruddin, S. M.; Grätzel, M. *J. Mater. Chem.* **2004**, 14, 1905.

138. Reng, Y.; Zhang, Z.; Gao, E.; Fang, S.; Cai, S. *J. Appl. Electrochem.* **2001**, 31, 445.

139. Kubo, W.; Kitamura,T.; Hanabusa, K.; Wada, Y.; Yanagida, S. *Chem. Commun.* **2002**, 374.

140. Stathtos, E.; Lianos, P.; Krontiras, C. *J. Phys. Chem. B* **2001**, 105, 3486.

141. Stathtos, E.; Lianos, P.; Stangar, U. L.; Orel, B. *Adv. Funct. Mater.* **2004**, 14, 45.

142. Stathtos, E.; Lianos, P. *Chem. Mater.* **2003**, 15, 1825.

143. Wu, J. H.; Lan, Z.; Lin, J. M.; Huang, M. L.; Hao, S. C.; Sato, T.; Yin, S. *Adv. Mater.* **2007**, 19, 4006.

144. Lan, Z.;Wu, J. H.; Lin,J. M.; Huang, M. L.; Yin, S.;Sato,T. *Electrochim. Acta.* **2007**, 52, 6673.

145. Wu, J. H.; Lan, Z.; Lin, J. M.; Huang, M. L.; Hao, S. C. *Electrochim. Acta* **2007**, 52, 7128.

146. Wu, J. H.; Lin, J. M.; Zhou, M. *Macromol. Rapid Commun.* **2000**, 21, 1032.

147. Lin, J. M.; Wu, J. H.; Yang, Z. F.; Pu, M. L. *Macromol. Rapid Commun.* **2001**, 22, 422.

148. Miettunen, K.; Halme, J.; Toivola, M.; Lund, P. *J. Phys. Chem. C* **2008**, 112, 4011.

149. Ma, T.; Fang, X.; Akiyama, M.; Inoue, K.; Noma, H.; Abe E. *J. Electroanal. Chem.* **2004**, 574, 77.

150. Fang, X.; Ma, T.; Akiyama M.; Guan, G.; Tsunematsu S.; Abe, E. *Thin Solid Films* **2005**, 472, 242.

151. Jun, Y.; Kim, J.; Kang, M. *Sol. Energy Mater. Sol. Cells.* **2007**, 91, 779.

152. Ito, S.; Ha, N-L.; Rothenberger, G.; Liska, P.; Comte, P.; Zakeeruddin, S.; Péchy, P.; Nazeeruddin, M.; Grätzel, M. *Chem. Commun.* **2006**, 4004.

153. Onoda, K.; Ngamsinlapasathian, S.; Fujieda, T.; Yoshikawa, S. *Sol. Energy Mater. Sol.Cells.* **2007**, 91, 1176.

154. Kang, M.; Park, N.; Ryu, K.; Chang, S.; Kim, K. *Chem. Lett.* **2005,** 34, 804.

155. Park, H.; Jun, Y.; Yun, H.; Lee, S.; Kang, M., *J. Electrochem.Soc.* **2008**, 155, F145.

156. Ke, L.; Dolmanan, S.; Shen, L.; Pallathadk, P.; Zhang, Z.; Lai, D.; Liu, H. *Sol. Energy Mater. Sol. Cells.* **2010**, 94, 323.

157. Kalyanasundaram, K.; Gra¨tzel, M. *Coord. Chem. Re*V. **1998**, 177, 347.

158. Murakoshi, K.; Kano, G.; Wada, Y.; Yanagida, S.; Miyazaki, H.; Matsumoto, M.; Murasawa, S. *J. Electroanal. Chem.* **1995**, 396, 27.

159. Ardo, S.; Meyer, G. J. *Chem. Soc. Rev.* **2009**, 38, 115.

160. Pechy, P.; Rotzinger, F. P.; Nazeeruddin, M. K.; Kohle, O.; Zakeeruddin, S. M.; Humphry-Baker, R.; Gra¨tzel, M. *J. Chem. Soc., Chem. Commun* **1995**, 1, 65.

161. Galoppini, E. *Coord. Chem. Rev.* **2004**, 248, 1283.

162. Wang, Z. S.; Hara, K.; Dan-Oh, Y.; Kasada, C.; Shinpo, A.; Suga, S.; Arakawa, H.; Sugihara, H. *J. Phys. Chem. B* **2005**, 109, 3907.

163. Nazeeruddin, M. K.; Humphry-Baker, R.; Liska, P.; Grätzel, M. *J. Phys. Chem. B* **2003**, 107, 8981.

164. Zhang, Z.; Zakeeruddin, S.; O'Regan, B.; Humphry-Baker, R.; Grätzel, M., *J. Phys. Chem.B* **2005**, 109, 21818.

165. Wang, P.; Zakeeruddin, S.; Grätzel, M., *J. Fluorine Chemistry.* **2004**, 125, 1241.

166. Tennakone, K.; Kumara, G.; Kottegoda, I.; Wijayantha, K.; Perera, V. *J. Phys. D: Appl. Phys.* **1998**, 31, 1492.

167. Kumara, G.; Konno, A.; Shiratsuchi, K.; Tsukahara, J.; Tennakone, K. *Chem. Mater.* **2002**, 14, 954.

168. Konno, A.; Kitagawa, T.; Kida, H.; Kumara, G.; Tennakone, K., *Current Applied Physics* **2005**, 5, 149.

169. O'Regan, B.; Lenzmann, F.; Muis, R.; Wienke, J., *Chem. Mater.* **2002**, 14, 5023.

170. Perera, V.; Senevirathna, M.; Pitigala, P.; Tennakone, K., *Sol. Energy Mater. Sol. Cells.* **2005**, 86, 443.

171. Krüger, J.; Plass, R.; Cevey, L.; Piccirelli, M.; Grätzel, M., *Appl. Phys. Lett.* **2001**, 79, 2085.

172. Krüger, J.; Plass, R.; Grätzel, M.; Matthieu, H-J., *Appl. Phys. Lett.* **2002**, 81, 367.

173. Schmidt-Mende, L.; Bach, U.; Humphry-Baker, R.; Horiuchi, T.; Miura, H.; Ito, S.; Uchida, S.; Grätzel, M. *Adv. Mater.* **2005**, 17, 813.

174. Saito, Y.; Fukuri, N.; Senadeera, R.; Kitamura, T.; Wada, Y.; Yanagida, S., *Electrochem. Commun.* **2004**, 6, 71.

175. Hauch, A.; Georg, A., *Electrochimica Acta* **2001**, 46, 3457.

176. Gorlov, M.; Kloo, L., *Dalton Transactions.* **2008**, 2655.

177. Gorlov, M.; Pettersson, H.; Hagfeldt, A.; Kloo, L., *Inorganic Chemistry* **2007**, 46, 3566.

178. O'Mahony, A.; Silvester, D.; Aldous, L.; Hardacre, C.; Compton, R., *Journal of Chemical and Engineering Data* **2008**, 53, 2884.

179. Papageorgiou, N.; Maier, W.; Grätzel, M. *J. Electrochem. Soc.* **1997**, 144, 876.

180. Hagfeldt, A.; Didriksson, B.; Palmqvist, T.; Lindström, H.; Södergren, S.; Rensmo, H.; Lindquist, S. E. *Sol. Energy Mater. Sol. Cells* **1994,** 31, 481.

181. Smestad, G.; Bignozzi, C. ; Argazzi, R. *Sol. Energy Mater. Sol. Cells*, **1994,** 32, 259.

182. Lee, S.; Jun, Y.; Kim, K. J.; Kim, D. *Sol. Energy Mater. Sol. Cells*, **2001**, 65, 193.

183. Olsen, E.; Hagen, G.; Lindquist, S. E. *Sol. Energy Mater. Sol. Cells*, **2000**, 63, 267.

184. Kay, A.; Grätzel, M. *Sol. Energy Mater. Sol. Cells.***1996**, 44, 99.

185. Murakami, T.; Grätzel, M. *Inorganica Chimica Acta* **2008**, 361, 572.

186. Bay, L; West, K; Jensen, B.W; Jacobsen, T; *Sol. Energy Mater. Sol. Cells.* **2006**, 90, 341.

187. Shibata, Y.; Kato, T.; Kado, T.; Shiratuchi, R.; Takashima, W.; Kaneto, K.; Hayase, S.*Chem. Commun.* **2003,** 2730.

188. Wang, M.; Anghel, A. M.; Marsan, B.; Cevey Ha, N. L.; Pootrakulchote, N.; Zakeeruddin, S. M.; Grätzel, M. *J. Am. Chem. Soc.***2009**, 131, 15976.

189. Kiess, H.; Rehwald, W. *Sol. Energy Mater. Sol. Cells* **1995**, 38, 45.

190. Gregg, B. A. *J. Phys. Chem. B* **2003**, 107, 4688.

191. Dyakonov, V. *Physica E* **2002**, 14, 53.

192. Martin, H. D. *Chimia*, **1995**, 49, 45.

193. Yamasaki, H.; Uefuji H.; Sakihama, Y. *Arch. Biochem. Biophys.* **1996**, 332, 183.

194. Hara, K.; Kurashige, M.; Dan Ho, Y.; Kasada, C.; Shippo, A.; Suga, S.; Sayama, Arakawa, K. H. *N. J. Chem.* **2003,** 27, 783.

195. Dai, Q.; Rabani, J. *N. J. Chem.* **2002**, 26, 421.

196. Kong, J. M.; Chia, L. S.; Goh, N. K., Chia, T. F.; Brouillard, R. *Phytochemistry.* **2003**, 64, 923.

197. Starck, D.; Vogt, T.; Schliemann, W. *Phytochemistry*, **2003**, 62, 247.

198. Calogero, G.; Marco, G. D.; Caramori, S.; Cazzanti, S.; Argazzi, R.; Bignozzi, C. A. *Energy.Environ. Sci.* **2009**, 2, 1162.

199. Serris, G. S.; and Biliaderis, C. G. *Journal of the Science of Food and Agriculture*, **1900**, 81,691.

200. Zhang, D.; Lanier, S. M.; Downing, J. A.; Avent, J. L.; Lum, J.; McHale, J. L. *J.Photochem.Photobiol A* **2008**, 195, 72.

201. http://en.wikipedia.org/wiki/Photophosphorylation-retrived on Jan 11,2012

202. Kay,A; Grätzel,M *J. Phys. Chem.* **1993**, 97, 6272.

203. Kay, A.; Humphry Baker R.; Grätzel, M. *J. Phys. Chem.* **1994**, 98, 952.

204. Amao, Y.; Yamada, Y. *Langmuir* **2005**, 21, 3008.

205. Wang, X. F.; Zhan, C. H.; Maoka, T.; Wada, Y.; Koyama,Y. *Chem. Phys. Lett.* **2007**, 447, 79.

206. Wang, X.F.;Kitao, O.;Zhou, H.; Tamiaki, H.; Sasaki, S.I. *J. Phys. Chem.C* **2009**, 113, 7954.

207. Aagae, S.; Nekoomanesh, H.M.; Booth, C.; Owen, J.R. *Solid State Ionics* **1992**, 53 – 56, 1118.

208. Fan, L.; Kang, S.; Wu, J.; Hao, S.; Lan, Z.; Lin, J. *Energy Sources* A. **2010**, 32,1559.

209. Castellar, R.; Obon, J. M.; Alacid, M.; Fernandez-lopez, J. A. *J. Agric. Food Chem.* **2003**, 51, 2772.

210. Sariciftci, N.S.; Smilowitz, L.; Heeger, A.J.; Wudl, F. *Science* **1992**, 258, 1474.

211. Yu, G.; Gao, J.; Hummelen, J.C.; Wudl, F.; Heeger, A.J. *Science* **1995**, 270, 1789.

212. Yang, C.Y.; Heeger, A.J. *Synth.Met.* **1996**, 83, 85.

213. Padinger, F.; Rittberger, R.S.; Sariciftci, N.S. *Adv. Funct.Mater.* **2003**, 13, 85.

214. Brabec, C.J.; Shaheen, S.E.;Winder, C.; Sariciftci, N. S.; Denk, P. *Appl. Phys. Lett.* **2002**, 80, 1288.

215. Ma, W.; Yang, C.; Gong, X.; Lee, K.; Heeger, A.J. *Adv. Funct. Mater.* **2005**, 15, 1617.

216. Reyes-Reyes, M.; Kim, K.; Carroll, D.L. *Appl. Phys. Lett.* **2005**, 87, 083506.

217. Chen, H.Y.; Hou, J.H.; Zhang, S.Q.; Liang, Y.Y. ; Yang, G.W. ; Yang, Y.; Yu, L.P.; Wu, Y.; Li, *Nat. Photonics G.* **2009,** 3, 649.

218. Li, G.; Shrotriya, V.; Huang, J.; Yao, Y.; Moriarty, T.; Emery, K.; Yang, Y. *Nat. Mater.* **2005,** 4, 864.

219. Kim, Y.; Cook, S.; Tuladhar, S.M.; Choulis, S.A.; Nelson, J.; Durrant, J.R.; Bradley, D.D.C.; Giles, M.; McCulloch, I.; Ha, C.-S.; Ree, M. *Nat. Mater.* **2006,** 5, 197.

220. Chiu, M.-Y.; Jeng, U.-S.; Su, C.-H.; Liang, K.S.; Wei, K.-H. *Adv. Mater.* **2008**, 20, 2573.

221. Liang, Y.; Feng, D.; Wu, Y.; Tsai, S.T.; Li, G.; Ray, C.; Yu, L. *J. Am. Chem. Soc.* **2009**, 131, 7792.

222. Liang, Y.; Xu, Z.; Xia, J.; Tsai, S. T.; Wu, Y., Li, G.; Ray, C.; Yu, L. *Adv. Mater.* **2010**, 22, E135.

223. Park, S.H.; Roy, A.; Beaupre, S.; Cho, S.; Coates, N.; Moon, J.S.; Moses, D.; Leclerc, M.; Lee, K.; Heeger, A.J. *Nat. Photonics* **2009,** 3, 297.

224. Hou, J.; Chen, H.Y.; Zhang, S.; Chen, R.I.; Yang, Y.; Wu, Y.; Li, G. *J. Am. Chem. Soc.* **2009,** 131, 15586.

225. Bundgaard, E.; Krebs, F.C. *Sol. Energy Mater. Sol. Cells* **2007**, 91, 954.

226. Maurano, A.; Hamilton, R.; Shuttle, C.G.; Ballantyne, A.M.; Nelson, J.; O'Regan, B.; Zhang, W.; Mcculloch, I.; Azimi, H.; Morana, M.; Brabec, C.J.; Durrant, J.R. *Adv. Mater.,* **2010,** 22, 4987.

227. Brabec, C.J.; Gowrisanker, S.; Halls, J.J.M.; Laird, D.; Jia, S.; Williams, S.P.; *Adv. Mater.,* **2010,** 22, 3839.

228. Yohannes, T.; Inganas, O. *Sol. Energy Mater. Sol. Cells* **1998**, 51, 193.

229. Adi, M.; Yohannes, T.; Solomon, T. *Sol. Energy Mater. Sol. Cells* **2004**, 83, 301.

230. Mengesha, U.; Yohannes T. *Sol. Energy Mater. Sol. Cells,* **2006**, 90, 3508.

231. Sirringhaus, H.; Tessler, N.; Friend, R.H. *Science* **1998**, 280, 1741.

232. Craven, J.R.; Mobbs, R.H.; Booth, C.; Giles, J.R.M.; *Makromol. Chem. Rapid Commun.* **1986,** 7, 81.

233. Craven, J.R.; Nicholas, C.V.; Webster, R.; Wilson, D.J.; Mobbs, R.H.; Morris, G.A.; Heatley, F.; Booth, C.; Giles, J.R.M. *Br. Polym. J.* **1987,** 19, 509.

234. Nicholas, C.V.; Wilson, D.J.; Booth, C.; Giles, J.R.M. *Br. Polym. J.* **1988**, 20, 289.

235. Linden, E.; Owen, J.R. *Br. Polym. J.* **1988**, 20, 237.

236. Nekoomanesh, M.; Nagae, H. S.; Booth, C.; Owen, J. R. *J. Electrochem. Soc.* **1992**, 139, 3046.

237. MacCallum, J. R.; Vincent, C. A. "Polymer Electrolyte Reviews-2", *Elsevier Applied science*, London, **1989**.

238. Skotheim, T.A.; Feldberg, S.W.; Armand, M.B. *J. Phys. Paris Colloq.* **1983**, C 3, 615.

239. Tan, M.X.; Laibinis, P.E.; Nguyen, S.T.; Kesselman, J.M.; Stanton, C.E. and Lewis, N.S. Principles and applications of semiconductor photochemistry. *Progress in inorganic Chemistry*, (Karlin, K.D. ed.) John Wiley & Sons Inc., California; **1994,** pp. 69 – 82.

240. Brabec, C. J.; Cravino, A.; Meissner, D.; Sariciftci, N. S.; Fromherz, T.; Rispens, M.T.; Sanchez, L.; Hummelen, J. C. *Adv. Funct. Mater.* **2001,** 11, 374.

241. Liu, J.; Shi, Y.; Yang, Y. *Adv. Funct. Mater* **2001,** 11, 420.

242. Al-Ibrahim Al-Ibrahim, M.; Rotha, H.-K; Zhokhavetsb, U.; Gobsch, G.; Sensfuss, S. *Sol. Energy Mater. & Sol.Cells* **2005,** 85, 13.

243. Meier, H.; *Organic Semiconductors*, Verlag Chemie, Berlin, **1974**, pp. 318 – 321.

244. Glenis, S.; Tourillon, G.; Garnier, F. *Thin Solid Films* **1986**, 139, 221.

245. Glenis, S.; Horowitz, G.; Tourillon, G.; Garnier, F. *Thin Solid Films* **1984**, 111, 93.

246. Loutfy, R.O.; Sharp, J.H.; Hsiao, C.K., Ho, R. *J. Appl. Phys.* **1981**, 52, 5218.

247. Sze S.M. and Ng. K. K. Photodetectors and Solar Cells. *Physics of Semiconductor Devices*, (3rd ed) John Wiley & Sons Inc., New Jersey; **2003**, pp. 719 - 736.

248. Nazeeruddin, M. K.; Péchy, P.; Renouard, T.; Zakeeruddin, S. M.; Humphry-Baker, R.; Comte P., Liska P.; Cevey, L.; Costa, E.; Shklover, V.; Spiccia, L.; Deacon, G. B.; Bignozzi, C. A.; Grätzel, M. *J. Am. Chem. Soc.* **2001,** 123, 1613.

249. Grätzel M. *J. Photochem. Photobiol. C: Photochem Rev.*, **2003**, 4, 145.

250. Nelson, J.; Chandler R. E. *Coord. Chem. Rev.* **2004**, 248, 1181.

251. Smestad, G. *Sol. Energy Mater. Sol. Cells.* **2003**, **76**, 1.

252. Nogueira, A.F.; Paoli, A.D.; Montanari, I. *J. Phys. Chem. B*, **2001**, 105, 7517.

253. Sergawie, A.; Yohannes, T.; Günes, S.; Neugebauer, H.; Sariciftci, N.S. *J. Braz. Chem. Soc.* **2007**, 18, 1189.

254. Ghosh, A.K.; Feng, T. *J. Appl. Phys.* **1978**, 49, 5.

255. Chamberlain, G.A. *Solar Cells* **1983**, 8, 47.

256. Chamberlain, G.A. *J. Appl. Phys.* **1982**, 53, 6262.

257. Fan, F.-R.; Faulkner, L.R. *J. Chem. Phys.* **1978**, 69, 3341.

258. Chen, S. -An.; Fang, Y. *Synth. Met.* **1993**, 60, 215.

259. Fang, Y.; Chen, S.-An. *Synth. Met.* **1992**, 52, 261.

260. Kumar, A.; Santangelo, P. G.; Lewis, N. S. *Phys. Chem. B*, **1992**, 96, 834.

261. Yum, J. H.; Walter, P.; Huber, S.; Rentsch, D.; Geiger, T.; Neusch, F.; DeAngelis, F.; Graetzel, M.; Nazeeruddin, M. K. *J. Am. Chem. Soc.* **2007**, 129, 10320.

262. Campbell, W. M.; Jolley, K. W.; Wagner, P.; Wagner, K.; Walsh, P. J.; Gordon, K. C.; Mende, L. S.; Nazeeruddin, M. K.; Wang, Q.; Graetzel, M.; Officer, D. L. *J. Phys. Chem. C* **2007**, 111, 11760.

263. Tian, H.; Yang, X.; Chen, R.; Hagfeldt, A.; Sun, L. *Energy Environ. Sci.* **2009**, 2, 674.

264. Odobel, F.; Blart, E.; Lagree, M.; Villieras, M.; Boujtita, H.; El Murr, N.; Caramori, S.; Bignozzi, C. A. *J. Mater.Chem.* **2003**, 13, 502.

265. Kamat, P. V.; Ford, W. E. *Chem. Phys. Lett.* **1987**, 135, 421.

266. Tennakone, K.; Kumara, G. R.R.A.; Kottegoda, I. R.M.; Wijayantha, K.G.U. *Semicond. Sci. Technol.* **1997**, 12, 128.

267. Frank T. et al. *J. Clin. Pharmacol.* **2005**, 45, 203.

268. Zhou, K.; Wu, L.; Gao, Y.; Ma, T. *J. Photochem. Photobiol. A* **2011**, 219, 188.

269. Reddy, C.S.; Han, X.; Zhu, Q.Y.; Mai, L.Q.; Chen, W. *Microelectron. Eng.* **2006**, 83, 281.

270. Hugo, W.B.; Newton, J.M. *J. Pharm. Pharmacol.* **1963**, 15, 731.

271. Richardt, C. *Chem. Rev.* **1994**, 94, 2319.

272. Meng, S.; Ren, J.; Kaxiras, E. *Nano Lett.* **2008**, 8, 3266.

273. Polo, A.S.; Murakami Iha, N.Y. *Sol. Energy Mater. Sol. Cells.* **2006**, 90, 1936.

274. Lapornik, B.; Prosek, M.; Wondra, A.G. *J. Food Eng.* **2005**, 71, 214.

275. Bakowska, A.; Kucharska, A.Z.; Oszmianski, J. *Food Chem.*, **2003**, 81, 349.

276. Kumara, G.R.A.; Kaneko, S.; Okuya, M.; Onwona-Agyeman, B.; Konno, A.; Tennakone, K. *Sol. Energy Mater. Sol. Cells* **2006**, 90, 1220.

277. Tennakone, K.; Kumarasinghe, A. R.; Kumara, G. R. R. A.; Wijayantha, K. G. U.; Sirimanne, P. M. *J. Photochem. Photobiol. A: Chem.* **1997**, 108, 193.

278. Cherepy, N.J.; Smestad, G.P.; Graetzel, M.; Zhang, G.J. *J. Phys. Chem. B.* **1997**, 101, 9342.

279. Dai, Q.; Rabani, J. *J. Photochem. Photobiol. A Chem.* **2002**, 148, 17.

280. Calogero, G.; Di Marco, G. *Sol. Energy Mater. Sol. Cells.* **2008**, 92, 1341.

281. Gao, F.G.; Bard, A.J.; Kispert, L.D. *J. Photochem. Photobiol. A: Chem.* **2000**, 130, 49.

282. Tesoriere, L.; Allegra, M.; Butera, D.; Livrea, M.A. *Am. J. Clin. Nutr.* **2004**, 80, 941.

283. Quin C.; Clark, A.E. *Chem. Phys. Lett.* **2007**, 438, 26.

284. Calogero, G.; Di Marco, G.; Cazzanti, S.; Caramori, S.; Argazzi, R.; Di Carlo A.; Bignozzi, C. A. *Int. J. Mol. Sci.* **2010**, 11, 254.

285. Chen, C.-T.; Marder, S.R.; Cheng, L.-T. *J. Am. Chem. Soc.* **1994**, 116, 3117.

286. Alex, S.; Santhosh, U.; Das, S. *J. Photochem. Photobiol. A: Chem.* **2005**, 172,63

287. Wongcharee, K.; Meeyoo, V.; Chavadej S. *Sol. Energy Mater. Sol. Cells.* **2007**, 91, 566.